OPERATION KOMOREBI

REALIZATION CALCULUS

CORE SERIES V

Multiresolution Signal Calculus

Exact coordinates, singular packets, and stable reconstruction

---

Exact coordinates reveal how a signal moves through filters, refinements, and reconstruction. Singular packets keep representation, approximation, and recovery distinct.

Komorebi P.

Modern Monograph • 20 October 2026

How to use this volume

Part I. The twenty-result formal core develops exact polyphase reconstruction, filter transfers, Hilbert packet operators, finite adaptive trees, edge error bounds, and Smith coordinates.

Part II. The complete extended development treats lattice coordinates, stable banks, singular packets, separated jump recovery, geometric error bounds, and multiscale localization.

Visual atlas. Forty worked plates close the volume. The separate visual guide provides the same examples, and the Lean guide gives the precise released formal contract.

Reading this edition

The two branches of Paper V answer related questions at different levels. Part I preserves the twenty results and twenty proofs of the later v1.1.0 manuscript. Part II preserves the broader standalone development with its sixty-three proofs and E-prefixed section numbers. Their overlap is intentional. The combined eighty-three proofs are a record of the two complete branches, rather than eighty-three independent or novel results.

For a first reading, follow Part I Sections 1–7. These sections establish the coordinate maps, filter transfers, exact reconstruction, and the separation of packet error from smooth approximation error. Section 11 develops finite adaptive selection. Sections 13–14 give the cyclic Smith realization. Continue with Part II Sections E2–E6 for lattice and stability generalizations, E7–E11 for singular packets and recovery, and E12–E14 for nonlinear and Cayley coordinates. Each visual plate identifies the corresponding manuscript result.

The inherited September 2026 release records 225 Lean theorem targets across 23 proof modules supporting all twenty Part I results. This scope does not extend automatically to Part II. The E-prefixed development has prose proofs and retains the mathematical corrections recorded in the prior edition's exact change ledger. No fresh Lean compilation is claimed for this monograph. The current computation review reran twenty exact-model tests with 305,933 counted assertions and sixteen verifier controls. The current companion suite passed thirty-three tests, with twenty-seven overlapping tests from the earlier snapshot also checked. The extended suite passed 11,052 checks in thirteen groups. Fifty-two saved floating-point metrics and eighteen discrete leaves reproduced exactly, and all eighteen companion figure pairs were regenerated. The visual examples passed their own symbolic checks and controls. These checks have finite scopes and are recorded separately in the accompanying verification files. Historical counts in Part I's reproducibility appendix keep their September provenance.

The two broad edge recovery conjectures remain open. Part II proves recovery for a declared one dimensional separated jump class under its sampling, contrast, and noise assumptions. These results do not supply universal image segmentation or infinite-tree consistency. Numerical illustrations keep the finite interpretation stated in their captions.

Contents

Reading this edition i

Part I: The released formal core 1

Part I: The released formal core 1

1 The signal realization of the seed calculus 2

2 Residue projectors and exact polyphase coordinates 3
2.1 Nested refinement . . . 5

3 Linear time-invariant operators as transfer matrices 5

4 Analysis banks, synthesis banks, and perfect reconstruction 7
4.1 The Haar bank . . . 8
4.2 Predict–update lifting . . . 8

5 Wavelet packets as addressed refinements 10

6 Known edge packets and spectral reconstruction 11

7 Mask, amplitude, and smooth-background error 12

8 One-dimensional numerical study 13

9 Two-dimensional edge packets 15
9.1 Curves, corners, and multiple amplitudes . . . 17

10 Sparse wavelet packets and global Fourier modes 18

11 Finite adaptive packet trees 19

12 Nonlinear signal packets 24

13 Smith coordinates as cyclic signal coordinates 24
13.1 Radial seeds and physical phase . . . 27

14 Dyadic–odd phase factorization and boundary weighting 29

15 Boundary-localized error and claim control 29

16 Implementation and reproducibility 31

17 Conclusions 32

A Algorithm statements 33
A.1 Exact polyphase filtering . . . 33
A.2 Conditional known-edge reconstruction . . . 33
A.3 Limited positive-contrast estimator . . . 33

B Numerical record 34

C Notation crosswalk 34

D Formalization and reproducibility record 35
D.1 What has been checked . . . 35
D.2 Result-by-result correspondence . . . 35
D.3 Three bridges that matter for the statement . . . 36
D.4 September 2026 checks and numerical conventions . . . 37
D.5 Pinned environment and rerunning the release . . . 38
D.6 What remains open . . . 38

Part II: Extended mathematical development 39

Part II: Extended mathematical development 39

E1 Introduction 39
E1.1 Main results . . . 40
E1.2 Notation . . . 42

E2 Signal seeds and lattice addresses 42

E3 Polyphase coordinates on finite index sublattices 43
E3.1 Refinement of sublattices . . . 44

E4 Convolution as a packet transfer matrix 46
E4.1 The one dimensional symbol . . . 47

E5 Filter banks, frame bounds, and lifting 48
E5.1 Haar analysis . . . 51
E5.2 Lifting steps . . . 51

E6 Wavelet packet trees and admissible bases 52
E6.1 Best basis recursion . . . 54

E7 Singular packets and exact reconstruction 56

E8 Exact error formulas for estimated packets 59
E8.1 Several regions . . . 60
E8.2 Boundary tube control . . . 62

E9 Stable recovery of separated jumps 62
E9.1 Sub Gaussian noise . . . 67
E9.2 Signals with values in a normed space . . . 68

E10 Haar localization and annihilating differences 68
E10.1 Haar coefficient separation . . . 68
E10.2 Two shifted grids . . . 69
E10.3 Higher differences . . . 71

E11 Packet separation and the Gibbs phenomenon 71

E12 Nonlinear interactions in residue coordinates 74

E13 Finite numerical illustrations 75

E14 Cyclic Cayley coordinates 77

E15 Limits and further directions 78

E16 Conclusion 79

Part III: Forty worked visual plates **81**

Part III: Forty worked visual plates **81**

List of Figures

1 Four-phase analysis of a finite signal. The channels are decimated coordinate packets; interleaving them gives the original signal exactly. . . . 4
2 The exact transfer matrix for a seven-tap FIR filter in four phases. Every cell records the delays and coefficients carrying one input packet into one output packet. . . . 6
3 Exact address comparison for a two-phase split. A delay of one original sample sends the odd channel into the even channel with a coarse delay, and the even channel into the odd channel without a coarse delay. A one-step channel delay moves both original residues by two samples. All plotted values are integer sample addresses. . . . 7
4 A piecewise-smooth signal and its first Haar low/detail packets. The low channel records local averages. The detail channel records adjacent-sample differences, including pairs that cross a jump. . . . 9
5 Energy of the sixteen depth-four Haar packet addresses for the test signal. The packet address is an operator word in the common seed grammar. . . . 11
6 An exact rational eight-coordinate example of retained packet cancellation. The supplied jump packet is kept, while the linear operator averages adjacent pairs in the smooth component. The two error vectors agree coordinate by coordinate. This model illustrates cancellation and does not test packet detection or a Fourier convergence rate. . . . 11
7 One-dimensional reconstruction and absolute error. The known packet removes the edge from the global spectral approximation. The estimated packet is visibly better than the global reconstruction in this limited test but retains smooth-background estimation error. . . . 14
8 Error as spectral resolution increases. The known packet follows only the smooth approximation error. The estimated reconstruction reaches a floor determined by background and amplitude estimation. . . . 15
9 A sharp disk on a smooth background. Global Fourier truncation produces a bright boundary halo and oscillatory interior and exterior error. Retaining the exact edge packet leaves only the smooth-background approximation error. . . . 16
10 The limited data-driven experiment. The observed image alone is thresholded into two intensity classes, cleaned topologically, harmonically filled, spectrally smoothed, and recombined with an estimated jump. . . . 17
11 Known-packet stress test with curved boundaries, corners, overlap, and different jump amplitudes. The exact packet is not a binary mask multiplied by one amplitude; it is the complete piecewise packet. . . . 18
12 Sparse approximation of the test signal. With very few coefficients the global Fourier basis is initially better. After the edge packets are resolved, the Haar packet error decays much faster in this example. . . . 19
13 A globally optimal mixed-depth Haar packet pruning. The selected antichain covers the full tree, so its synthesis is exact even though different branches stop at different depths. 23
14 The dynamic-programming optimum agrees with exhaustive enumeration. A positive gap larger than twice the declared perturbation envelope certifies that the selected tree is stable. . . . 23
15 Norms of pairwise product interactions for five residue phases. The label in each cell gives the output phase $(i + j) \bmod 5$. . . . 25
16 The classical Smith grid equipped with sixteen exact phase rays and four radial seed orbits. The Cayley transform creates the chart; the projector calculus supplies the nested cyclic coordinate system. . . . 27

17 The same reflection circle at phase orders $2, 4, 8, 16, 32$. Each coarse phase ray appears in every finer grid whose order is a multiple of its order. The exact residue-projector refinement law concerns coefficient packets, not sums of impedance points. 28
18 The proposed symmetric refinement weight becomes large near the open- and short-circuit boundary points. It is a condition-based adaptive coordinate, not an asserted optimal sampling law. 30
19 Error restricted to a narrow boundary band. Global truncation concentrates large error on the jump. The known-packet reconstruction has only the small smooth-packet error in the same band. 30
20 Proof and claim boundary. Finite adaptive-tree selection is now proved; the remaining open rows concern universal recovery and infinite-tree or asymptotic selection. 31
E1 A signal and its four exact residue channels. Interleaving the channels returns the original samples without approximation. 45
E2 Absolute tap weight in the transfer blocks of the four phase operator in example E4.6. . 48
E3 Pointwise singular value bounds govern both the original frame and its perturbed analysis bank. 51
E4 A complete packet tree and one admissible pruning. Retained nodes may occur at different depths. 54
E5 An additive best basis recursion compares the cost of retaining a packet with the total cost of splitting it. 55
E6 Truncated power packets encode jumps in a function and in its successive derivatives. . 58
E7 A global Fourier approximation must represent the jumps. A retained packet approximation applies the Fourier truncation only to the smooth component. 59
E8 An overlap matrix records both correct regions and every type of misclassification. The exact packet norm weights each entry by the corresponding value difference. 61
E9 A sufficient threshold interval from exact rational contrast bounds. With the displayed model parameters, smooth and noise contrasts are at most $1/10$ and jump contrasts are at least $9/10$. Every threshold strictly between those values separates the cells under the sampling assumptions stated below. The figure does not assert an optimal threshold for other observation models. 63
E10 Separated jumps create isolated adjacent sample contrasts above the smooth and noise background. 66
E11 The smooth contribution decays like $L^{3/2}$, while a separated jump contribution decays like $L^{1/2}$. 70
E12 The boundaries of the two grids interlace. Every jump is well inside a cell in at least one grid. 70
E13 Global Fourier truncation represents the jump and exhibits an oscillatory boundary layer. Packet separation retains the jump and approximates only the smooth component. . . . 74
E14 One finite sparse approximation comparison. Fourier coordinates are better at the smallest budget, while the fixed Haar packet basis becomes better after localized edge coordinates are resolved. 76
E15 The cyclic action is an ordinary phase rotation in the reflection disk and a fractional linear action in the impedance half plane. 79

List of Tables

1 Sparse approximation errors for the one-dimensional test signal. 18
2 Numerical companion modules. 31

3 Main edge-study measurements. 34
4 Main software artifacts. 34
5 Notation crosswalk. 34
6 The twenty manuscript results and their Lean statement scopes. 35
E1 Finite sparse approximation record for one test signal. 76
E2 Finite edge reconstruction record from the original computational study. 77

Part I: The released formal core

Coordinates first, decisions second

A residue decomposition changes the coordinates of a signal without changing its information. Filtering then acts between those coordinates. Approximation enters when an operator compresses a component or when a decision discards coefficients. The formal core follows these operations in that order.

Overview

This paper develops the signal realization of the projector-resolved seed calculus. The impulse δ_0 is taken as a primitive signal seed and its shift orbit supplies the address system. Residue projectors split a sequence into exact polyphase channels, nested divisibility gives exact refinement, and every finite impulse-response operator becomes a matrix of packet transfers. The standard perfect-reconstruction condition for a filter bank is therefore an analysis–synthesis identity in the common operator language of the series. Haar analysis and every finite-depth wavelet-packet transform are treated on complex ℓ^2, together with concrete finite-signal models and a predict–update lifting step. The edge problem is separated into two statements. When a discontinuity packet is known and retained exactly, approximation error is exactly the approximation error of the remaining smooth packet. No spectral approximation of the jump is performed. When the packet is estimated, a symmetric-difference bound isolates mask error, amplitude error, and smooth-background error. Numerical studies compare global Fourier truncation, exact known-packet reconstruction, and a deliberately narrow positive-contrast estimator in one and two dimensions, including curved boundaries, corners, and multiple amplitudes. The same cyclic phase action is then placed on the Smith reflection disk. Its pullback through the Cayley transform is a Möbius action on impedance, and the two-phase case is precisely impedance–admittance inversion. Nonlinear coefficient products obey cyclic packet convolution. The preserved September 2026 release integrates a Lean formalization of all twenty theorem-like statements under the hypotheses stated below: 225 supporting theorem targets in 23 modules. Eighteen regenerated figures, machine-readable numerical results, the 33-test original companion suite, and 36 additional exact-model and verifier tests accompany the paper. Exact signal theorems, limited numerical estimators, classical constructions, and open recovery problems are kept distinct throughout.

Scope and claim boundary

The paper proves exact polyphase reconstruction, exact finite filter-transfer identities, perfect reconstruction for the stated filter banks, the conditional known-edge theorem, mask and amplitude perturbation bounds, nonlinear residue-convolution laws, and the Smith-coordinate phase action. It does not claim that every discontinuity can be detected automatically, that every form of Gibbs ringing has been eliminated, or that the simple two-class estimator supplied with the release is a universal segmentation method. The estimator is included as one reproducible finite example. For every finite packet refinement tree, the paper now proves existence of a globally optimal complete pruning, an exact dynamic-programming selector for additive costs, and a deterministic margin-stability certificate. Wavelets, filter banks, the Cayley transform, and the classical Smith grid are treated as classical inputs organized in the common seed–packet–refinement language.

Verification convention. "Lean-checked" refers to the explicitly scoped theorem statements and their supporting declarations, accepted by the pinned Lean kernel. It does not certify the English text automatically, the floating-point Python implementation, physical modelling choices, or the two conjectures. The manuscript-to-declaration correspondence has been reviewed manually. Appendix D records it result by result. The September 2026 release records a rerun of the numerical experiments. The current final-edition checks are distinguished in the opening reading note.

1 The signal realization of the seed calculus

Let $\ell^2(\mathbb{Z};\mathbb{C})$, abbreviated $\ell^2(\mathbb{Z})$, be the Hilbert space of square-summable complex discrete signals. The inner product is conjugate-linear in its first argument. A superscript $*$ on a bounded operator denotes its Hilbert adjoint. Write δ_n for the unit impulse at address n and let the bilateral shift be

$$(Sx)[n] = x[n-1].$$

Then

$$S^n\delta_0 = \delta_n.$$

The primitive signal seed is therefore $s = \delta_0$, the address operators are the shift words S^n, and the completion is the ℓ^2 norm.

Theorem 1.1 (Impulse seed theorem). *The closed shift-generated hull of δ_0 is all of $\ell^2(\mathbb{Z})$:*

$$\boxed{\overline{\operatorname{span}\{S^n\delta_0 : n \in \mathbb{Z}\}}^{\ell^2} = \ell^2(\mathbb{Z}).}$$

Every finitely supported signal has the exact finite expression

$$x = \sum_{n\in\mathbb{Z}} x[n]S^n\delta_0.$$

Proof. The shift orbit is the standard orthonormal basis $\{\delta_n\}_{n\in\mathbb{Z}}$. For $x \in \ell^2$, the finite truncations

$$x_F = \sum_{n\in F} x[n]\delta_n, \qquad F \subset \mathbb{Z} \text{ finite},$$

satisfy $\|x - x_F\|_2^2 = \sum_{n\notin F} |x[n]|^2 \to 0$ as the finite sets exhaust $\mathbb{Z}$. Thus the unordered Hilbert-space sum $\sum_n x[n]\delta_n$ converges to x, and the finite-support statement is exact. The shift is a surjective isometry because $n \mapsto n-1$ is a bijection of $\mathbb{Z}$, with inverse shift $n \mapsto n+1$. This proves the closed-span assertion. □

This realization fixes the language used below:

$$\text{impulse seed} \longrightarrow \text{shift address} \longrightarrow \text{packet projection} \longrightarrow \text{filter transfer}$$
$$\longrightarrow \text{refinement} \longrightarrow \text{reconstruction}.$$

Remark 1.2 (Several completions). The same algebraic seed description applies to finite sequences, ℓ^1, ℓ^2, periodic sequences, tempered distributions, and multidimensional lattices. The topology decides which infinite reconstructions are legitimate. Finite-dimensional experiments in this paper use ordinary Euclidean norms; theorem statements specify the ambient norm when it matters.

2 Residue projectors and exact polyphase coordinates

A packet has two useful representations

The masked packet keeps its original sample addresses and sets the other phases to zero. The decimated channel stores only the retained addresses, now indexed by the coarse coordinate. They carry the same values, but their domains differ. Refinement sums belong on the original lattice. Interleaving converts the channels back to that lattice.

Fix an integer $N \geq 1$. For $0 \leq r < N$, define

$$(P_{N,r}x)[n] = \mathbf{1}_{n \equiv r \,(\mathrm{mod}\, N)} x[n].$$

The corresponding decimated channel is

$$x_r[q] = x[Nq + r].$$

Theorem 2.1 (Polyphase projector theorem)**.** *The maps $P_{N,r}$ are bounded orthogonal projectors on ℓ^2, with operator norm at most one, and satisfy*

$$P_{N,r}P_{N,s} = \delta_{rs}P_{N,r}, \qquad \sum_{r=0}^{N-1} P_{N,r} = I.$$

Consequently,

$$\boxed{x = \sum_{r=0}^{N-1} P_{N,r}x}$$

with no approximation.

Proof. Each integer belongs to exactly one residue class modulo N. Multiplying the two indicator functions gives zero for distinct classes and the same indicator for equal classes. Summing all residue indicators gives one at every address. Moreover,

$$\|P_{N,r}x\|_2^2 = \sum_{n \equiv r \,(\mathrm{mod}\, N)} |x[n]|^2 \leq \|x\|_2^2, \qquad \langle P_{N,r}x, y\rangle = \langle x, P_{N,r}y\rangle.$$

The mask is real-valued, so the inner-product identity follows term by term. Hence each projector is self-adjoint, and the ranges of different residue projectors are orthogonal. □

Define the analysis and synthesis maps

$$\mathcal{A}_N x = (x_0, \dots, x_{N-1}), \qquad \mathcal{S}_N(x_0, \dots, x_{N-1})[Nq + r] = x_r[q].$$

Corollary 2.2 (Analysis–synthesis identity)**.**

$$\boxed{\mathcal{S}_N\mathcal{A}_N = I.}$$

On the product of the channel spaces one also has $\mathcal{A}_N\mathcal{S}_N = I$. Equip this finite product with the Hilbert norm

$$\|(x_0, \dots, x_{N-1})\|_{\mathrm{ch}}^2 = \sum_{r=0}^{N-1} \|x_r\|_2^2.$$

Then $\mathcal{A}_N$ is a linear isometric equivalence and

$$\|x\|_2^2 = \sum_{r=0}^{N-1} \|x_r\|_2^2.$$

Proof. Euclidean division gives a unique pair (r, q) with $0 \le r < N$ and $n = Nq + r$, including negative n. The address maps $n \mapsto (n \bmod N, n \operatorname{div} N)$ and $(r, q) \mapsto Nq + r$ are inverse. Analysis and synthesis are reindexing by this bijection. Reindexing the nonnegative sum $\sum_n |x[n]|^2$ proves the norm identity and shows that both maps preserve square summability. In Lean the target is $\ell^2(\{0, \dots, N-1\} \times \mathbb{Z})$, which realizes exactly this Hilbert norm. □

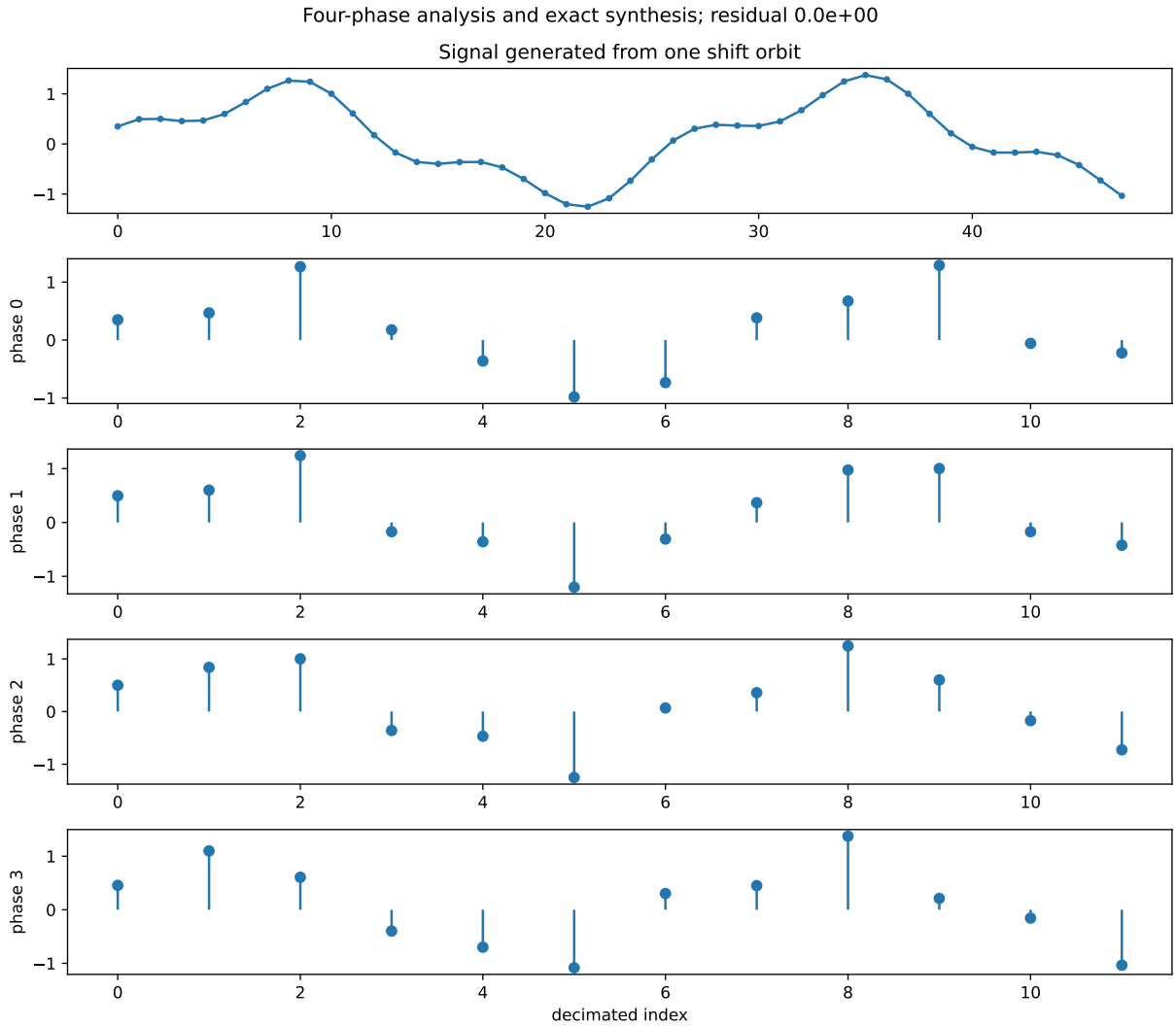


Figure 1. Four-phase analysis of a finite signal. The channels are decimated coordinate packets; interleaving them gives the original signal exactly.

2.1 Nested refinement

Suppose $N, M \geq 1$ and $N \mid M$. Every coarse phase has a disjoint family of fine descendants:

$$\mathrm{Child}_M(N, r) = \{s : 0 \leq s < M,\ s \equiv r \pmod{N}\}.$$

Theorem 2.3 (Exact nested refinement). *For $N, M \geq 1$ and $N \mid M$,*

$$\boxed{P_{N,r} = \sum_{\substack{0 \leq s < M \\ s \equiv r \,(\mathrm{mod}\, N)}} P_{M,s}.}$$

Proof. An integer n satisfies $n \equiv r \pmod{N}$ exactly when its unique residue $s = n \bmod M$ lies among the listed descendants. The fine indicators are disjoint, so their sum is the coarse indicator. □

This identity is the signal form of the refinement law introduced in Paper II. It is not merely a denser sampling rule. The coarse masked packet, represented on the original integer lattice, is exactly the sum of its fine masked descendants. Decimated channels at different moduli must first be placed in these common coordinates before being added.

3 Linear time-invariant operators as transfer matrices

Let h be a finite impulse response and

$$y = h * x, \qquad y[n] = \sum_{q \in \mathbb{Z}} h[q]x[n-q].$$

Resolve both input and output into N phases. For output phase k and input phase s, define the transfer kernel

$$\boxed{h_{ks}[m] = h[Nm + k - s].}$$

Out-of-range taps are understood to be zero.

Theorem 3.1 (Exact FIR polyphase transfer law). *The output channels satisfy*

$$\boxed{y_k[n] = \sum_{s=0}^{N-1} \sum_{m \in \mathbb{Z}} h_{ks}[m] x_s[n-m].}$$

For the numerical channel transform, take $z \in \mathbb{C} \setminus \{0\}$ and assume

$$\sum_{n \in \mathbb{Z}} |x_s[n] z^{-n}| < \infty \quad (0 \leq s < N).$$

Define $X_s(z) = \sum_n x_s[n] z^{-n}$. The output series then also converge absolutely, and

$$\boldsymbol{Y}(z) = \boldsymbol{H}^{(N)}(z)\boldsymbol{X}(z), \qquad H_{ks}^{(N)}(z) = \sum_m h[Nm + k - s] z^{-m}.$$

Proof. Evaluate y at address $Nn + k$ and partition every input index by its residue s:

$$\begin{aligned} y[Nn + k] &= \sum_{q} h[q]x[Nn + k - q] \\ &= \sum_{s=0}^{N-1} \sum_{m} h[Nm + k - s]x[N(n - m) + s]. \end{aligned}$$

For a fixed output phase k, the change of tap address $q = Nm + k - s$ is a bijection between $\mathbb{Z}$ and the pairs (s, m) with $0 \leq s < N$: choose $s \equiv k - q \pmod{N}$ and then $m = (q - k + s)/N$. Thus this is a reindexing of the finite filter support, valid for every bilateral input sequence, without a convergence assumption on x.

The last factor is $x_s[n-m]$, giving the time-domain formula. Under the additional transform hypothesis, each delayed channel has transform

$$\sum_{n} x_s[n - m]z^{-n} = z^{-m} \sum_{j} x_s[j]z^{-j}.$$

Absolute summability permits this bijective reindexing, and only finitely many delayed channels are combined. Taking their finite linear combination gives the matrix formula. The time-domain theorem therefore remains valid even when no numerical bilateral transform exists. □

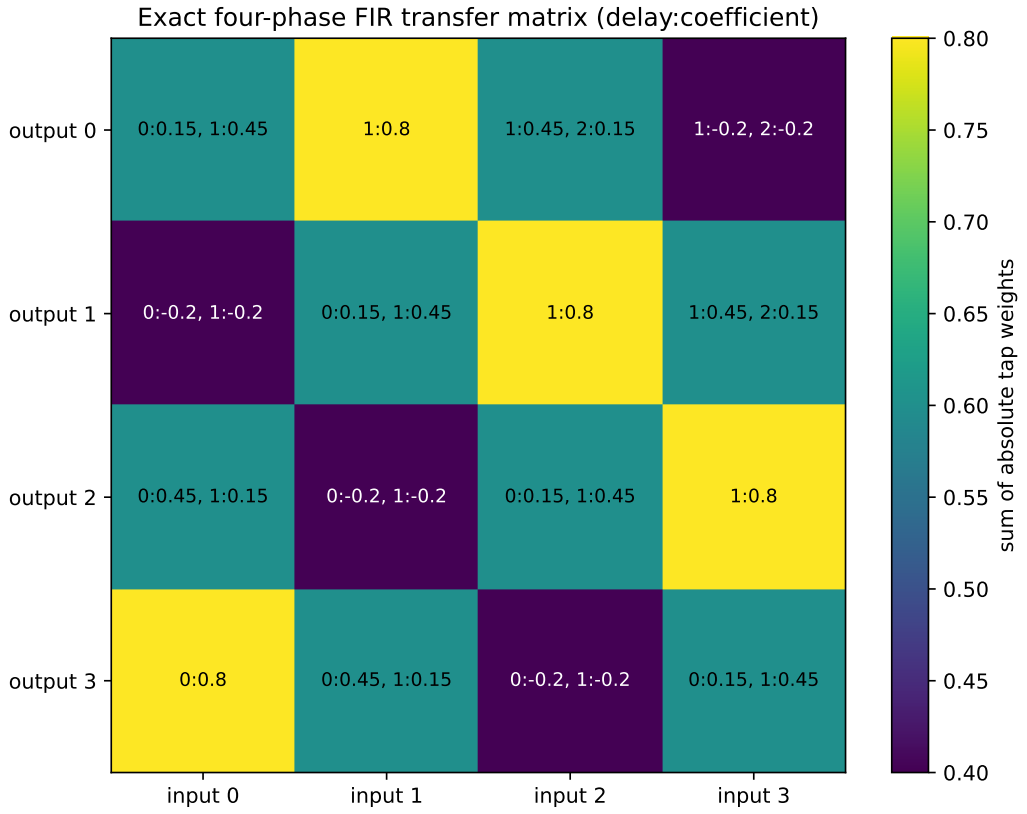


Figure 2. The exact transfer matrix for a seven-tap FIR filter in four phases. Every cell records the delays and coefficients carrying one input packet into one output packet.

Remark 3.2 (Operator-block form). If H denotes convolution by h, the same identity is

$$H = \sum_{k,s} P_{N,k} H P_{N,s}.$$

Thus the familiar polyphase matrix is exactly the transfer-block matrix of the seed calculus.

4 Analysis banks, synthesis banks, and perfect reconstruction

Read the delay in the coordinate system used

A step in one decimated channel crosses a full block of original samples. A one-sample shift also permutes the residue labels. At two phases, these operations have different matrices. The following calculation keeps the original sample delay visible instead of hiding it in a channel convention.

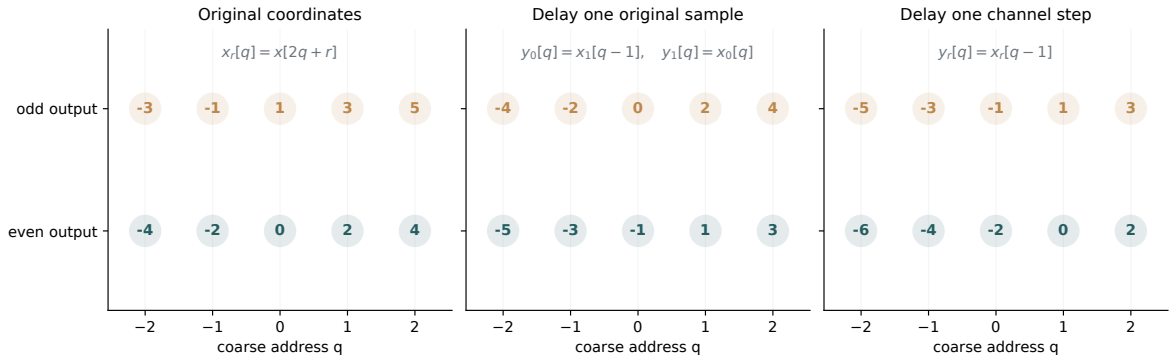


Figure 3. Exact address comparison for a two-phase split. A delay of one original sample sends the odd channel into the even channel with a coarse delay, and the even channel into the odd channel without a coarse delay. A one-step channel delay moves both original residues by two samples. All plotted values are integer sample addresses.

Work with finite impulse-response banks. Let $\mathcal{L} = \mathbb{C}[z, z^{-1}]$ be the Laurent-polynomial algebra, with the monomial z^{-m} acting on a bilateral sequence by $x[n] \mapsto x[n-m]$. Let $\boldsymbol{E} \in \mathrm{Mat}_{N\times N}(\mathcal{L})$ and $\boldsymbol{R} \in \mathrm{Mat}_{N\times N}(\mathcal{L})$ be analysis and synthesis matrices. Their composition acts on all bilateral channel sequences by finite convolutions. At a nonzero z where the input transforms are absolutely convergent, this gives

$$\widehat{\boldsymbol{X}}(z) = \boldsymbol{R}(z)\boldsymbol{E}(z)\boldsymbol{X}(z).$$

Theorem 4.1 (Perfect-reconstruction criterion)**.** *For $d \in \mathbb{Z}$, such a bank reconstructs every input up to a delay of d* channel indices *exactly when the following Laurent-polynomial identity holds:*

$$\boxed{\boldsymbol{R}(z)\boldsymbol{E}(z) = z^{-d} I_N.}$$

If the right side is $cz^{-d}I_N$ with $c \neq 0$, reconstruction holds up to gain c and channel delay d. After interleaving, this is a delay of Nd original samples. A negative delay denotes an advance.

Proof. Finite convolution represents Laurent-polynomial multiplication: composing shifts adds their delays, and distributivity handles finite sums. Thus the matrix identity implies the asserted action. Conversely, let $\boldsymbol{B} = \boldsymbol{RE} - cz^{-d}I_N$ and suppose its action vanishes on every channel sequence. Insert

an impulse at channel s, address zero, with every other channel zero. Output channel k reads the coefficients of the Laurent polynomial B_{ks} at all addresses. All of these coefficients vanish, so $B_{ks} = 0$ for every k, s. The representation is faithful, proving necessity as a polynomial identity rather than merely equality at one evaluation point. The displayed unit-gain case is $c = 1$. □

Original-sample delay. For an arbitrary original-sample delay $D \in \mathbb{Z}$, the output phase k has

$$y_k[n] = x_{r_k}[n + q_k], \qquad r_k = (k - D) \bmod N, \qquad q_k = (k - D) \operatorname{div} N.$$

Its channel matrix has the sole nonzero entry z^{q_k} in row k, column r_k. In particular, a one-sample delay at $N = 2$ has matrix

$$\begin{pmatrix} 0 & z^{-1} \\ 1 & 0 \end{pmatrix},$$

whereas $z^{-1} I_2$ delays the original signal by two samples. The general address identity is valid for negative sample addresses as well.

4.1 The Haar bank

The Haar analysis matrix is

$$\boldsymbol{E}_{\mathrm{H}} = \frac{1}{\sqrt{2}} \begin{pmatrix} 1 & 1 \\ 1 & -1 \end{pmatrix}.$$

It is orthogonal, so $\boldsymbol{R}_{\mathrm{H}} = \boldsymbol{E}_{\mathrm{H}}^{\mathsf{T}}$ and

$$\boldsymbol{R}_{\mathrm{H}} \boldsymbol{E}_{\mathrm{H}} = I_2.$$

The channels are

$$a[n] = \frac{x[2n] + x[2n+1]}{\sqrt{2}}, \qquad d[n] = \frac{x[2n] - x[2n+1]}{\sqrt{2}}.$$

Corollary 4.2 (Haar energy identity)**.**

$$\boxed{\|x\|_2^2 = \|a\|_2^2 + \|d\|_2^2.}$$

Proof. For any $u, v \in \mathbb{C}$, the parallelogram identity gives

$$\left|\frac{u+v}{\sqrt{2}}\right|^2 + \left|\frac{u-v}{\sqrt{2}}\right|^2 = |u|^2 + |v|^2.$$

Apply this to $u = x[2n]$, $v = x[2n+1]$ and sum over $n \in \mathbb{Z}$. Each summand is nonnegative; the right side is $\|x\|_2^2$ by the two-channel address equivalence. This also proves that the literal low and detail channels belong to ℓ^2. The real Haar matrix is unitary over $\mathbb{C}$, so the finite-signal statement is the same calculation with a finite sum. □

4.2 Predict–update lifting

Split x into even and odd channels e, o. Define

$$d = o - e, \qquad s = e + \frac{1}{2} d.$$

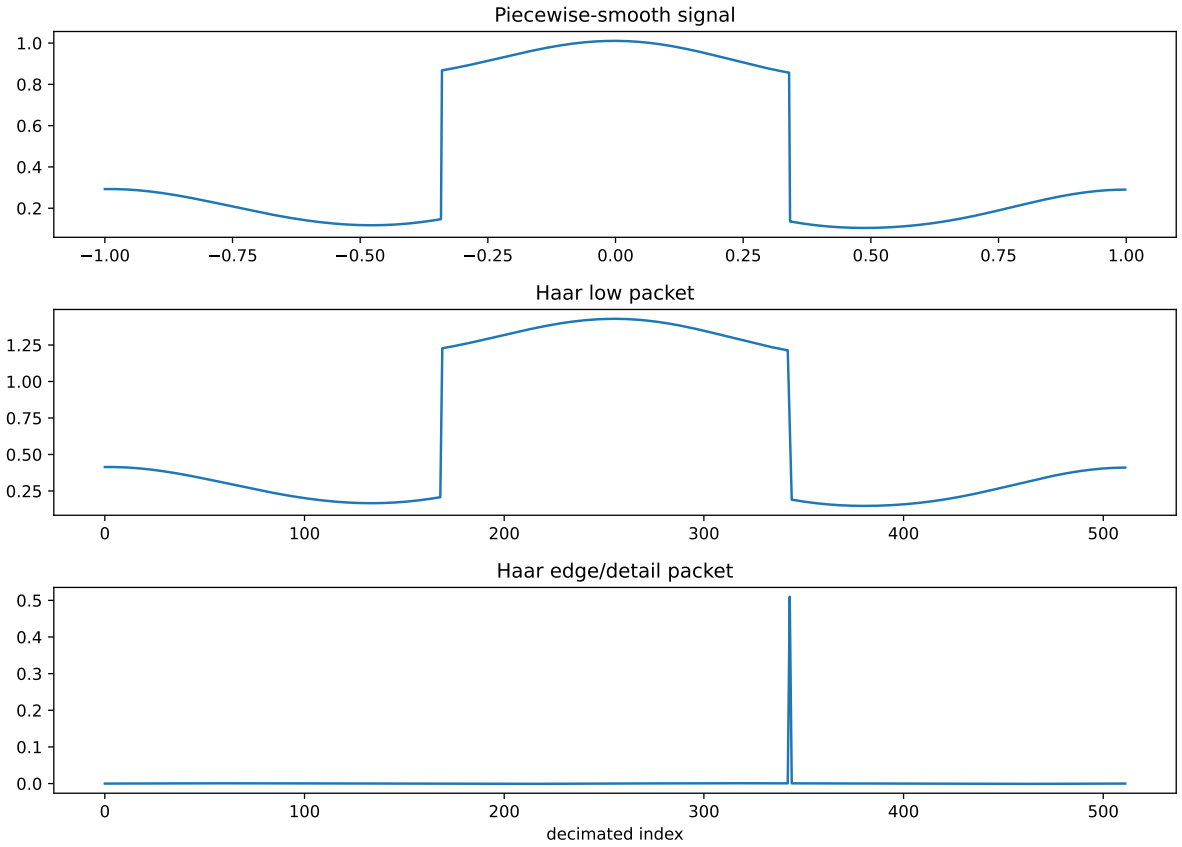


Figure 4. A piecewise-smooth signal and its first Haar low/detail packets. The low channel records local averages. The detail channel records adjacent-sample differences, including pairs that cross a jump.

The inverse is

$$e = s - \frac{1}{2}d, \qquad o = d + e.$$

Theorem 4.3 (Exact lifting reconstruction). *The predict–update map $(e, o) \mapsto (s, d)$ is invertible with determinant one and the displayed inverse. Consequently the associated finite transform reconstructs every even-length signal exactly.*

Proof. The forward matrix is

$$\begin{pmatrix} s \\ d \end{pmatrix} = \begin{pmatrix} 1/2 & 1/2 \\ -1 & 1 \end{pmatrix} \begin{pmatrix} e \\ o \end{pmatrix},$$

whose determinant is one. Direct substitution gives the inverse formulas. □

5 Wavelet packets as addressed refinements

On $\ell^2(\mathbb{Z}; \mathbb{C})$, apply the Haar analysis to both children at each stage. For a finite input, assume its length is divisible by 2^ℓ when a depth-ℓ transform is used. A binary word $\alpha \in \{0, 1\}^\ell$ addresses a depth-ℓ packet, denoted $W_{\ell,\alpha}x$. Appending 0 or 1 selects the low or high child.

Theorem 5.1 (Wavelet-packet reconstruction and energy). *At every finite depth ℓ,*

$$\boxed{x = \sum_{\alpha \in \{0,1\}^\ell} W_{\ell,\alpha}^* W_{\ell,\alpha} x,}$$

and

$$\boxed{\|x\|_2^2 = \sum_{\alpha \in \{0,1\}^\ell} \|W_{\ell,\alpha} x\|_2^2.}$$

Proof. Write H_0, H_1 for the literal low and detail operators. The preceding energy identity implies $\|H_b x\|_2 \le \|x\|_2$, so both have bounded Hilbert adjoints. At depth zero the only packet operator is the identity. If the energy identity holds at depth ℓ, apply the one-level identity to each $W_{\ell,\alpha}x$ and sum; this proves it at depth $\ell + 1$.

Set $A = \sum_\alpha W_{\ell,\alpha}^* W_{\ell,\alpha}$. This is a finite sum of bounded operators. The energy result says $\langle x, Ax\rangle = \langle x, x\rangle$ for every x. Complex polarization, applied also to $x + y$ and $x + \mathrm{i}y$, gives $\langle y, (A - I)x\rangle = 0$ for all x, y, hence $A = I$. Applying the operator identity to x proves synthesis. This argument uses the actual Hilbert adjoints of the decimation operators, not a separately postulated inverse symbol. □

Classical Input 5.2 (Wavelet boundary). The existence and perfect-reconstruction theory of wavelets and filter banks are classical. Their role here is structural: they provide a fully developed realization in which seed generation, packet addressing, refinement, transfer blocks, and exact synthesis can all be read literally in the common operator language.

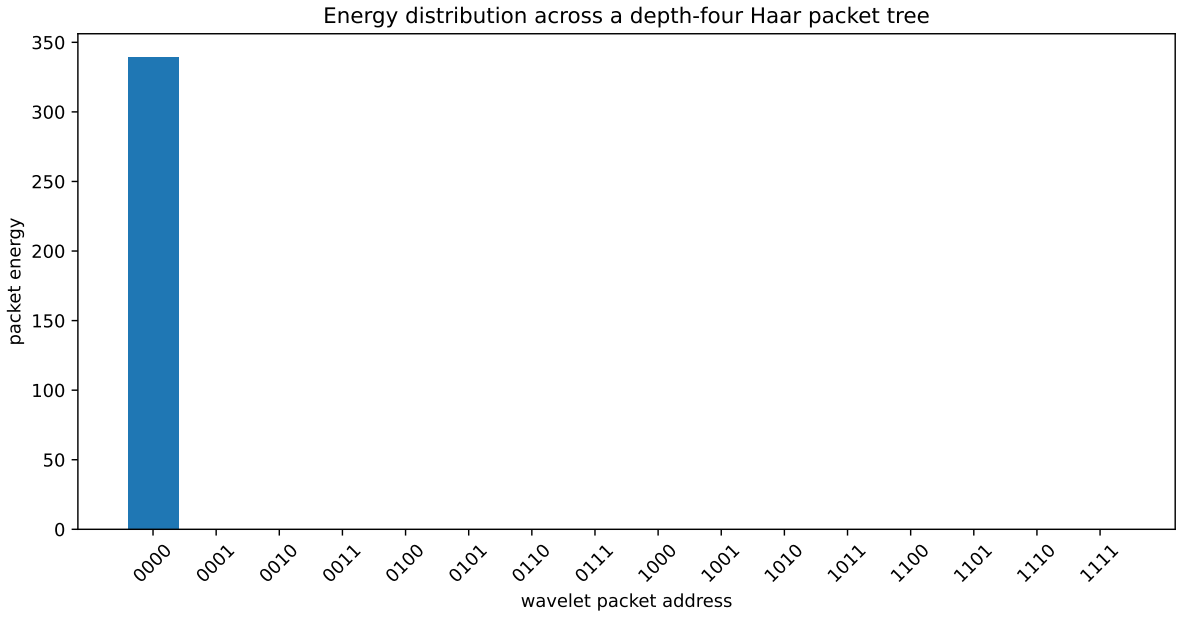


Figure 5. Energy of the sixteen depth-four Haar packet addresses for the test signal. The packet address is an operator word in the common seed grammar.

6 Known edge packets and spectral reconstruction

> **Retention changes the approximation target**
>
> The retained packet is supplied as part of the model. It passes through synthesis exactly. The approximation operator acts on the smooth remainder, so its error can be studied without forcing a global smooth basis to reproduce the jump. Finding that packet from observations is a separate recovery problem.

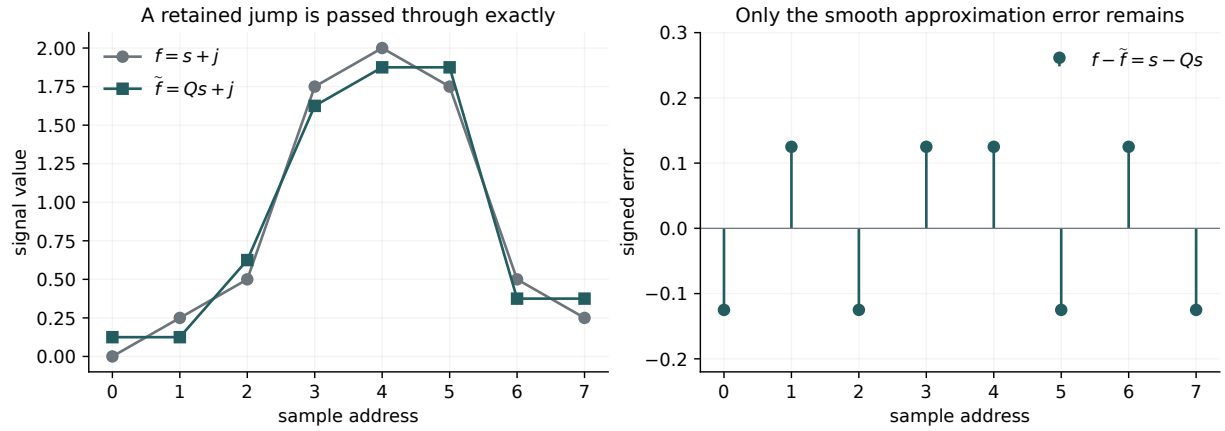


Figure 6. An exact rational eight-coordinate example of retained packet cancellation. The supplied jump packet is kept, while the linear operator averages adjacent pairs in the smooth component. The two error vectors agree coordinate by coordinate. This model illustrates cancellation and does not test packet detection or a Fourier convergence rate.

The central distinction is between approximating a jump globally and retaining it as its own packet.

Let

$$f = s + j$$

where s belongs to a smooth approximation class and j is a known discontinuity packet. Let Q_m be any approximation operator applied only to s, and define

$$\tilde{f}_m = Q_m s + j.$$

Theorem 6.1 (Exact known-edge theorem). *For every norm for which the expressions are defined,*

$$\boxed{f - \tilde{f}_m = s - Q_m s, \qquad \|f - \tilde{f}_m\| = \|s - Q_m s\|.}$$

No approximation of j occurs.

Proof. Subtract:

$$f - \tilde{f}_m = (s + j) - (Q_m s + j) = s - Q_m s.$$

Taking the norm gives the second identity. □

Corollary 6.2 (Several exact edge packets). *If*

$$f = s + \sum_{q=1}^{M} j_q$$

and every j_q is retained exactly, then

$$\left\| f - \left(Q_m s + \sum_{q} j_q \right) \right\| = \|s - Q_m s\|.$$

Curved edges, corners, and different jump amplitudes do not alter the identity.

Proof. The finite sum $j = \sum_{q=1}^{M} j_q$ is a single retained packet. Applying the preceding cancellation identity gives the result; the empty family $M = 0$ is included with sum zero. □

Boundary 6.3 (What the theorem does and does not say). The theorem explains why global ringing caused by spectrally approximating a known jump is absent from the reconstructed jump packet. It does not discover the packet. If the packet is wrong, its error is reconstructed exactly as well. Nor does the theorem prevent unrelated truncation errors in the smooth packet, domain-boundary errors, noise, or model mismatch.

7 Mask, amplitude, and smooth-background error

Let (X, Σ, μ) be a measure space, with measurable masks $\Omega, \widehat{\Omega} \subseteq X$ and scalar amplitudes $a, \hat{a} \in \mathbb{C}$ (real amplitudes are a special case). Suppose a scalar jump packet is

$$j = a\mathbf{1}_{\Omega},$$

and an estimated packet is

$$\hat{j} = \hat{a}\mathbf{1}_{\widehat{\Omega}}.$$

Theorem 7.1 (Packet perturbation bound)**.** *For $1 \le p < \infty$, interpreted first as an inequality of extended L^p seminorms,*

$$\boxed{\|j - \hat{j}\|_{L^p} \le |a - \hat{a}|\, \mu(\Omega)^{1/p} + |\hat{a}|\, \mu(\Omega \triangle \widehat{\Omega})^{1/p}.}$$

If $\mu(\Omega)$ and $\mu(\Omega \triangle \widehat{\Omega})$ are finite, all terms in this displayed jump bound are finite and it is an ordinary real-valued L^p inequality. For the pointwise supremum, and consequently also the essential L^∞ seminorm,

$$\|j - \hat{j}\|_\infty \le |a - \hat{a}| + |\hat{a}|\, \mathbf{1}_{\Omega \triangle \widehat{\Omega} \neq \emptyset}.$$

Proof. Write

$$a\mathbf{1}_\Omega - \hat{a}\mathbf{1}_{\widehat{\Omega}} = (a - \hat{a})\mathbf{1}_\Omega + \hat{a}(\mathbf{1}_\Omega - \mathbf{1}_{\widehat{\Omega}}).$$

Apply the triangle inequality and use

$$\|\mathbf{1}_\Omega - \mathbf{1}_{\widehat{\Omega}}\|_{L^p} = \mu(\Omega \triangle \widehat{\Omega})^{1/p}.$$

For the supremum estimate, $|\mathbf{1}_\Omega - \mathbf{1}_{\widehat{\Omega}}| \le 1$ pointwise, and this function vanishes everywhere when the symmetric difference is empty. The same pointwise bound also bounds the essential supremum. Nonempty null symmetric differences need not contribute to the essential norm; the stated bound remains valid in that case and need not be sharp. Measurability justifies the L^p triangle inequality and the indicator norm formula. □

If $s, \hat{s}$ are measurable smooth-background models, the same triangle inequality gives, for finite p,

$$\boxed{\|f - (\hat{s} + \hat{j})\|_p \le \|s - \hat{s}\|_p + |a - \hat{a}|\mu(\Omega)^{1/p} + |\hat{a}|\mu(\Omega \triangle \widehat{\Omega})^{1/p}.}$$

This is the correct separation of errors. Detection error is not hidden inside a generic reconstruction score.

Conjecture 7.2 (Stable edge-packet recovery)**.** For specified piecewise-smooth classes, contrast bounds, separation conditions, and noise models, there should exist a multiscale packet estimator whose symmetric-difference error and amplitude error converge at rates controlled independently of the smooth approximation rate. A theorem of this kind would turn the conditional known-edge result into a stable data-driven reconstruction theorem. No universal version is asserted here.

8 One-dimensional numerical study

The one-dimensional signal contains a smooth non-bandlimited background and a positive rectangular packet. Three reconstructions are compared:

(i) global Fourier truncation of the complete signal;

(ii) Fourier truncation of the known smooth packet plus the exact jump packet;

(iii) a two-class estimated packet followed by harmonic background filling, spectral smoothing, and jump-amplitude estimation.

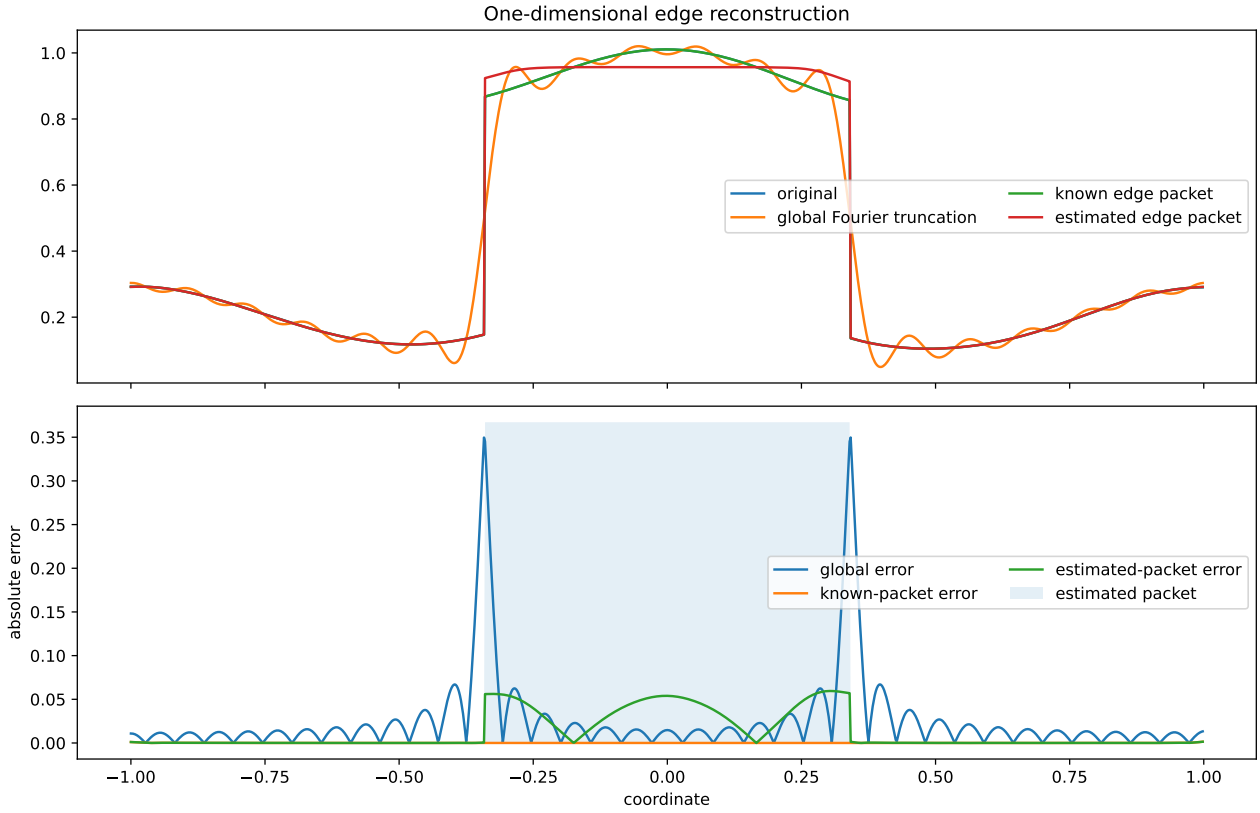


Figure 7. One-dimensional reconstruction and absolute error. The known packet removes the edge from the global spectral approximation. The estimated packet is visibly better than the global reconstruction in this limited test but retains smooth-background estimation error.

Numerical Certificate 8.1 (One-dimensional errors). For 1024 samples on $[-1, 1)$ and Fourier cutoff $m = 18$, the retained frequency indices are $-18, \dots, 18$: 37 bins including the zero-frequency bin. The measured values were

method	RMSE	maximum absolute error
global Fourier truncation	5.4023×10^{-2}	3.4968×10^{-1}
known edge packet	1.3692×10^{-4}	1.4503×10^{-3}
estimated edge packet	2.4029×10^{-2}	5.9530×10^{-2}

The simple estimator recovered the binary mask exactly in this deliberately separated two-class example. That result is a property of this test, not a universal guarantee.

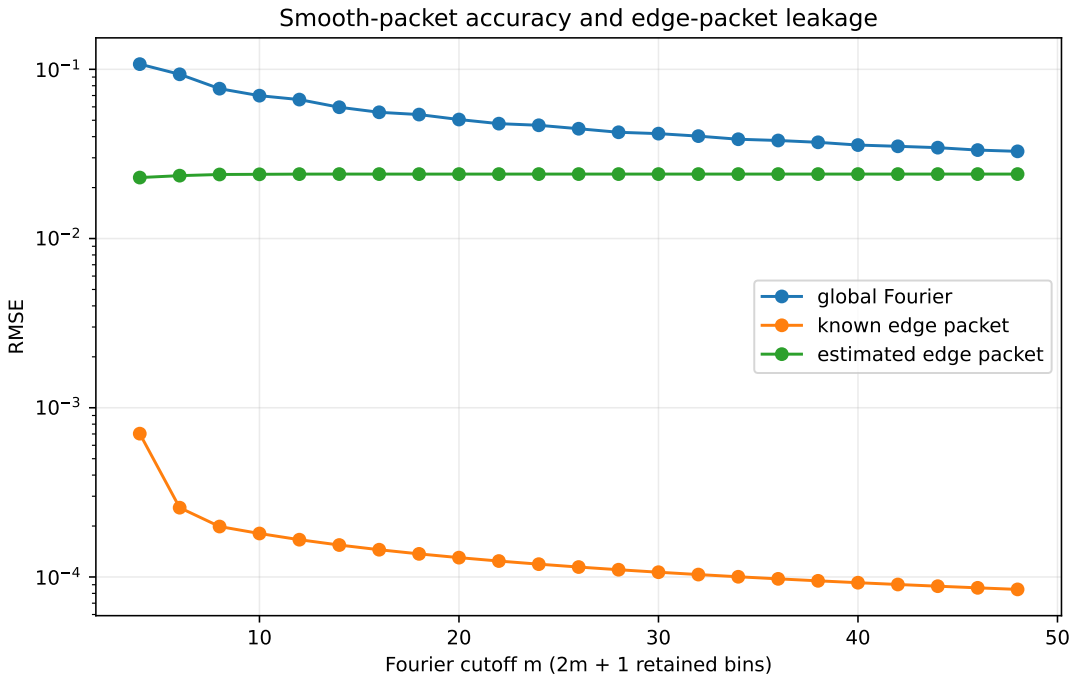


Figure 8. Error as spectral resolution increases. The known packet follows only the smooth approximation error. The estimated reconstruction reaches a floor determined by background and amplitude estimation.

9 Two-dimensional edge packets

The first image consists of a smooth background and one sharp disk. The same three logical levels must remain separate:

(a) the exact theorem using the known decomposition;

(b) a limited estimator designed for a positive-contrast two-class packet;

(c) the open problem of recovering arbitrary edge packets under noise and model ambiguity.

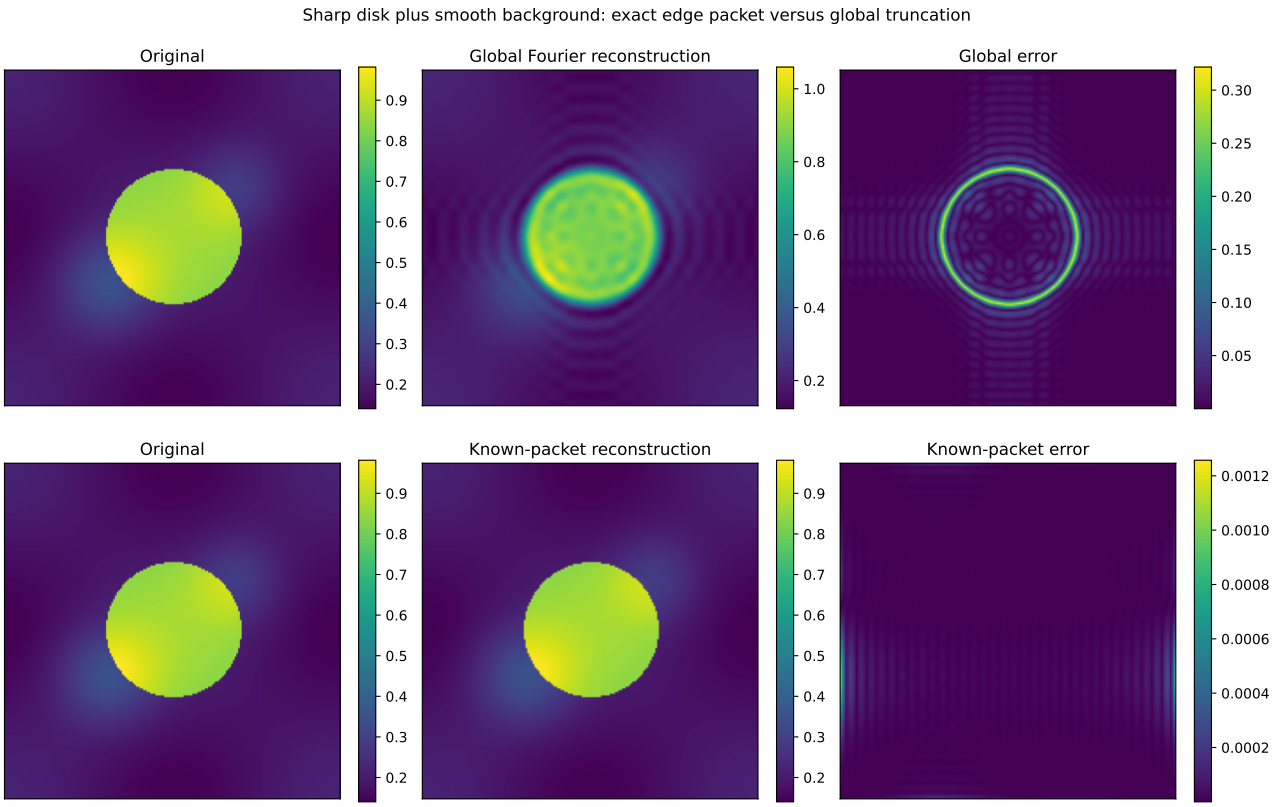


Figure 9. A sharp disk on a smooth background. Global Fourier truncation produces a bright boundary halo and oscillatory interior and exterior error. Retaining the exact edge packet leaves only the smooth-background approximation error.

Numerical Certificate 9.1 (Two-dimensional errors). For the 192×192 disk experiment, a square Fourier mask retains indices $|k_x|, |k_y| \le 16$, or $33^2 = 1089$ bins. The reported errors are

method	full-image RMSE	boundary-band RMSE
global Fourier truncation	3.7643×10^{-2}	1.8541×10^{-1}
known edge packet	6.4752×10^{-5}	1.2709×10^{-5}
estimated edge packet	3.4043×10^{-3}	8.8834×10^{-3}

The mask intersection-over-union was one in this positive-contrast synthetic case. The amplitude was estimated rather than inserted from the generating model.

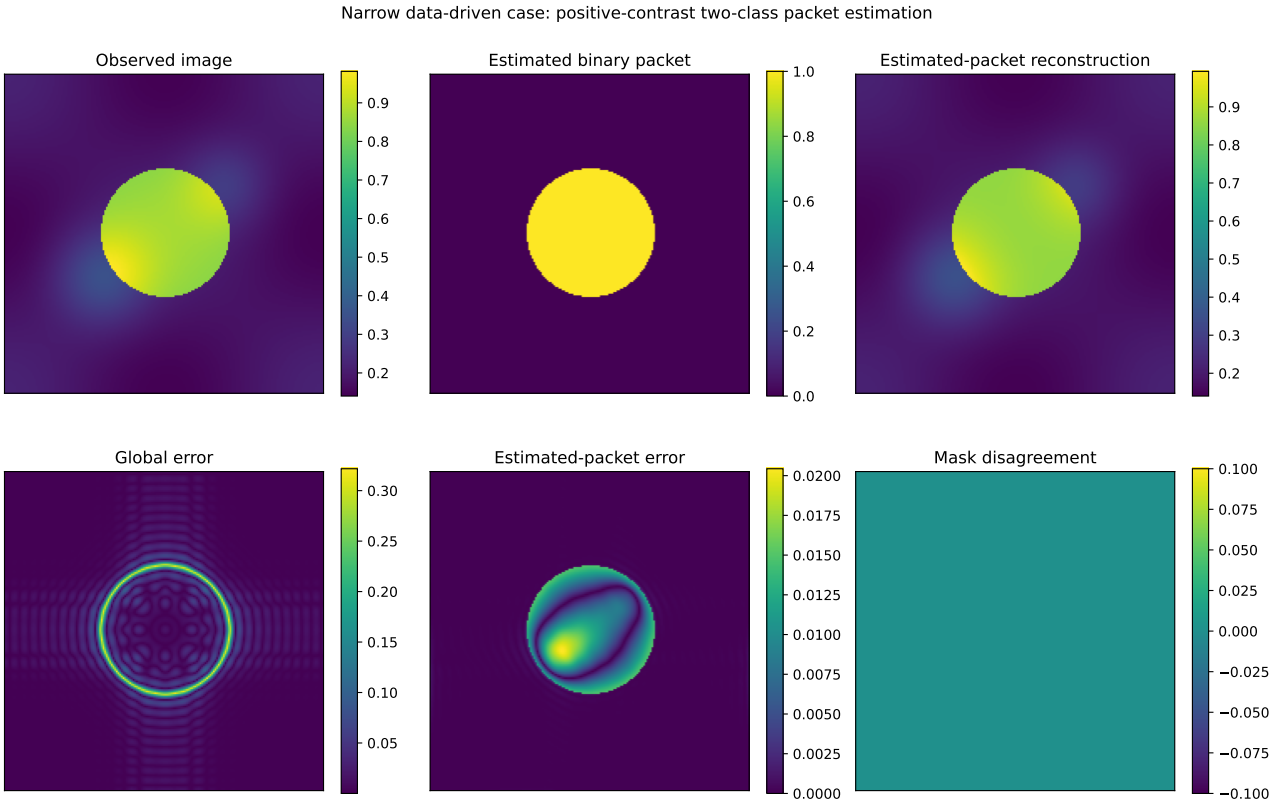


Figure 10. The limited data-driven experiment. The observed image alone is thresholded into two intensity classes, cleaned topologically, harmonically filled, spectrally smoothed, and recombined with an estimated jump.

9.1 Curves, corners, and multiple amplitudes

The exact theorem does not depend on the shape of the known edge packet. The next experiment contains a disk, a square, and a diamond with different jump amplitudes.

Numerical Certificate 9.2 (Multiedge errors). The global reconstruction had RMSE 3.3740×10^{-2} and maximum error 3.2807×10^{-1}. The known-packet reconstruction had only the remaining smooth-background error. The experiment checks the finite implementation of the theorem for a composite packet; it is not a data-driven multiregion segmentation result.

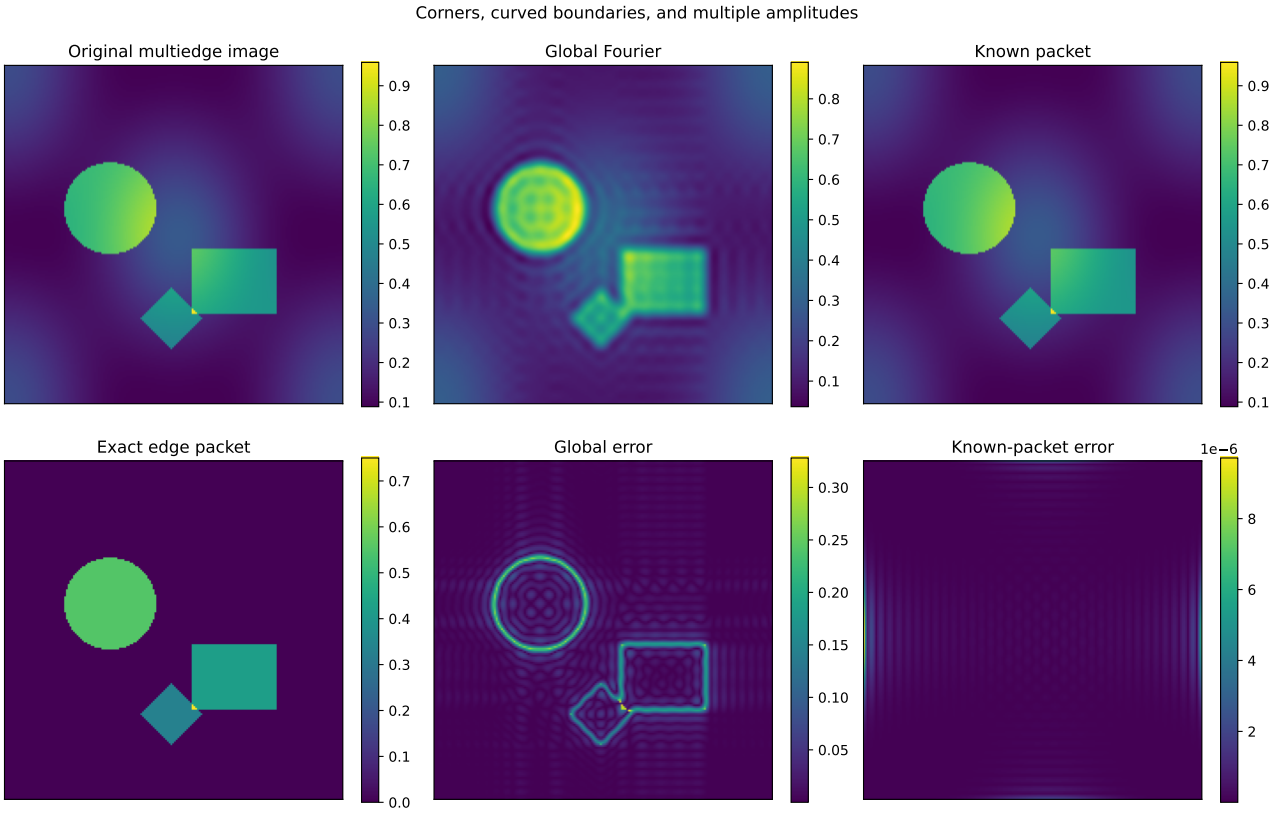


Figure 11. Known-packet stress test with curved boundaries, corners, overlap, and different jump amplitudes. The exact packet is not a binary mask multiplied by one amplitude; it is the complete piecewise packet.

10 Sparse wavelet packets and global Fourier modes

A sharp edge is spatially local but spectrally global. Wavelets often provide a more economical coordinate system once enough localized coefficients are retained. To keep the comparison explicit, the numerical study subtracts the signal mean, keeps the largest coefficients in a fixed depth-five Haar packet basis, and compares them with the same number of largest-magnitude discrete Fourier coefficients. These are coefficient-count budgets, not equal bit-storage budgets. The Fourier reconstruction uses the real part of the inverse transform; for the five reported budgets, the selected nonzero-frequency bins occur in conjugate pairs, so this operation removes only floating-point imaginary residuals.

Table 1. Sparse approximation errors for the one-dimensional test signal.

retained coefficients	Haar packet RMSE	Fourier RMSE
16	1.7999×10^{-1}	6.6522×10^{-2}
32	3.8414×10^{-2}	4.9153×10^{-2}
64	1.6267×10^{-2}	3.8056×10^{-2}
128	1.7387×10^{-3}	2.5631×10^{-2}
256	1.5870×10^{-4}	1.7424×10^{-2}

Boundary 10.1 (Basis selection). This table compares two fixed finite coordinate systems for one signal. It does not prove that Haar packets are optimal, that Fourier is inferior on smooth or oscillatory data, or that a single packet tree is best for every edge geometry. The point is that the seed calculus records both systems with the same analysis, transfer, refinement, and synthesis maps.

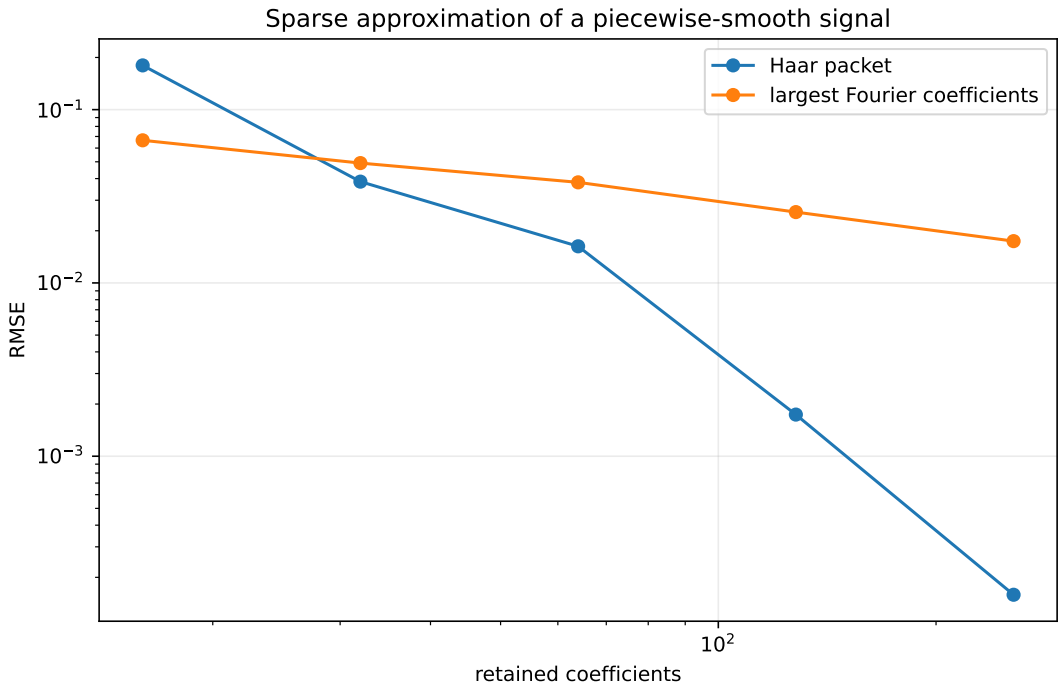


Figure 12. Sparse approximation of the test signal. With very few coefficients the global Fourier basis is initially better. After the edge packets are resolved, the Haar packet error decays much faster in this example.

11 Finite adaptive packet trees

> **Three levels of a finite tree decision**
>
> First choose a complete pruning, so every terminal path is represented once and synthesis remains exact. Then assign a finite objective to those feasible choices. Additivity permits the local dynamic recursion. Finally, a positive cost gap protects the selected pruning against a declared perturbation envelope. Each step uses a different hypothesis.

The preceding sparse comparison used one fixed depth-five packet basis. A refinement tree permits a stronger choice: different branches may stop at different depths while the selected packets still form one complete coordinate system.

Definition 11.1 (Complete packet pruning)**.** Let $\mathcal{T}$ be a finite rooted refinement tree. Every node v carries a projector P_v, the root satisfies $P_\emptyset = I$, and every internal node satisfies

$$P_v = \sum_{u \in \mathrm{ch}(v)} P_u, \qquad P_u P_w = 0 \quad (u \neq w \text{ in } \mathrm{ch}(v)).$$

A set Λ of nodes is a complete pruning if it is an antichain and every root-to-terminal path meets Λ exactly once.

Theorem 11.2 (Exact synthesis from every complete pruning). *For every complete pruning Λ,*

$$\boxed{\sum_{v\in\Lambda} P_v = I,} \qquad \boxed{x = \sum_{v\in\Lambda} P_v x.}$$

Thus changing the selected tree changes the coordinates but does not introduce reconstruction error.

Proof. Starting from the root identity $P_\emptyset = I$, replace every unselected internal node by the exact sum of its children. If a complete pruning contains the root it contains no other node. Otherwise its restriction to each child subtree is itself a complete pruning: every terminal path through that child must be met exactly once. Induction on the finite tree therefore justifies the substitution and its termination precisely at Λ. Child subtrees have distinct node addresses, so their selected-node sets form a disjoint union. The sum identity uses only root identity and parent-to-child conservation; sibling orthogonality gives the additional interpretation as nonoverlapping projector packets. Applying the resulting identity to x gives the synthesis formula. □

Let y denote the observed data. For a complete pruning Λ, consider any finite criterion

$$J_y(\Lambda) = R_y(\Lambda) + \eta L_y(\Lambda) + \tau K(\Lambda),$$

where R_y is a representation cost, L_y is a cross-packet leakage cost, and K is a tree-complexity penalty. Here R_y, L_y, K take finite real values, and η, τ are fixed real weights (usually nonnegative in applications). No additivity is needed for the first theorem.

Theorem 11.3 (Finite globally optimal stable selector). *Let $\mathfrak{P}(\mathcal{T})$ be the finite set of complete prunings of $\mathcal{T}$.*

(i) A global minimizer

$$\Lambda_y^* \in \operatorname*{argmin}_{\Lambda\in\mathfrak{P}(\mathcal{T})} J_y(\Lambda)$$

always exists.

(ii) If the minimizer is unique and at least one competing pruning exists, its gap

$$\Gamma_y = \min_{\Lambda\neq\Lambda_y^*} \left(J_y(\Lambda) - J_y(\Lambda_y^*)\right)$$

is attained and strictly positive. If the pruning set is a singleton, its only element minimizes every criterion; no real-valued minimum over an empty competitor set is introduced.

(iii) In the case with competitors, if new data y' satisfy

$$\sup_{\Lambda\in\mathfrak{P}(\mathcal{T})} |J_{y'}(\Lambda) - J_y(\Lambda)| < \frac{\Gamma_y}{2},$$

then $\Lambda_{y'}^* = \Lambda_y^*$.

(iv) Every selected minimizer preserves the exact synthesis identity of the preceding theorem.

Proof. The root-only pruning exists, and every pruning is a subset of the finite node set, so the feasible set is nonempty and finite. Thus the minimum is attained. If competitors exist, their finitely many differences from a unique optimum are strictly positive, so their minimum is positive and is achieved by a competitor. In the singleton case there is no alternative selector under any objective change. In the remaining case, for any competing pruning $\Lambda \neq \Lambda_y^*$,

$$\begin{aligned} J_{y'}(\Lambda) - J_{y'}(\Lambda_y^*) &\geq J_y(\Lambda) - J_y(\Lambda_y^*) - 2 \sup_{\Xi} |J_{y'}(\Xi) - J_y(\Xi)| \\ &> \Gamma_y - \Gamma_y = 0. \end{aligned}$$

Hence the same pruning remains uniquely optimal. Exact synthesis depends only on completeness of the pruning, not on the cost used to select it. □

For tree-local costs, the optimum can be found without enumerating all prunings.

Theorem 11.4 (Dynamic-programming best packet basis)**.** *Suppose*

$$J_y(\Lambda) = \sum_{v \in \Lambda} c_v(y).$$

For a node v, define recursively

$$V_y(v) = \begin{cases} c_v(y), & v \text{ terminal}, \\ \min\left\{ c_v(y), \sum_{u \in \mathrm{ch}(v)} V_y(u) \right\}, & v \text{ internal}. \end{cases}$$

Stop at v when $c_v(y) \leq \sum_u V_y(u)$, including equality; refine otherwise. This deterministic rule produces a globally optimal complete pruning. With the node costs supplied and child values cached, the evaluator uses one comparison per internal node, one visit per node, and at most $|\mathcal{T}| - 1$ additions. Its arithmetic-and-visit count is therefore at most $3|\mathcal{T}|$. This is a unit-cost statement about the specified evaluator; it excludes evaluation of the local costs, bit complexity of scalar arithmetic, and materialization or sorting of packet-address strings.

Proof. Proceed upward from the terminal nodes. Every complete pruning below an internal node v has exactly two possible forms: it either stops at v, with cost $c_v(y)$, or it refines and is the union of complete child prunings, whose minimum total cost is the sum of the already computed child minima. The recursion therefore gives the exact minimum on every subtree, in particular at the root. This characterization also proves both directions of the correspondence between recursive cuts and complete covering antichains, for arbitrary positive finite branching, including unary branches. Summing cached child values charges at most one addition per child edge; a finite rooted tree has $|\mathcal{T}| - 1$ such edges. The number of internal nodes is at most $|\mathcal{T}|$, which gives the stated work bound. Ties do not affect optimality, but the stop-on-ties rule makes the selected pruning unambiguous. □

Corollary 11.5 (Local perturbation certificate)**.** *Assume*

$$|c_v(y') - c_v(y)| \leq \varepsilon_v.$$

Define

$$E(v) = \begin{cases} \varepsilon_v, & v \text{ terminal}, \\ \max\left\{ \varepsilon_v, \sum_{u \in \mathrm{ch}(v)} E(u) \right\}, & v \text{ internal}. \end{cases}$$

For the complete prunings $\mathfrak{P}_v$ below v, the envelope is exactly

$$E(v) = \max_{\Lambda \in \mathfrak{P}_v} \sum_{a \in \Lambda} \varepsilon_a.$$

The maximum is attained. Every complete-pruning cost changes by at most $E(\emptyset)$, and the two globally optimal values differ by at most this quantity. Consequently, for a unique optimum with competitors,

$$\boxed{\Gamma_y > 2E(\emptyset)}$$

is a deterministic certificate that the globally optimal pruning is unchanged. A singleton pruning set is stable without a gap condition. Assume the random node costs and the joint local-error event are measurable. If a noise model supplies all *local bounds simultaneously on one event of probability at least $1-\delta$, and the displayed strict-gap condition holds, the same selector is recovered with probability at least $1-\delta$. Individual nodewise probabilities alone do not give this joint confidence without an additional argument, such as a union bound.*

Proof. For any pruning of the subtree rooted at v, either v itself is selected, producing perturbation at most ε_v, or the pruning is the disjoint union of child prunings, producing perturbation at most the sum of the child envelopes. The same decomposition applied to the nonnegative weights ε_a proves equality with the maximum weight: at each node choose either the stop option or a maximizing pruning in each child, whichever gives the larger total. Finiteness ensures these choices attain their maxima. Evaluating each cost at a minimizer of the other cost bounds the difference of the two optimal values by the uniform envelope. The selector statement follows from the strict-gap theorem. The finite deterministic comparisons defining the selector make its preservation event measurable when the random node costs are measurable. The joint local-error event is contained in the selector-preservation event, so monotonicity of probability proves the probabilistic assertion. □

Numerical Certificate 11.6 (Adaptive-tree optimum). For the depth-five example, the complete binary tree has $458{,}330$ admissible prunings. Dynamic programming and exhaustive enumeration returned the same minimum with residual 0. The selected pruning was

$$\{000, 001, 0100, 0101, 011, 1\},$$

and mixed-depth synthesis reconstructed the signal with maximum residual 8.88×10^{-16}. The optimum gap was 3.1909×10^{-4}, while twice the declared perturbation envelope was 6.4×10^{-5}, so the finite selector is certified stable.

Boundary 11.7 (Finite versus asymptotic selection). The theorem resolves the finite adaptive-tree existence, exact-synthesis, global-optimality, and margin-stability problem. It does not by itself prove minimax rates, statistical consistency on an infinite tree, or a universal choice of representation and leakage costs for every signal class.

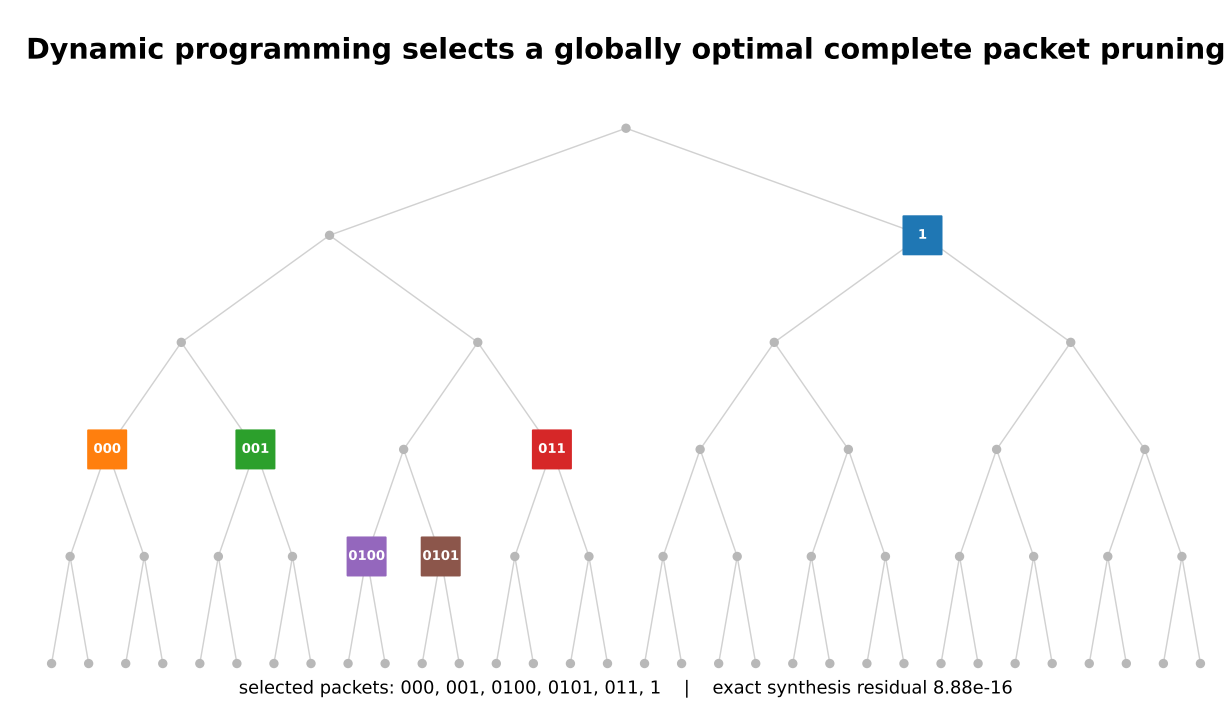


Figure 13. A globally optimal mixed-depth Haar packet pruning. The selected antichain covers the full tree, so its synthesis is exact even though different branches stop at different depths.

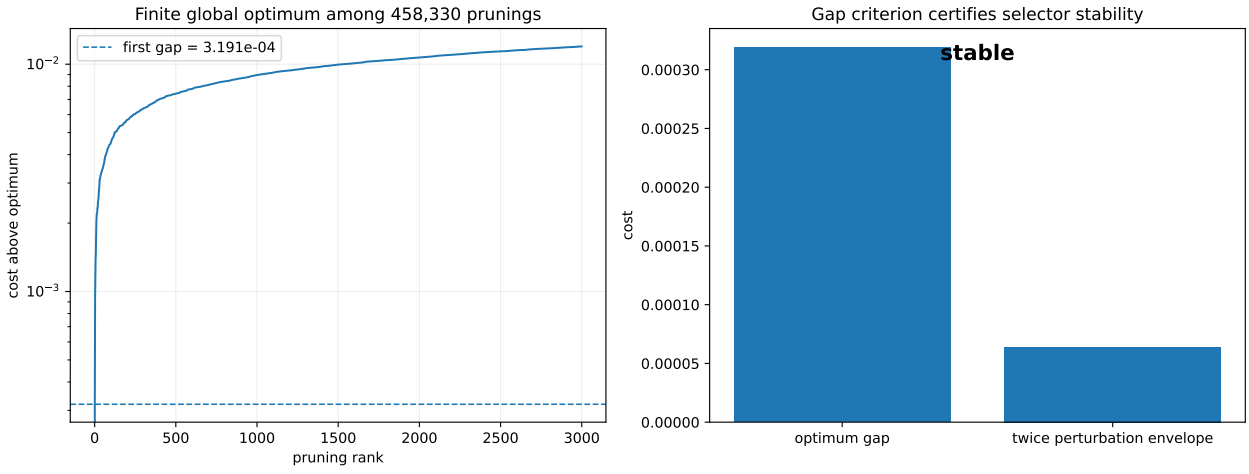


Figure 14. The dynamic-programming optimum agrees with exhaustive enumeration. A positive gap larger than twice the declared perturbation envelope certifies that the selected tree is stable.

12 Nonlinear signal packets

Linear time invariance is not required for exact packet coordinates. Let A and B be formal power series over a commutative coefficient ring (in particular $\mathbb{C}$). Set

$$A(z) = \sum_{n \geq 0} a_n z^n, \qquad A_i = P_{N,i} A.$$

All phase indices range from 0 to $N-1$. For another representation $B(z)$, multiplication gives a nonlinear or bilinear interaction.

Theorem 12.1 (Cyclic product law)**.**

$$\boxed{P_{N,k}(AB) = \sum_{i+j \equiv k \,(\mathrm{mod}\, N)} A_i B_j.}$$

For $q \in \mathbb{N}$, the qth-power identity is

$$P_{N,k}(A^q) = \sum_{i_1 + \cdots + i_q \equiv k} A_{i_1} \cdots A_{i_q}.$$

Proof. Every coefficient in $A_i B_j$ has degree congruent to $i + j$ modulo N. At any fixed degree n, the Cauchy coefficient sum is finite. Sorting these terms by the residues of their two indices gives the first identity coefficient by coefficient. For the power identity, use induction on q and the finite product law. At $q = 0$, the index set contains the single empty tuple, its product is 1, and its residue sum is 0; hence the right side is 1 for $k = 0$ and 0 otherwise, as required. No convergence is needed for these formal identities. For analytic power series, the same identities hold wherever the series are absolutely convergent and their Cauchy products may be evaluated. □

For a finite nonlinear shift operator

$$F(x)[n] = x[n] + \alpha x[n] x[n-1],$$

the exact packet coordinates are simply

$$F_r((x_s)_s) = P_{N,r} F \left(\sum_s P_{N,s} x \right).$$

Analysis followed by this packet system and synthesis reproduces the direct nonlinear output exactly. The numerical residual in the companion implementation was zero to machine representation.

13 Smith coordinates as cyclic signal coordinates

Let $Z_0 > 0$ be a reference impedance and

$$z = \frac{Z}{Z_0} = r + \mathrm{i}x.$$

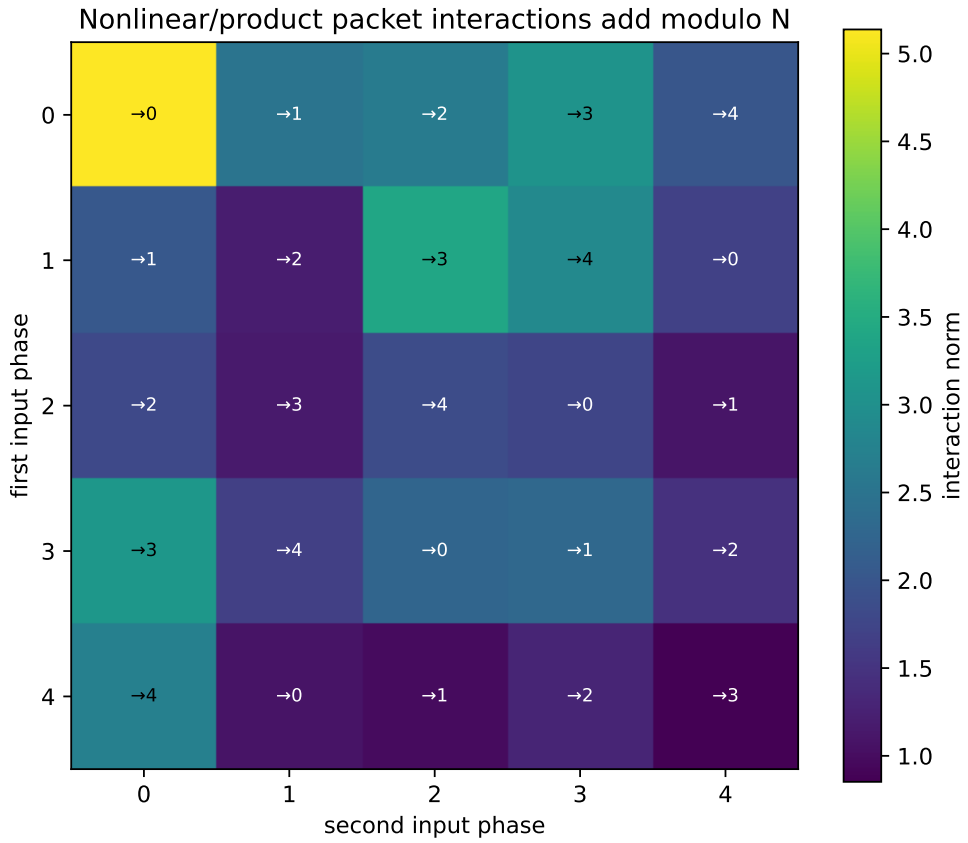


Figure 15. Norms of pairwise product interactions for five residue phases. The label in each cell gives the output phase $(i + j) \bmod 5$.

The reflection coefficient is

$$\boxed{\Gamma = \frac{z-1}{z+1}, \qquad z = \frac{1+\Gamma}{1-\Gamma}.}$$

Classical Input 13.1 (Cayley geometry). The map sends the finite passive half-plane $r \geq 0$ onto the closed unit disk with $\Gamma = 1$ omitted. Adjoining the point at infinity in impedance adds that missing boundary point; the open right half-plane maps conformally onto the open disk. Constant resistance and reactance become the familiar Smith circles. This conformal geometry is classical and is not replaced by polyphase refinement.

Writing $\Gamma = u + \mathrm{i}v$, the grid equations are

$$\left(u - \frac{r}{1+r}\right)^2 + v^2 = \frac{1}{(1+r)^2},$$

and, for $x \neq 0$,

$$(u-1)^2 + \left(v - \frac{1}{x}\right)^2 = \frac{1}{x^2}.$$

Fix

$$\omega_N = e^{2\pi \mathrm{i}/N}$$

and rotate the reflection coefficient by

$$R_{N,k}(\Gamma) = \omega_N^k \Gamma.$$

Theorem 13.2 (Polyphase Möbius action). *Regard normalized impedance as the projective line $\mathbb{P}^1(\mathbb{C}) = \mathbb{C} \cup \{\infty\}$. For $N \geq 1$, the pullback is a globally defined projective action. In the finite chart, wherever the denominator is nonzero, it is*

$$\boxed{T_{N,k}(z) = \frac{(1+\omega_N^k)z + (1-\omega_N^k)}{(1-\omega_N^k)z + (1+\omega_N^k)}.}$$

As maps on $\mathbb{P}^1(\mathbb{C})$ it satisfies

$$T_{N,k} \circ T_{N,\ell} = T_{N,k+\ell \,(\mathrm{mod}\, N)}.$$

Proof. Let $C(z) = (z-1)/(z+1)$. Then

$$T_{N,k} = C^{-1} \circ R_{N,k} \circ C.$$

For a division-free construction, represent a point by a nonzero pair $[u : v]$, identifying $[cu : cv] = [u : v]$ for $c \neq 0$. With $w = \omega_N^k$, use the matrix

$$A(w) = \frac{1}{2}\begin{pmatrix} 1+w & 1-w \\ 1-w & 1+w \end{pmatrix}.$$

It has determinant $w \neq 0$, preserves nonzero pairs, and commutes with rescaling, so it induces a projective map. Direct multiplication gives $A(w)A(w') = A(ww')$ and $A(1) = I$. Since $\omega_N^N = 1$, this proves the cyclic composition law modulo N. The Cayley coordinate of $[u : v]$ is $[u - v : u + v]$, and applying $A(w)$ changes this pair to $[w(u-v) : u+v]$. This proves the conjugacy also at poles. For $[z : 1]$, taking the coordinate ratio gives the displayed finite-chart formula. □

Corollary 13.3 (Impedance–admittance is the two-phase split). *For $N = 2$ and finite $z \neq 0$,*

$$\boxed{T_{2,1}(z) = z^{-1}.}$$

On the full projective line it exchanges 0 and ∞. Thus a half-turn of the reflection disk exchanges normalized impedance and admittance.

Proof. $\omega_2 = \exp(\pi \mathrm{i}) = -1$, so $A(\omega_2)[u : v] = [v : u]$. The finite ratio is $1/z$ when $z \neq 0$; the coordinate swap also gives $[0 : 1] \leftrightarrow [1 : 0]$. No ordinary division by zero is used to represent infinity. □

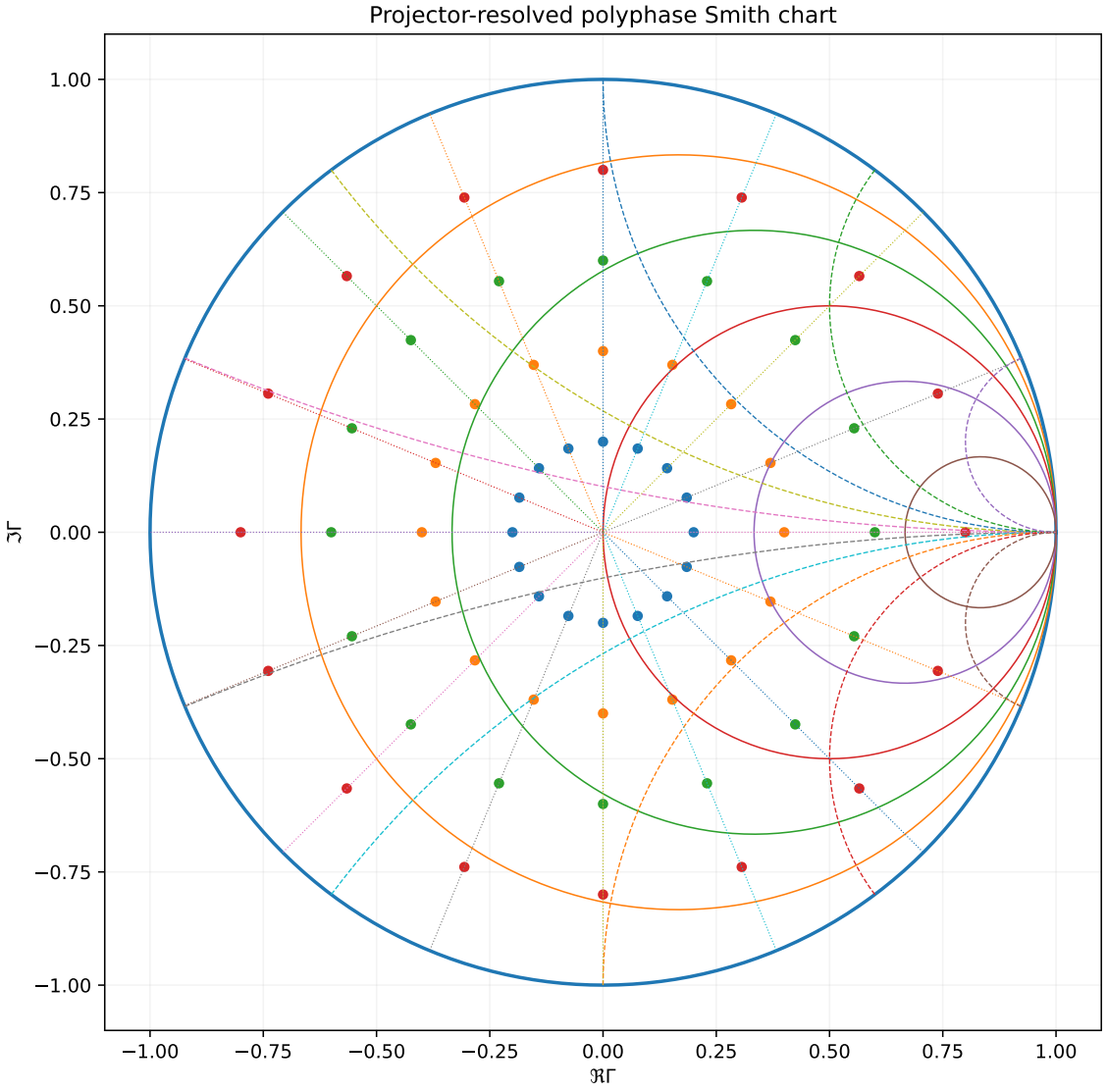


Figure 16. The classical Smith grid equipped with sixteen exact phase rays and four radial seed orbits. The Cayley transform creates the chart; the projector calculus supplies the nested cyclic coordinate system.

13.1 Radial seeds and physical phase

For $0 \leq \rho < 1$ and angle θ,

$$\Gamma = \rho e^{\mathrm{i}\theta}$$

gives

$$z(\rho,\theta)=\frac{1+\rho e^{\mathrm{i}\theta}}{1-\rho e^{\mathrm{i}\theta}},$$

with

$$r(\rho,\theta)=\frac{1-\rho^2}{1-2\rho\cos\theta+\rho^2},\qquad x(\rho,\theta)=\frac{2\rho\sin\theta}{1-2\rho\cos\theta+\rho^2}.$$

A fixed ρ is a constant-mismatch circle. Refining N increases angular resolution without changing ρ.

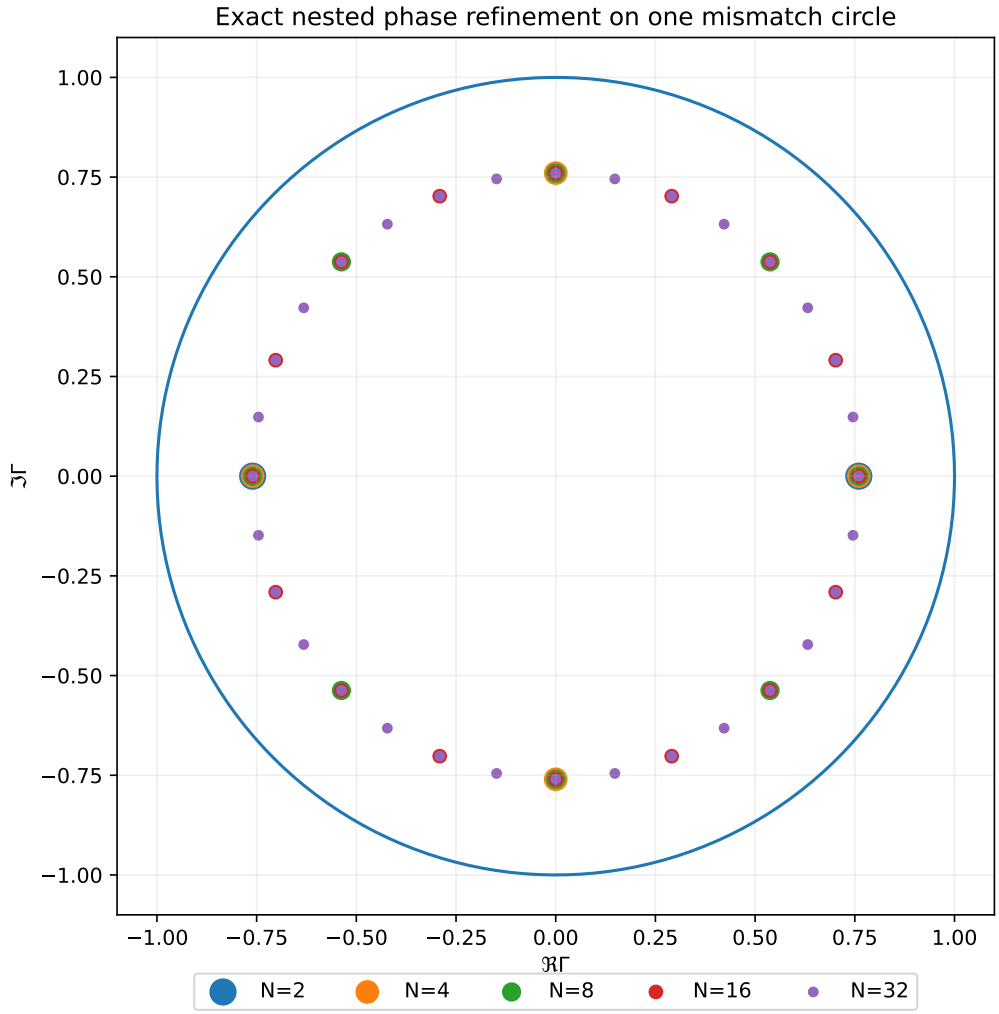


Figure 17. The same reflection circle at phase orders $2, 4, 8, 16, 32$. Each coarse phase ray appears in every finer grid whose order is a multiple of its order. The exact residue-projector refinement law concerns coefficient packets, not sums of impedance points.

For a lossless transmission line,

$$\Gamma_{\mathrm{in}}=\Gamma_L e^{-2\mathrm{i}\beta\ell}.$$

One N-phase step corresponds to a line-length increment $\lambda/(2N)$, up to the chosen orientation convention. Hence the phase address has a direct electrical interpretation.

14 Dyadic–odd phase factorization and boundary weighting

Write

$$N = 2^s M, \qquad M \text{ odd}.$$

The cyclic index splits by the Chinese remainder theorem:

$$\mathbb{Z}/N\mathbb{Z} \cong \mathbb{Z}/2^s\mathbb{Z} \times \mathbb{Z}/M\mathbb{Z}.$$

Proposition 14.1 (Dyadic–odd packet factorization)**.** *After identifying the residue labels by the Chinese remainder map, the phase projector factors as*

$$\boxed{P_{N,j} = P_{2^s,j_2} P_{M,j_o}.}$$

Proof. The two congruence conditions are independent because 2^s and M are coprime. Their indicator functions multiply to the indicator of the unique residue class modulo N satisfying both. □

The first dyadic step is exceptional in Smith coordinates because it is the inversion $z \mapsto z^{-1}$. Higher dyadic levels refine the open/short duality into quarter-, eighth-, and finer phase sectors.

Away from its pole $\Gamma = 1$, the inverse Cayley map has derivative

$$\frac{dz}{d\Gamma} = \frac{2}{(1-\Gamma)^2},$$

while normalized admittance has derivative proportional to $(1+\Gamma)^{-2}$. Away from $\Gamma = \pm 1$, this motivates the symmetric sensitivity

$$\boxed{w_{\text{Smith}}(\Gamma) = \frac{1}{|1-\Gamma|^2} + \frac{1}{|1+\Gamma|^2}.}$$

Boundary 14.2 (Weighted refinement). The sensitivity formula follows directly from the exact coordinate derivatives. Using it to choose an optimal adaptive grid, interpolation rule, or measurement design is a separate numerical problem. The release visualizes the weight but does not prove optimality.

15 Boundary-localized error and claim control

The strongest visual distinction between global Fourier reconstruction and exact packet retention is seen in a band around the discontinuity.

Conjecture 15.1 (Edge-packet approximation class)**.** There should exist natural function spaces in which a signal is represented as

$$f = s + \sum_q a_q \mathbf{1}_{\Omega_q},$$

with separate norms for smooth approximation, boundary geometry, packet amplitude, and packet identification. A projector-resolved approximation theory on such spaces should yield rates that do not mix smooth truncation error with discontinuity-location error.

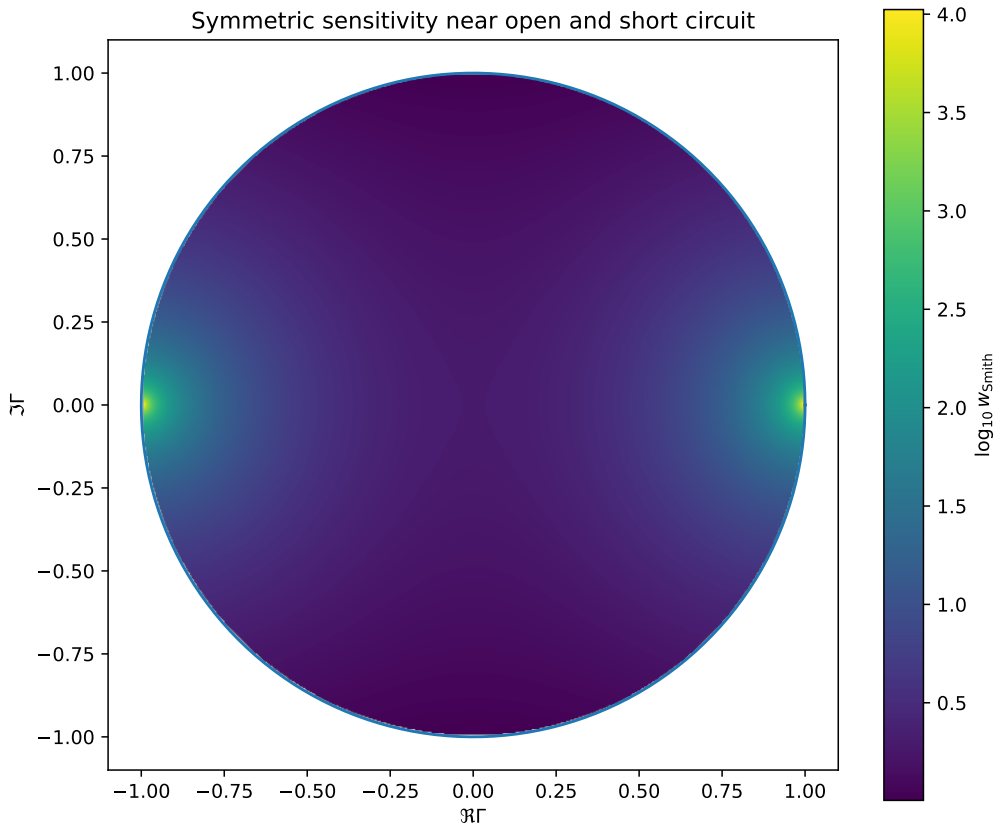


Figure 18. The proposed symmetric refinement weight becomes large near the open- and short-circuit boundary points. It is a condition-based adaptive coordinate, not an asserted optimal sampling law.

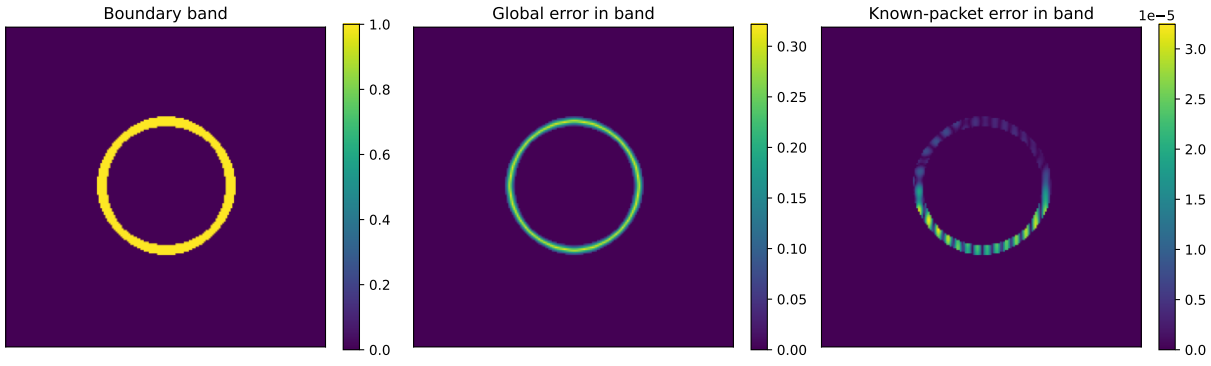


Figure 19. Error restricted to a narrow boundary band. Global truncation concentrates large error on the jump. The known-packet reconstruction has only the small smooth-packet error in the same band.

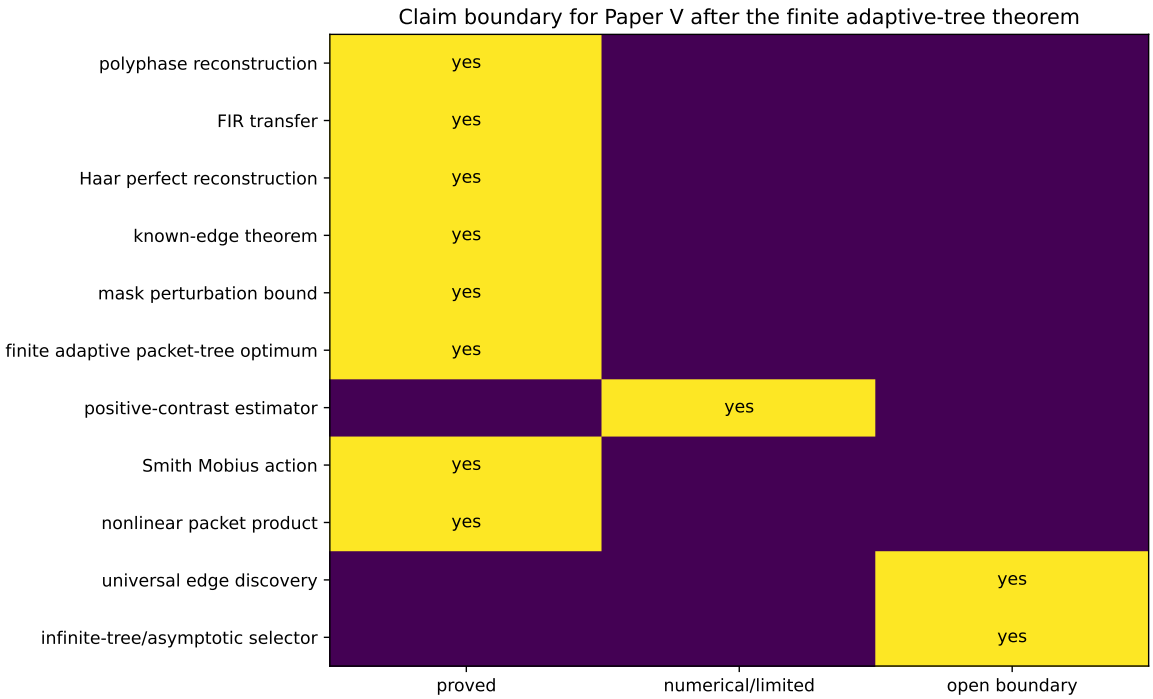


Figure 20. Proof and claim boundary. Finite adaptive-tree selection is now proved; the remaining open rows concern universal recovery and infinite-tree or asymptotic selection.

16 Implementation and reproducibility

The companion package is organized by mathematical layer:

Table 2. Numerical companion modules.

module	implemented content
`polyphase.py`	residue projectors, analysis/synthesis, refinement, exact FIR transfer kernels, polyphase convolution
`filterbanks.py`	Haar analysis/synthesis, complete Haar packet trees, energy accounting, predict–update lifting
`adaptive.py`	complete-pruning enumeration, exact mixed-depth synthesis, dynamic-programming optimization, and stability certificates
`edges.py`	one- and two-dimensional Fourier truncation, known-packet reconstruction, narrow two-class estimators, harmonic filling, error metrics
`smith.py`	Cayley coordinates, cyclic Möbius action, Smith circles, sensitivity weight, coefficient projectors
`nonlinear.py`	coefficient packets, cyclic product convolution, nonlinear shifted packet reconstruction
`experiments.py`	all machine-readable numerical certificates and tabular summaries
`visuals.py`	the eighteen figure pairs used in the paper

The September 2026 release records recovery and rerunning of the original companion source: its 33 tests passed, and all 18 figure pairs and numerical tables were regenerated. The Lean package con-

tributes 20 independent exact-model tests and 16 tests of the verifier itself; these account for another 36 passing tests. The exact-model suites count 305,933 assertions. These counts are separate from the 225 Lean theorem targets.

All numerical computations are CPU-based. Floating-point residuals measure finite implementations and may vary at rounding level with the scientific libraries. The universal mathematical statements are supported by the Lean proofs; the Python modules are not compiled or verified by Lean. The adaptive-tree certificate uses floating-point costs and an exhaustive finite comparison, so its displayed gap is numerical evidence rather than an interval-arithmetic proof about those computed costs. Appendix D explains the verification boundary.

Numerical Certificate 16.1 (Finite numerical residuals). The largest recorded residuals were

identity	residual
polyphase reconstruction	0
nested refinement	0
polyphase convolution	4.44×10^{-16}
Haar reconstruction	8.88×10^{-16}
wavelet-packet reconstruction	2.22×10^{-15}
adaptive-tree optimum versus exhaustive search	0
adaptive mixed-depth synthesis	8.88×10^{-16}
lifting reconstruction	4.44×10^{-16}
Smith rotation conjugacy	3.34×10^{-16}
Smith impedance–admittance duality	0
nonlinear product-packet reconstruction	1.33×10^{-15}
nonlinear shifted-filter reconstruction	0

The Haar and wavelet energy residuals were 5.68×10^{-14} and 2.27×10^{-13}, respectively.

17 Conclusions

The signal realization makes the seed, address, packet, transfer, refinement, and synthesis operations concrete. The objects and laws can be read directly:

$$\begin{aligned}
\text{seed} &= \delta_0, \\
\text{address} &= S^n, \\
\text{packet} &= P_{N,r}x, \\
\text{transfer} &= P_{N,k}HP_{N,s}, \\
\text{refinement} &= P_{N,r} = \sum_{s \succ r} P_{M,s}, \\
\text{synthesis} &= \sum_r P_{N,r}x, \\
\text{nonlinearity} &= P_{N,r}F\left(\sum_s P_{N,s}x\right).
\end{aligned}$$

Filter banks, wavelet packets, adaptive complete prunings, edge packets, and Smith coordinates inhabit the same operator grammar, but their claims differ. Polyphase and filter-bank identities are exact.

Wavelet perfect reconstruction is exact. The known-edge theorem is exact conditional on the decomposition. Estimated-edge performance depends on a detection model. The Smith chart remains the classical Cayley geometry equipped with an exact cyclic refinement algebra. Keeping those distinctions explicit is part of the calculus, not an editorial afterthought.

The next paper in the series turns from discrete signal transfer to semigroups, resolvents, conditioning, stochastic evolution, fractional powers, and PDE kernels.

A Algorithm statements

A.1 Exact polyphase filtering

Given x, h, and N:

1. Form $x_s[n] = x[Nn + s]$ for $0 \le s < N$.
2. Form every transfer kernel $h_{ks}[m] = h[Nm + k - s]$.
3. Compute
$$y_k[n] = \sum_s \sum_m h_{ks}[m] x_s[n - m].$$
4. Interleave the y_k channels.

The algorithm is algebraically identical to direct convolution; its purpose is to expose independent and interacting packets for block computation and refinement.

A.2 Conditional known-edge reconstruction

Given a decomposition $f = s + j$:

1. Apply the selected smooth approximation Q_m to s only.
2. Retain j exactly.
3. Return $Q_m s + j$.

The error certificate is $\|s - Q_m s\|$.

A.3 Limited positive-contrast estimator

The included finite estimator does the following:

1. Split the observed values into two classes by an Otsu threshold.
2. Keep coherent connected components and fill holes.
3. Harmonically fill the selected packet to estimate the missing background.
4. Smooth the filled background spectrally.
5. Estimate one packet amplitude by a robust median residual.

6. Recombine the estimated smooth and edge packets.

This procedure is useful for the supplied separated synthetic case. It assumes a positive-contrast two-class packet and is not promoted to a general edge theorem.

B Numerical record

Table 3. Main edge-study measurements.

case	global RMSE	known-packet RMSE	estimated RMSE
1D rectangular packet	5.4023×10^{-2}	1.3692×10^{-4}	2.4029×10^{-2}
2D disk packet	3.7643×10^{-2}	6.4752×10^{-5}	3.4043×10^{-3}
2D multiedge packet	3.3740×10^{-2}	known composite packet only	

Table 4. Main software artifacts.

artifact	purpose
`results/numerical_results.json`	complete machine-readable certificate record
`tables/numerical_summary.csv`	flat summary of errors and residuals
`tables/sparse_representation.csv`	wavelet/Fourier coefficient study
`tests/`	automated finite identity and estimator tests
`figures/`	PNG and vector-PDF figure pairs
`VERIFY_PAPER.py`	combined manuscript, numerical, and Lean checks

C Notation crosswalk

Table 5. Notation crosswalk.

common symbol	**signal realization**	**interpretation**
s	δ_0	primitive signal seed
A_n	S^n	address operator
$P_{N,r}$	residue mask	phase packet projector
T_{ks}	$P_{N,k}HP_{N,s}$	input-to-output phase transfer
E, R	analysis and synthesis matrices	coordinate conversion and reconstruction
$W(\gamma)$	filter or path weight	refinement or implementation cost
$\Delta(F)$	coarse/fine signal defect	aliasing, leakage, or estimator inconsistency
$\mathrm{Hol}(\gamma)$	closed phase transfer	cycle consistency in a network
Γ	reflection coefficient	Smith-disk coordinate

D Formalization and reproducibility record

D.1 What has been checked

The preserved Part I manuscript has twenty theorem-like statements: Theorems, Propositions, and Corollaries, counted together. The Lean project contains 225 explicit supporting theorem targets in 23 proof modules. All twenty statements have an explicit scope row and principal declaration targets. The September 2026 release records a successful build and axiom audit with warnings treated as errors. No fresh Lean build is asserted for this October final edition. The audit inspected all 827 declarations in the project namespace, including definitions and automatically generated declarations. The latter is an implementation census, not a count of 827 mathematical theorems.

The accepted axiom dependencies are `propext`, `Classical.choice`, and `Quot.sound`. No admitted proof or additional project axiom is permitted. The verifier checks the imported modules, registered theorem inventory, dependency pins, source hashes, and coverage of the twenty-row scope contract. Its successful status is `LEAN_CHECKS_PASS`. The correspondence between a mathematical sentence in this PDF and its Lean type is a manual mathematical review, not an automated semantic-equivalence test.

The source-level formalization was completed before this manuscript revision. The revision integrates those checked hypotheses and conclusions into the paper itself; it does not increase the Lean theorem count by counting editorial changes as new proofs. Eleven foundational formal-power-series proofs in `CyclicSeries` are adaptations of Paper IV and are identified as such in the provenance record.

D.2 Result-by-result correspondence

The following table summarizes the reviewed statement boundary. Full qualified declaration names, source locations, and supplementary targets appear in `MANUSCRIPT_TARGET_MAP.md` and the machine-readable scope contract. Every row below has supporting kernel-checked declarations; numerical certificates, classical-input paragraphs, remarks, and conjectures are not additional theorem rows.

Table 6. The twenty manuscript results and their Lean statement scopes.

Result	Principal modules	Checked mathematical content
1.1	HilbertPackets	Complex ℓ^2 impulse expansion, finite-support identity, unitary shifts, and closed shift-generated span.
2.1	HilbertPackets	Bounded self-adjoint residue projectors, pairwise annihilation, completeness, and orthogonal ranges.
2.2	IntegerPolyphase; HilbertPackets	Signed quotient/remainder coordinates, both inverse identities, and the joint Hilbert norm of the channels.
2.3	HilbertPackets	Literal bounded-projector refinement for positive divisible moduli.
3.1	FIRTransfer; ZTransform	Finite-support tap reindexing for all bilateral inputs; numerical channel transforms under weighted absolute summability.
4.1	FilterBank; FiniteTransforms	Finite Laurent/FIR bank composition, faithful action on sequences, gain-delay reconstruction criterion, and the Nd original-sample delay.
4.2	HaarChannels; HaarHilbert	Literal even/odd input samples, normalized complex low/detail channels, and ℓ^2 energy equality.
4.3	Lifting; FiniteTransforms	Predict/update inverse maps, determinant one, and both flat finite-signal inverse identities.

Result	Principal modules	Checked mathematical content
5.1	WaveletPackets	Every finite depth of literal Haar packet operators, energy equality, and reconstruction using actual Hilbert adjoints.
6.1	KnownEdge	Exact cancellation of one retained packet, and equality of approximation errors.
6.2	KnownEdge	Finite families of retained packets, with no geometry assumption on the packets.
7.1	MaskPerturbation	Measurable-mask symmetric-difference norm, extended finite-p error bound, pointwise and essential supremum bounds, and smooth-background error.
11.2	CompletePrunings; PruningSums	Recursive cuts correspond to complete covering antichains; literal finite node sums preserve synthesis.
11.3	PruningSums	Finite arbitrary-objective minimization, attained positive gap with competitors, strict stability, and the singleton case.
11.4	FiniteAdaptive; PruningAlgorithm	Deterministic stop-on-ties selector, global optimum, arbitrary positive finite branching, and the stated unit-operation count.
11.5	PruningSums; PruningAlgorithm	Attained maximum error envelope, optimal-value perturbation, strict-gap selector stability, and probability transfer from a joint event.
12.1	CyclicSeries	Formal Cauchy-product residue convolution and the finite-tuple power identity, including the empty product at exponent zero.
13.2	SmithAction; SmithCyclic	Nonzero homogeneous pairs modulo scaling, Cayley conjugacy, the actual exponential phase, and cyclic composition on the projective line.
13.3	SmithCyclic	Two-phase coordinate swap, $0 \leftrightarrow \infty$, and finite impedance inversion when $z \neq 0$.
14.1	CRT	Signed integer residue-mask factorization for coprime moduli, including the dyadic–odd case.

The remaining foundational modules `Packets`, `FiniteSelection`, and `BinaryAdaptive` provide generic coordinate, finite-minimum, and binary-tree lemmas used or retained alongside the concrete constructions. The Hilbert target is the square-summable space on a product of indices; it is not the supremum-norm function space that Lean would otherwise assign to an unqualified finite family of channels.

D.3 Three bridges that matter for the statement

Finite filters and numerical transforms. The filter-bank proof is an algebraic theorem about finite Laurent-polynomial kernels acting faithfully on bilateral sequences. Equality at a single complex value of z would be insufficient to prove a polynomial identity; the impulse argument avoids that error. The separate transform theorem proves the finite-filter action agrees with evaluation wherever the weighted input series converge absolutely. An arbitrary bilateral ℓ^2 sequence need not have an absolutely convergent numerical z-transform. The all-sequence time-domain theorem makes no such assumption.

Recursive trees and set-valued prunings. The formal tree permits any positive finite arity at an internal node, including arity one. A node has a position in the tree, so equal data labels on distinct nodes do not identify the nodes. A recursive cut is either a stop or a collection of child cuts. Its equivalence with a covering antichain is proved in both directions. The cost, envelope, and operator sums are then

shown to equal actual finite sums over the selected node set. This connects the recursive optimizer to the manuscript's set-valued definition instead of assuming that connection.

Hilbert operators and finite experiments. The coordinate maps, literal Haar channels, and packet operators are constructed on complex ℓ^2. Square summability and boundedness are established before adjoints are used. The finite Python experiments separately check indexing, reconstruction, and energy at finite lengths. They illustrate these operators but are not the objects executed by the Lean kernel. Likewise, the Python Smith routine evaluates only finite charts; the Lean projective construction supplies the pole-safe universal statement.

D.4 September 2026 checks and numerical conventions

Check family	Accepted count
Original numerical companion tests	33
Independent exact-model tests	20
Verifier positive and negative controls	16
Total tests in these three families	69
Exact assertions inside the independent model suites	305,933
Registered Lean theorem targets	225
Lean proof modules	23
Regenerated figure pairs	18

The September 2026 record states that all scalar entries in the recovered numerical-results JSON reproduced exactly in its environment. This includes the 458,330-pruning depth-five comparison, its selected six-node pruning, the optimum gap, and the reconstruction residuals. The five Fourier sparse-approximation budgets were also checked for conjugate-pair closure. The revised figures and tables use the regenerated data. This exact replay of the stored floating-point numbers is stronger than a visual similarity check, but it is not a promise of bitwise equality on every platform.

For the one-dimensional low-pass experiment, "cutoff 18" means 37 signed frequency bins, not 18 retained coefficients. The disk experiment uses a square 33×33 frequency mask, not a radial cutoff. The sparse comparison uses largest-coefficient budgets instead of either low-pass convention. The full-image and boundary-band RMSEs are normalized by the number of samples in the respective comparison set. The supplied inpainting routines perform a fixed finite number of periodic neighbor-averaging iterations; "harmonic filling" describes that iteration, not a separately proved exact continuum Dirichlet solver.

The independent exact-model suite checks signed polyphase/FIR addresses, exact lifting and normalized Haar arithmetic, mask bounds, and exhaustive finite-tree objectives. Its tree census includes all 626 ordered rooted tree shapes with one through eight nodes and 129,958 node subsets. These finite checks can catch implementation or convention errors; they are not substitutes for the universal Lean proofs. The verifier controls exercise failure paths, including incomplete scope contracts and unregistered proof targets. Mandatory verification conditions use explicit exceptions rather than Python assertions, so optimized Python cannot silently remove them.

D.5 Pinned environment and rerunning the release

The Lean toolchain is `leanprover/lean4:v4.34.0-rc2`. The project pins mathlib to

`aeb72f1e9981b6d35b426b16dca7759be3e7ba06`.

The Lake manifest records the remaining dependency revisions. The numerical environment versions are recorded in `verification/numerical_environment.json`. Source and artifact hashes appear in `SHA256SUMS.txt`. The original manuscript, source, numerical data, and figures remain available under provenance for comparison; the expanded PDF and its TeX are the manuscript of that September 2026 release.

From the preserved release root (`source/complete/original_snapshot` in the final package), the combined verification entry point is:

```
python3 VERIFY_PAPER.py
```

This runs the Lean verifier, companion tests, numerical regeneration/comparison, and manuscript consistency checks. Lean, Lake, the pinned dependencies, the Python requirements, and a TeX installation must be available for the corresponding full checks. Missing prerequisites or failed checks return failure; static checks alone never report kernel verification. The individual numerical generation command is

```
cd companion
python3 run_all.py
python3 -m pytest -q tests
```

The TeX source resolves the eighteen vector figures from the manuscript's figure directory. The checked build uses repeated pdfLaTeX passes, then text, cross-reference, and page-render inspection. Different pdfTeX versions can produce different binary PDF hashes even when the rendered document is unchanged.

In the September 2026 release environment, a disclosed runtime adapter was needed for Lean executable-path discovery: it redirects a read of the current process's numeric `/proc` executable link to `/proc/self/exe`. It does not modify the Lean binary, elaborator, kernel, axioms, or proof terms. The adapter source and invocation are retained with the verification evidence; ordinary installations can run the pinned toolchain directly.

D.6 What remains open

The September 2026 finite theorem scope is complete in the stated sense: all twenty theorem-like statements have reviewed, accepted formal counterparts, and that release records a rerun of the numerical companion. The two edge-recovery conjectures remain open research directions. No universal segmentation theorem, infinite-tree consistency result, minimax rate, or optimal Smith sampling theorem is inferred from the finite results. Classical Smith-grid and transmission-line formulae provide application context; those physical and historical assertions are not additional Lean-certified theorem rows.

Across the available Papers I–V manuscripts there are 168 theorem-like results. Their release maps contain 1,456 raw theorem targets; removing two shared qualified names and eleven known Paper-IV-to-V adaptations leaves 1,443 after those known duplicate removals. This is a source census, not a claim of that many independent or novel mathematical results. Papers I–IV were counted from their release material and bundled audit records; only Paper V was freshly built for that September 2026 release. These historical cross-paper counts are not a current census of the October final companions.

Part II: Extended mathematical development

Multiresolution Signal Calculus, Singular Packets, and Stable Reconstruction

This part preserves the complete standalone mathematical branch, with the explicit audit repairs recorded in the accompanying source ledger. Its sixty-three proofs are prose proofs; no additional Lean coverage is asserted. Section and result numbers carry the prefix E to distinguish this scope from Part I.

Overview

Signals on a lattice admit exact coordinates indexed by the residue classes of every finite index sublattice. Convolution becomes a matrix of packet transfers, while filter banks and packet trees become exact changes of coordinates. We develop this structure on sequence spaces, prove quantitative stability for imperfect and perturbed banks, and give an exact dynamic recursion for adaptive packet trees. A singular signal is written as a smooth component plus step or truncated power packets that record jumps in the signal and its derivatives. Retaining the correct packets leaves only the smooth approximation error. Estimated packets are governed by exact formulas involving value error, region overlap, boundary displacement, and the norm of the smooth approximation operator. The main recovery result treats separated jumps sampled on a uniform grid. An explicit contrast gap gives exact recovery of every jump cell, grid scale location accuracy, amplitude control, and finite norm consistency. Probability bounds cover sub Gaussian noise and repeated measurements. Haar coefficients, two shifted grids, and annihilating differences give complementary localization results. The final sections treat Gibbs oscillation, nonlinear residue interactions, numerical illustrations, and cyclic Cayley coordinates.

E1 Introduction

Polyphase decompositions, filter banks, lifting schemes, and wavelet packets are standard parts of multirate signal processing and harmonic analysis. Their classical development is described in [CR83, Vai93, VK95, SN96, Dau92, Mal09]. These theories are often introduced through several parallel languages. Residue classes appear in polyphase analysis. Matrix symbols appear in filter banks. Trees appear in wavelet packets. Singularities are handled through a different approximation or detection method. The first aim of this article is to place these constructions in one exact coordinate system.

The second aim is to separate representation from recovery. If a signal has already been written as

$$f = s + j$$

with a smooth part s and a singular packet j, then

$$\tilde{f} = Qs + j$$

satisfies

$$f - \tilde{f} = s - Qs.$$

This identity is exact, but it does not discover j. A useful signal theory must therefore distinguish three errors. The first is the approximation error of the smooth component. The second is the error in the

estimated singular packet. The third is the amplification caused by applying a reconstruction operator to that packet error. The middle sections of the paper isolate all three terms.

The singular packets considered here range from indicator functions of regions to truncated powers

$$\frac{(t-\tau)_+^m}{m!}.$$

The latter encode jumps in derivatives of order m. They permit a piecewise smooth function to be reduced to a globally Sobolev remainder under explicit trace assumptions. This gives a precise version of the informal statement that a discontinuity should be represented directly rather than approximated by a global smooth basis.

The recovery theory begins with one dimensional separated jumps. For bounded deterministic noise, thresholding adjacent sample contrasts recovers the exact grid cells containing the jumps whenever the jump size exceeds the combined smooth variation and noise by an explicit margin. The same proof gives location and amplitude bounds. A sub Gaussian version follows from a union bound. Averaging repeated measurements reduces the required threshold in the expected way. Haar coefficients provide a second detection mechanism. Two grids shifted by half a cell guarantee that every jump is well placed in at least one grid, which removes the most elementary dyadic alignment failure.

The literature on singularity detection is much broader than the results proved here. Wavelet modulus maxima are developed in [MH92]. Best basis selection in packet libraries was introduced in [CW92]. Nonlinear approximation is surveyed in [DeV98]. Geometric image models, wedgelets, and curvelets appear in [Don99, CD04]. The present article does not replace those theories. Its narrower purpose is to give a common exact calculus in which coordinate reconstruction, adaptive basis selection, singular packet estimation, and smooth approximation remain logically separate.

The article is organized as follows. Appendices E2 and E3 develop lattice addresses and exact residue coordinates in any dimension. Appendices E4 and E5 express convolution and filter banks in those coordinates, including stability under imperfect reconstruction and filter perturbation. Appendix E6 treats arbitrary pruned packet trees and stability of the best basis decision. Appendices E7 and E8 introduce step and higher order singular packets, exact reconstruction identities, and error formulas. Appendices E9 and E10 prove deterministic and probabilistic recovery results. Appendices E11 and E12 treat Gibbs oscillation and nonlinear interactions. The final sections record finite numerical illustrations and a secondary cyclic Cayley realization.

Several conclusions are deliberately excluded. The paper does not prove a universal image segmentation theorem. Exact recovery of separated jumps in one dimension does not imply stable recovery of arbitrary boundaries in higher dimensions. Retaining a correct singular packet does not remove noise or model error. An adaptive tree selected by an additive objective need not remain optimal when global hardware costs or cross packet interactions are introduced. The Cayley coordinate section is a secondary conformal realization and is not used in the recovery theorems.

E1.1 Main results

The first result is an exact coordinate theorem. Let L be a finite index sublattice of $\mathbb{Z}^d$, and let R contain one representative from every coset. The analysis map

$$x \longmapsto (x_r)_{r\in R}, \qquad x_r(\ell) = x(r+\ell),$$

is an isometric isomorphism on every ℓ^p space. This statement includes the usual one dimensional polyphase decomposition, but it also applies to arbitrary finite index lattice packets in several dimen-

sions. If $L' \leq L$, the coarse packets split exactly into their fine descendants. A convolution operator becomes a matrix of convolution operators on L, with entries

$$h_{rs}(m) = h(r - s + m).$$

The matrix is therefore a coordinate representation of the original operator, not a reduced model.

The filter bank results distinguish exact reconstruction from quantitative near reconstruction. Exact recovery with delay d is the pointwise matrix identity

$$R(z)E(z) = z^{-d}I.$$

When this identity fails, the reconstruction error is controlled by the essential supremum of the delay compensated multiplier defect. If the filters themselves are perturbed, theorem E5.4 separates the analysis error, the synthesis error, and their product. The frame bound in theorem E5.7 shows that a lower singular value gap survives every sufficiently small perturbation. This makes the distinction between algebraic invertibility and stable numerical reconstruction explicit.

The packet tree results treat every admissible pruning, not only complete trees of a fixed depth. Unitary local splits give a unitary global transform. Local frame bounds propagate recursively in the nonunitary case. If the cost of a pruning is additive over retained nodes, then

$$F(v) = \min \left\{ c(v), \sum_{w \in \mathrm{child}(v)} F(w) \right\}$$

gives the exact optimal tree. The cost and the selected basis are stable when the node costs change by less than the gap separating the optimal pruning from its competitors.

The singular packet results begin with trace data. If a piecewise smooth function has a jump in its derivative of order m at τ_q, then the packet

$$\left[f^{(m)}\right]_{\tau_q} \frac{(t - \tau_q)_+^m}{m!}$$

removes exactly that trace jump. Subtracting all packets through order $r - 1$ leaves a global $W^{r,p}$ remainder. The packet coefficients are uniquely determined by the one sided trace jumps. This gives a finite and explicit singular part for the class covered by theorem E7.2.

The reconstruction formula with an estimated packet is

$$f - \hat{f}_m = (I - Q_m)s + (I - Q_m)(j - \hat{j}).$$

This identity identifies the two terms that must be controlled. The exact packet formulas in appendix E8 then evaluate or bound $\|j - \hat{j}\|$ from amplitude error, region overlap, boundary displacement, and the order of a derivative jump. A value jump has location modulus $|\tau - \hat{\tau}|^{1/p}$ in finite L^p, while every positive order truncated power packet is Lipschitz in its location.

The principal recovery theorem uses adjacent sample contrasts. Let

$$b_h = Mh + 2\varepsilon$$

be the largest contrast that can be produced by a Lipschitz background and bounded noise in one grid cell. If

$$a_{\min} > 2b_h,$$

then every threshold between b_h and $a_{\min} - b_h$ detects exactly the cells containing jumps. The jump locations are recovered within $h/2$, and each amplitude error is at most b_h. The probability theorem replaces the deterministic noise term by

$$2\sigma\sqrt{\log(2n/\delta)}.$$

Two half shifted Haar grids provide a second recovery mechanism. Every point is at least one quarter of a cell away from the boundary of one of the grids, so the Haar coefficient gap can be made independent of dyadic alignment.

E1.2 Notation

The following symbols recur throughout the article.

symbol	meaning
$L \le \mathbb{Z}^d$	a finite index sublattice
R	a set of representatives for $\mathbb{Z}^d/L$
P_r	the coordinate projector onto the coset $r + L$
$\mathcal{A}_L, \mathcal{S}_L$	lattice analysis and interleaving synthesis
E, R	filter bank analysis and synthesis symbols
Q_m	a bounded linear approximation operator acting on the smooth part
$j, \hat{j}$	the true and estimated singular packets
H_τ	the step packet $\mathbf{1}_{[\tau,1]}$
$\phi_{m,\tau}$	the truncated power packet $(t-\tau)_+^m/m!$
h	the grid spacing in the recovery theorems

E2 Signal seeds and lattice addresses

Let $1 \le p \le \infty$. For a countable set G, write $\ell^p(G)$ for the usual complex sequence space. For an integer $d \ge 1$, when $G = \mathbb{Z}^d$, translation by $a \in \mathbb{Z}^d$ is

$$(T_a x)(n) = x(n-a).$$

Let δ_0 be the impulse at the origin.

Theorem E2.1 (Impulse generation). *For $1 \le p < \infty$,*

$$\overline{\operatorname{span}\{T_a\delta_0 : a \in \mathbb{Z}^d\}}^{\ell^p} = \ell^p(\mathbb{Z}^d).$$

The same statement holds in $c_0(\mathbb{Z}^d)$ with the supremum norm. In $\ell^\infty(\mathbb{Z}^d)$, the closed span of the translation orbit is exactly $c_0(\mathbb{Z}^d)$.

Proof. The translation orbit is the standard coordinate family $(\delta_a)_{a\in\mathbb{Z}^d}$. Its finite span is the space of finitely supported sequences. Finitely supported sequences are dense in ℓ^p for finite p and in c_0. Their closure in the supremum norm is c_0, which is a proper closed subspace of ℓ^∞. □

Remark E2.2. The distinction at $p = \infty$ is structural. The impulse generates every finitely supported signal algebraically, but it is not a topological cyclic seed for all bounded signals.

Proposition E2.3 (Finite periodic signals)**.** *Let $G = \mathbb{Z}^d/L$, where $L \le \mathbb{Z}^d$ has finite index. The translation orbit of the impulse at the identity is a basis of $\mathbb{C}^G$. In particular, one impulse generates every signal on the finite periodic lattice.*

Proof. Translation sends the impulse at the identity to the impulse at each element of G. These impulses form the standard basis of $\mathbb{C}^G$. □

E3 Polyphase coordinates on finite index sublattices

Let $L \le \mathbb{Z}^d$ be a sublattice of finite index q. Choose a set $R \subset \mathbb{Z}^d$ containing one representative from every coset in $\mathbb{Z}^d/L$. Thus

$$\mathbb{Z}^d = \bigsqcup_{r\in R} (r + L).$$

For $x : \mathbb{Z}^d \to \mathbb{C}$, its channel at r is the sequence on L

$$x_r(\ell) = x(r + \ell).$$

Definition E3.1 (Lattice packet)**.** For $r \in R$, define the coordinate projector

$$(P_r x)(n) = \mathbf{1}_{r+L}(n)x(n).$$

The family $(P_r)_{r\in R}$ is called the packet system associated with L and R.

For finite p, equip $\bigoplus_{r\in R} \ell^p(L)$ with

$$\|(u_r)\|^p = \sum_{r\in R} \|u_r\|_p^p.$$

For $p = \infty$, use the maximum norm.

Theorem E3.2 (Exact lattice polyphase decomposition)**.** *For every $1 \le p \le \infty$, the analysis map*

$$\mathcal{A}_L : \ell^p(\mathbb{Z}^d) \longrightarrow \bigoplus_{r\in R} \ell^p(L), \qquad \mathcal{A}_L x = (x_r)_{r\in R},$$

is an isometric isomorphism. Its inverse is the interleaving map

$$\mathcal{S}_L(u)(r + \ell) = u_r(\ell).$$

The projectors satisfy

$$P_r P_s = \delta_{rs} P_r, \qquad \sum_{r\in R} P_r = I.$$

Proof. Every address has a unique representation $r + \ell$. For finite p,

$$\|x\|_p^p = \sum_{r\in R}\sum_{\ell\in L} |x(r+\ell)|^p = \sum_{r\in R} \|x_r\|_p^p.$$

The corresponding supremum identity is immediate when $p = \infty$. Unique address representation proves that analysis and interleaving are inverse maps. The projector identities follow from the disjoint coset partition. □

Corollary E3.3 (One dimensional residue coordinates)**.** *For $L = N\mathbb{Z}$ and $R = \{0, \dots, N-1\}$,*

$$x_r(k) = x(Nk + r)$$

and

$$\ell^p(\mathbb{Z}) \cong \bigoplus_{r=0}^{N-1} \ell^p(\mathbb{Z})$$

isometrically.

Proof. Apply theorem E3.2 to the standard residue representatives. □

Proposition E3.4 (Translation covariance)**.** *Fix $a \in \mathbb{Z}^d$. For every $r \in R$, write uniquely*

$$r - a = r_a + \lambda_{a,r}, \qquad r_a \in R, \quad \lambda_{a,r} \in L.$$

Then

$$(\mathcal{A}_L T_a x)_r(\ell) = x_{r_a}(\ell + \lambda_{a,r}).$$

Thus a fine translation permutes the lattice packets and applies an internal translation on L.

Proof. Evaluate at $r + \ell$:

$$(T_a x)(r+\ell) = x(r+\ell-a) = x(r_a + \ell + \lambda_{a,r}).$$

This is the stated channel formula. □

E3.1 Refinement of sublattices

Let $L' \le L \le \mathbb{Z}^d$, with both indices finite. Choose representative systems R for $\mathbb{Z}^d/L$ and R' for $\mathbb{Z}^d/L'$. For $r \in R$, define

$$\mathrm{Child}(r) = \{s \in R' : s + L' \subset r + L\}.$$

Theorem E3.5 (Exact lattice refinement)**.** *For every coarse packet,*

$$P_r^L = \sum_{s\in \mathrm{Child}(r)} P_s^{L'}.$$

The fine packets in the sum are pairwise disjoint. Refinement through several nested sublattices is transitive.

Proof. The coset $r + L$ is the disjoint union of the L' cosets contained in it. Multiplying by the corresponding indicator functions gives the projector identity. A nested partition of a coset is independent of whether the intermediate level is inserted, which proves transitivity. □

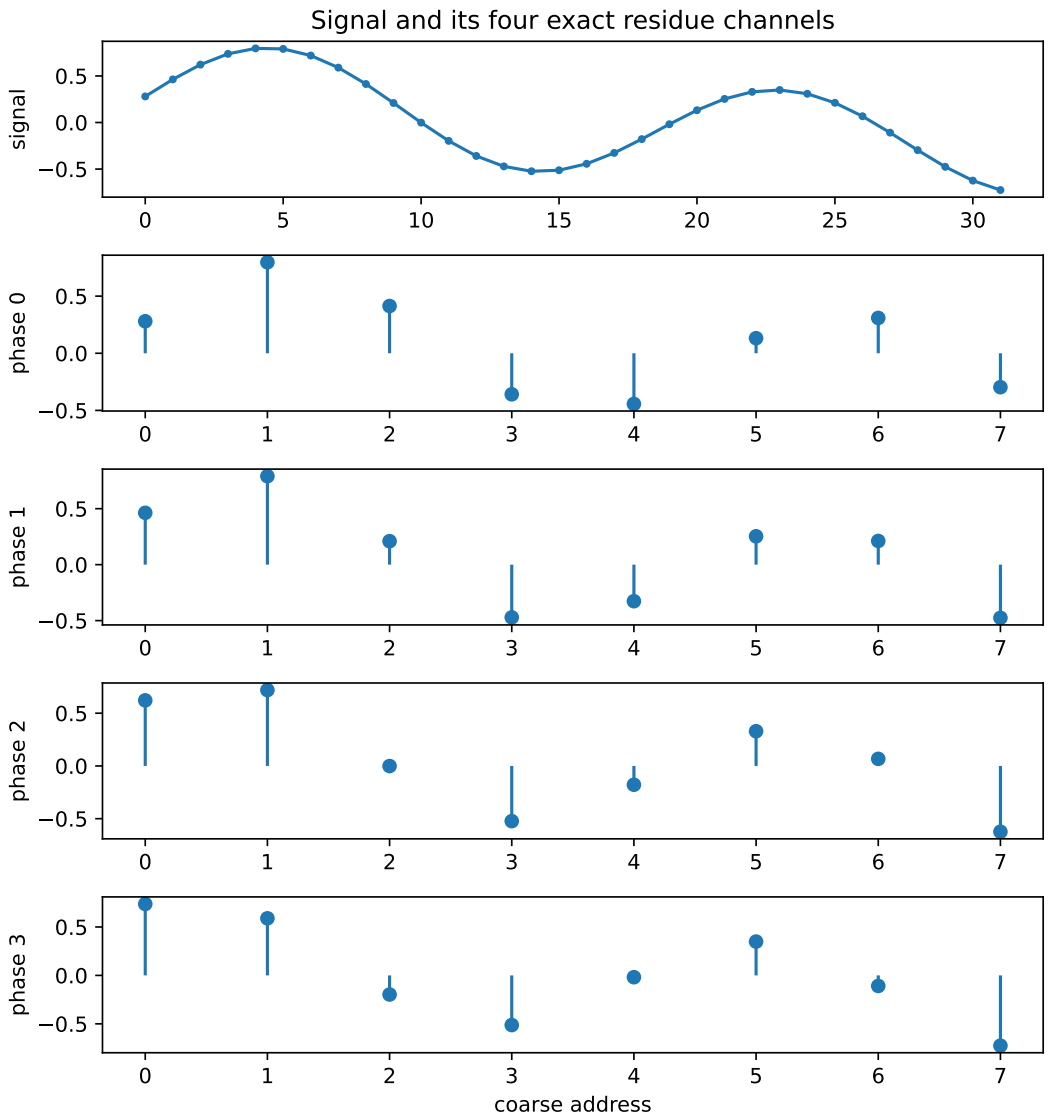


Figure E1. A signal and its four exact residue channels. Interleaving the channels returns the original samples without approximation.

Example E3.6 (Rectangular image phases)**.** For

$$L = M\mathbb{Z} \times N\mathbb{Z} \subset \mathbb{Z}^2,$$

one may take

$$R = \{0, \dots, M-1\} \times \{0, \dots, N-1\}.$$

The analysis map separates an image into MN exact phases. Refining (M, N) to (M', N'), where $M \mid M'$ and $N \mid N'$, splits every coarse phase into

$$\frac{M'}{M}\frac{N'}{N}$$

fine phases.

E4 Convolution as a packet transfer matrix

Let $h \in \ell^1(\mathbb{Z}^d)$ and $x \in \ell^p(\mathbb{Z}^d)$, with $1 \le p \le \infty$, and define

$$(Hx)(n) = (h * x)(n) = \sum_{q \in \mathbb{Z}^d} h(q)x(n-q).$$

Young's inequality gives

$$\|Hx\|_p \le \|h\|_1 \|x\|_p$$

for every $1 \le p \le \infty$.

Definition E4.1 (Packet transfer kernel)**.** For output residue $r \in R$ and input residue $s \in R$, define a kernel on L by

$$h_{rs}(m) = h(r - s + m), \qquad m \in L.$$

Theorem E4.2 (Exact convolution transfer law)**.** *Let $y = h * x$. Then*

$$y_r(\ell) = \sum_{s \in R} \sum_{m \in L} h_{rs}(m) x_s(\ell - m).$$

Equivalently,

$$\mathcal{A}_L H \mathcal{A}_L^{-1} = (H_{rs})_{r,s \in R},$$

where H_{rs} is convolution on L by h_{rs}.

Proof. Evaluate the output at $r + \ell$. Write every input address as $s + \ell'$. The convolution offset is

$$(r + \ell) - (s + \ell') = (r - s) + (\ell - \ell').$$

Setting $m = \ell - \ell'$ gives the formula. □

Proposition E4.3 (Transfer norm control)**.** *For every output residue r,*

$$\sum_{s \in R} \|h_{rs}\|_{\ell^1(L)} = \|h\|_{\ell^1(\mathbb{Z}^d)}.$$

The packet transfer matrix acts on the polyphase direct sum with norm at most $\|h\|_1$ on every ℓ^p space.

Proof. For fixed r, every $q \in \mathbb{Z}^d$ has a unique representation $q = r - s + m$ with $s \in R$ and $m \in L$. This proves the equality of the absolute sums. The operator norm bound also follows by conjugating Young's inequality through the isometric analysis map. □

Proposition E4.4 (Composition of transfer matrices)**.** *If G and H are convolution operators with packet matrices (G_{rs}) and (H_{rs}), then the packet matrix of GH is*

$$(GH)_{rt} = \sum_{s \in R} G_{rs} H_{st}.$$

In one dimensional transform notation, the corresponding matrix symbols multiply pointwise.

Proof. Conjugation by $\mathcal{A}_L$ preserves composition:

$$\mathcal{A}_L GH \mathcal{A}_L^{-1} = (\mathcal{A}_L G \mathcal{A}_L^{-1})(\mathcal{A}_L H \mathcal{A}_L^{-1}).$$

Reading the (r, t) block gives the formula. □

E4.1 The one dimensional symbol

For $L = N\mathbb{Z}$ with $N \geq 1$, first take $|z| = 1$. The assumption $h \in \ell^1(\mathbb{Z})$ makes the following symbol series absolutely convergent. Define

$$H_{ks}(z) = \sum_{m \in \mathbb{Z}} h(Nm + k - s) z^{-m}.$$

For $x \in \ell^1(\mathbb{Z})$, the channel transforms converge absolutely on the unit circle and satisfy

$$\boldsymbol{Y}(z) = \boldsymbol{H}_N(z) \boldsymbol{X}(z).$$

For $x \in \ell^2(\mathbb{Z})$, the same identity holds almost everywhere in the L^2 Fourier sense. For finite impulse-response kernels it also holds at nonzero z wherever the input channel transforms are weighted absolutely summable. This is the classical polyphase matrix. It is the exact block matrix of the original convolution operator.

Corollary E4.5 (Finite impulse response closure)**.** *If h has finite support, every packet kernel h_{ks} has finite support. Matrix multiplication of polyphase symbols agrees with composition of the original finite impulse response operators.*

Proof. Finite support is preserved by taking residue subsequences. The composition statement is proposition E4.4. □

Example E4.6 (A four phase finite impulse response operator)**.** Let

$$h(0) = 1, \quad h(1) = 2, \quad h(2) = 3, \quad h(3) = 4, \quad h(4) = 5,$$

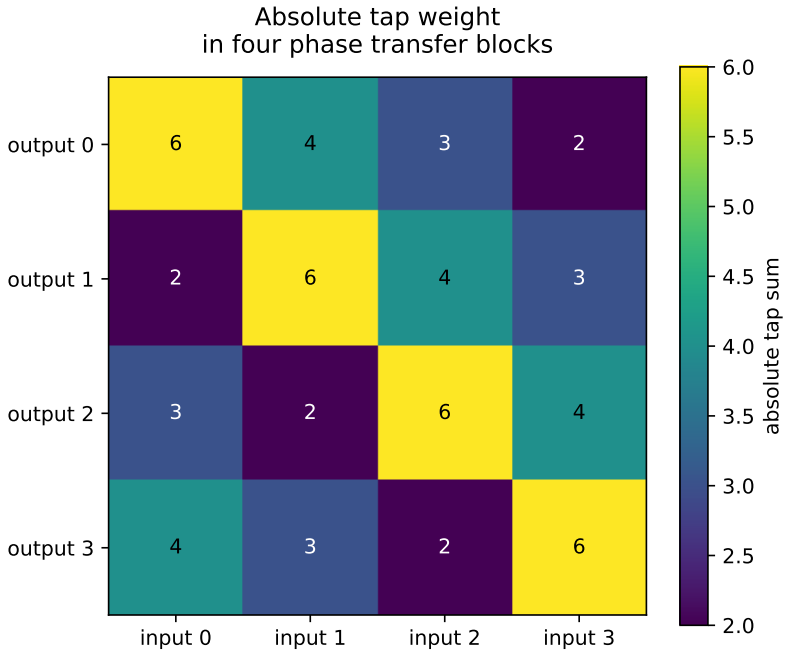


Figure E2. Absolute tap weight in the transfer blocks of the four phase operator in example E4.6.

with all other taps zero. For four residue channels, the transfer symbol is

$$\boldsymbol{H}_4(z) = \begin{pmatrix} 1+5z^{-1} & 4z^{-1} & 3z^{-1} & 2z^{-1} \\ 2 & 1+5z^{-1} & 4z^{-1} & 3z^{-1} \\ 3 & 2 & 1+5z^{-1} & 4z^{-1} \\ 4 & 3 & 2 & 1+5z^{-1} \end{pmatrix}.$$

The delay term records the tap that crosses a coarse cell boundary. No approximation is introduced by the matrix representation.

E5 Filter banks, frame bounds, and lifting

Throughout this section the banks act boundedly on the relevant polyphase ℓ^2 spaces. A finite channel analysis bank acts in Fourier coordinates by a matrix $E(z)$. A synthesis bank acts by a matrix $R(z)$. The matrices may be square or rectangular. Their entries are Laurent polynomials for finite filters and bounded measurable functions for general stable filters.

Theorem E5.1 (Perfect reconstruction criterion). *Let $E(z)$ be an M by N analysis matrix and let $R(z)$ be an N by M synthesis matrix. The bank reconstructs every input with a delay of d coarse channel samples, equivalent to Nd original samples in the one dimensional N-phase convention, exactly if and only if*

$$R(z)E(z) = z^{-d} I_N$$

for almost every point on the unit circle. A nonzero scalar factor gives exact reconstruction up to gain and delay.

Proof. The channel Fourier transform turns analysis followed by synthesis into multiplication by $R(z)E(z)$. If the matrix identity holds, inverse transformation gives the delayed input. Conversely, if every input is reconstructed with that delay, the difference matrix annihilates every vector valued Fourier datum and must vanish almost everywhere. □

Theorem E5.2 (Quantitative imperfect reconstruction)**.** *Define the delay compensated defect*

$$D(\mathrm{e}^{\mathrm{i}\omega}) = \mathrm{e}^{\mathrm{i}d\omega} R(\mathrm{e}^{\mathrm{i}\omega}) E(\mathrm{e}^{\mathrm{i}\omega}) - I_N.$$

If

$$\varepsilon_{\mathrm{rec}} = \operatorname*{ess\,sup}_{\omega} \|D(\mathrm{e}^{\mathrm{i}\omega})\|_{\mathrm{op}} < \infty,$$

then the delay compensated reconstruction $\tilde{x}$ satisfies

$$\|\tilde{x} - x\|_2 \le \varepsilon_{\mathrm{rec}} \|x\|_2.$$

The constant is sharp as an operator norm.

Proof. In polyphase Fourier coordinates, the error is $D(\mathrm{e}^{\mathrm{i}\omega})\boldsymbol{X}(\mathrm{e}^{\mathrm{i}\omega})$. Pointwise multiplication and Plancherel's theorem give the upper bound. The operator norm of a measurable matrix multiplier is its essential supremum, which proves sharpness. □

Example E5.3 (A reconstruction certificate)**.** Suppose a two channel bank has delay compensated defect

$$D(\mathrm{e}^{\mathrm{i}\omega}) = \begin{pmatrix} 0.01\cos\omega & 0 \\ 0 & 0.02\sin\omega \end{pmatrix}.$$

Then

$$\operatorname*{ess\,sup}_{\omega} \|D(\mathrm{e}^{\mathrm{i}\omega})\|_{\mathrm{op}} = 0.02.$$

Every input therefore has relative reconstruction error at most two percent in ℓ^2. The estimate is independent of the input length.

Theorem E5.4 (Stability under filter perturbation)**.** *Assume $RE = z^{-d} I_N$. Let*

$$\widetilde{E} = E + \Delta E, \qquad \widetilde{R} = R + \Delta R.$$

Set

$$e_0 = \operatorname{ess\,sup} \|E\|_{\mathrm{op}}, \qquad r_0 = \operatorname{ess\,sup} \|R\|_{\mathrm{op}},$$
$$\delta_E = \operatorname{ess\,sup} \|\Delta E\|_{\mathrm{op}}, \quad \delta_R = \operatorname{ess\,sup} \|\Delta R\|_{\mathrm{op}}.$$

Then the delay compensated reconstruction defect obeys

$$\varepsilon_{\mathrm{rec}} \le r_0 \delta_E + e_0 \delta_R + \delta_R \delta_E.$$

Proof. Expand

$$\widetilde{R}\widetilde{E} - RE = R\Delta E + \Delta R E + \Delta R \Delta E.$$

Take pointwise operator norms, then the essential supremum. Multiplication by the delay factor has unit modulus. □

Theorem E5.5 (Frame bounds from the polyphase symbol)**.** *Assume that*

$$AI_N \le E(\mathrm{e}^{\mathrm{i}\omega})^* E(\mathrm{e}^{\mathrm{i}\omega}) \le BI_N$$

for almost every ω, where $0 < A \le B < \infty$. Then the analysis bank satisfies

$$A\|x\|_2^2 \le \|\mathcal{A}_E x\|_2^2 \le B\|x\|_2^2.$$

The pointwise matrix

$$R_{\mathrm{can}}(\mathrm{e}^{\mathrm{i}\omega}) = (E^*E)^{-1}E^*$$

is a bounded left inverse and gives the canonical dual synthesis bank.

Proof. Apply the matrix inequality to the polyphase Fourier vector at every frequency and integrate. Plancherel's theorem gives the frame inequalities. The lower bound makes E^*E invertible almost everywhere, and direct multiplication gives $R_{\mathrm{can}}E = I_N$. The same spectral bounds show that the canonical dual is bounded. □

Corollary E5.6 (Coefficient noise under canonical synthesis)**.** *Under the hypotheses of theorem E5.5, suppose the observed coefficient vector is*

$$c = \mathcal{A}_E x + \nu.$$

Canonical synthesis gives

$$\hat{x} = R_{\mathrm{can}} c$$

and

$$\|\hat{x} - x\|_2 \le \frac{1}{\sqrt{A}}\|\nu\|_2.$$

Proof. The smallest singular value of E is at least $\sqrt{A}$, so the pointwise norm of its pseudoinverse is at most $1/\sqrt{A}$. Apply Plancherel's theorem to $R_{\mathrm{can}}\nu$. □

Theorem E5.7 (Perturbation of frame bounds)**.** *Under the hypotheses of theorem E5.5, let $\widetilde{E} = E + \Delta E$ and suppose*

$$\delta = \operatorname*{ess\,sup}_{\omega} \|\Delta E(\mathrm{e}^{\mathrm{i}\omega})\|_{\mathrm{op}} < \sqrt{A}.$$

Then $\widetilde{E}$ is a frame analysis bank with bounds

$$(\sqrt{A} - \delta)^2 \quad \textit{and} \quad (\sqrt{B} + \delta)^2.$$

Proof. For every vector v,

$$\|\widetilde{E}v\| \ge \|Ev\| - \|\Delta E v\| \ge (\sqrt{A} - \delta)\|v\|.$$

The upper bound follows from

$$\|\widetilde{E}v\| \le (\sqrt{B} + \delta)\|v\|.$$

Square the inequalities and integrate in frequency. □

Remark E5.8. Even when E is a Laurent polynomial matrix, the canonical dual need not have finite impulse response. Finite support of both analysis and synthesis is an additional algebraic condition.

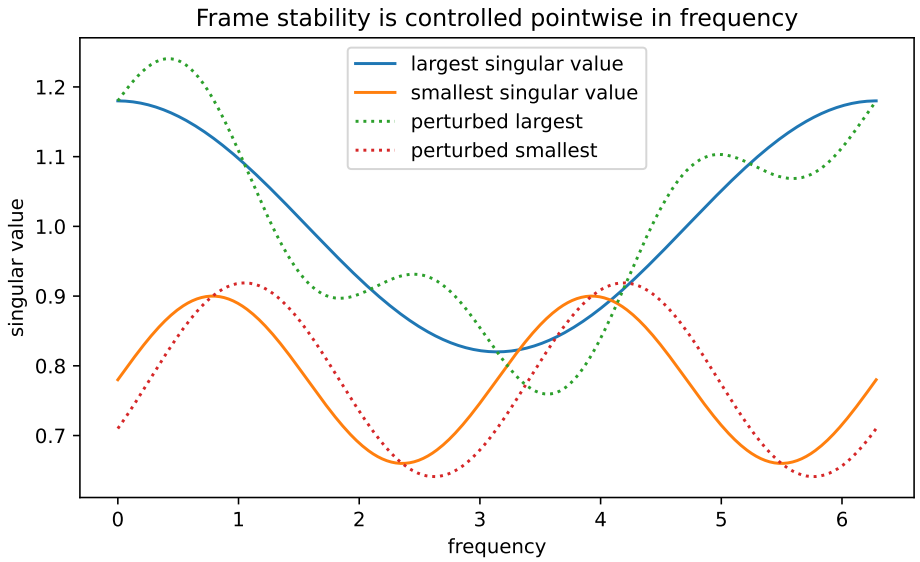


Figure E3. Pointwise singular value bounds govern both the original frame and its perturbed analysis bank.

Corollary E5.9 (Paraunitary bank)**.** *If $E(z)^* E(z) = I_N$ on the unit circle, then analysis is an isometry and synthesis may be chosen as $R(z) = E(z)^*$.*

Proof. Use theorem E5.5 with $A = B = 1$, then multiply the matrices. □

E5.1 Haar analysis

The Haar matrix is

$$E_H = \frac{1}{\sqrt{2}} \begin{pmatrix} 1 & 1 \\ 1 & -1 \end{pmatrix}.$$

For even and odd samples $e(n) = x(2n)$ and $o(n) = x(2n+1)$, the low and high coordinates are

$$a(n) = \frac{e(n) + o(n)}{\sqrt{2}}, \qquad d(n) = \frac{e(n) - o(n)}{\sqrt{2}}.$$

Corollary E5.10 (Haar reconstruction and energy)**.** *The Haar bank reconstructs exactly and*

$$\|x\|_2^2 = \|a\|_2^2 + \|d\|_2^2.$$

Proof. The matrix E_H is unitary. □

E5.2 Lifting steps

Let $P(z)$ and $Q(z)$ be Laurent polynomials. Define

$$L_P(z) = \begin{pmatrix} 1 & 0 \\ P(z) & 1 \end{pmatrix}, \qquad U_Q(z) = \begin{pmatrix} 1 & Q(z) \\ 0 & 1 \end{pmatrix}.$$

Theorem E5.11 (Exact lifting update)**.** *The lifting matrices are invertible with*

$$L_P^{-1} = L_{-P}, \qquad U_Q^{-1} = U_{-Q}.$$

If $R_0 E_0 = I$, then every finite product V of lifting matrices gives another exact bank by

$$E = VE_0, \qquad R = R_0 V^{-1}.$$

Every lifting step has determinant one.

Proof. Direct multiplication proves the inverse formulas and the determinant statement. The reconstructed product is

$$RE = R_0 V^{-1} V E_0 = R_0 E_0 = I.$$

□

Example E5.12 (A two neighbor predict and update transform)**.** Split a sequence into even and odd samples. Define

$$d(n) = o(n) - \frac{e(n) + e(n+1)}{2}$$

and

$$s(n) = e(n) + \frac{d(n-1) + d(n)}{4}.$$

The inverse is obtained in reverse order:

$$e(n) = s(n) - \frac{d(n-1) + d(n)}{4},$$

then

$$o(n) = d(n) + \frac{e(n) + e(n+1)}{2}.$$

Thus reconstruction is exact over every coefficient field in which two is invertible. This is a standard compactly supported biorthogonal lifting pattern [CDF92, Swe96, DS98].

E6 Wavelet packet trees and admissible bases

A packet transform is built by deciding at each node whether to retain the current coordinate space or to split it into children. The proof of reconstruction is local and does not depend on a particular wavelet family.

Definition E6.1 (Unitary packet tree)**.** A finite unitary packet tree consists of Hilbert spaces $\mathcal{H}_v$ at its vertices and, at every internal vertex v, a unitary map

$$U_v : \mathcal{H}_v \longrightarrow \bigoplus_{w \in \mathrm{child}(v)} \mathcal{H}_w.$$

An admissible pruning is a set of vertices that meets every root to terminal path exactly once.

Theorem E6.2 (Reconstruction on a pruned packet tree)**.** *Every admissible pruning $\mathcal{L}$ defines a unitary analysis map*

$$\mathcal{A}_{\mathcal{L}} : \mathcal{H}_{\text{root}} \longrightarrow \bigoplus_{v \in \mathcal{L}} \mathcal{H}_v.$$

Its inverse is obtained by applying the adjoints of the local splits from the leaves toward the root. In particular,

$$\|x\|^2 = \sum_{v \in \mathcal{L}} \|x_v\|^2.$$

Proof. Proceed by induction on the depth of the retained subtree. If the root is retained, the statement is immediate. If the root is split, apply the unitary map U_{root}, then apply the induction hypothesis independently in each child subtree. A direct sum of unitary maps is unitary. Reversing the maps with adjoints gives synthesis. □

Corollary E6.3 (Coefficient perturbations in a unitary tree)**.** *Let $c = \mathcal{A}_{\mathcal{L}} x$ be the leaf coefficients of an admissible unitary pruning, and let $\hat{c} = c + e$. If $\hat{x}$ is synthesized from $\hat{c}$, then*

$$\|\hat{x} - x\| = \|e\|.$$

Thus coefficient quantization and coefficient noise are neither amplified nor attenuated by exact unitary synthesis.

Proof. The synthesis map is unitary by theorem E6.2. Hence

$$\hat{x} - x = \mathcal{A}_{\mathcal{L}}^{-1} e$$

has the same norm as e. □

Proposition E6.4 (Bounds for nonunitary local splits)**.** *Suppose every internal node has an analysis map U_v and constants $0 \le A_v \le B_v < \infty$ satisfying*

$$A_v \|x\|^2 \le \sum_{w \in \text{child}(v)} \|(U_v x)_w\|^2 \le B_v \|x\|^2.$$

Define recursively

$$a(v) = \begin{cases} 1, & v \text{ retained}, \\ A_v \min_w a(w), & v \text{ split}, \end{cases}$$

and

$$b(v) = \begin{cases} 1, & v \text{ retained}, \\ B_v \max_w b(w), & v \text{ split}. \end{cases}$$

Then the leaf analysis of the pruned tree has bounds $a(\text{root})$ and $b(\text{root})$.

Proof. Assume the child subtree bounds have been proved. Then

$$\sum_w \sum_{\ell \in \mathcal{L}_w} \|x_\ell\|^2 \ge \min_w a(w) \sum_w \|(U_v x)_w\|^2 \ge A_v \min_w a(w) \|x\|^2.$$

The upper bound follows in the same way with the maximum and B_v. Induction completes the proof. □

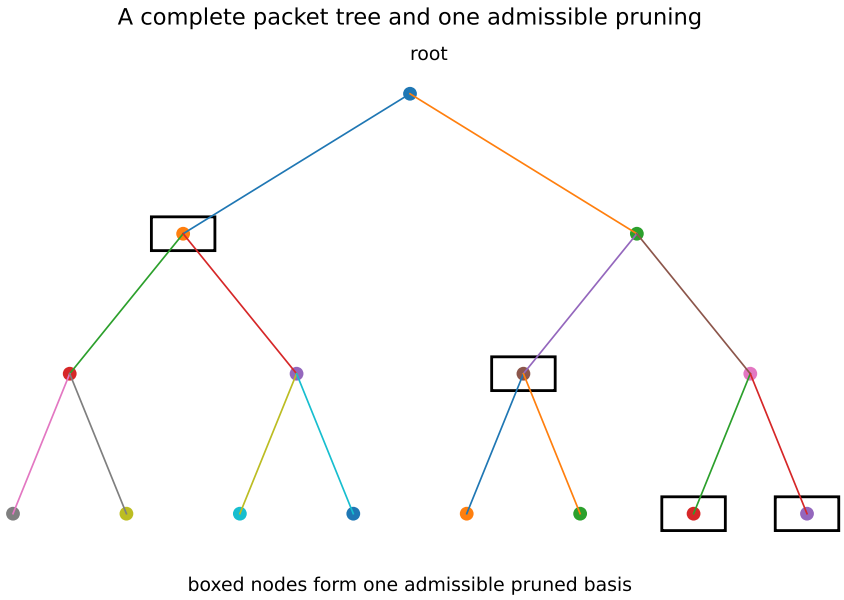


Figure E4. A complete packet tree and one admissible pruning. Retained nodes may occur at different depths.

E6.1 Best basis recursion

> **The minimum is taken over feasible prunings**
>
> The value at a node is the least cost among all admissible prunings of the subtree rooted there. It is one optimal value. Individual competing prunings may have larger costs. The recursion compares retaining the node with the sum of the already optimal child values, with retention chosen on a tie.

Assign a real cost $c(v)$ to retaining each node. For an admissible pruning $\mathcal{L}$, let

$$C(\mathcal{L}) = \sum_{v \in \mathcal{L}} c(v).$$

The cost may measure entropy, coefficient count, an approximation penalty, or any other additive local objective.

Theorem E6.5 (Exact additive best basis recursion)**.** *For each vertex define*

$$F(v) = \min \left\{ c(v), \sum_{w \in \mathrm{child}(v)} F(w) \right\},$$

with $F(v) = c(v)$ at terminal vertices. Then $F(v)$ is the minimum cost of every admissible pruning of the subtree rooted at v. A minimizing pruning is recovered by retaining v when the first term is no larger than the second and splitting it otherwise.

Proof. Every admissible pruning of the subtree has exactly two forms. It either retains v, with cost $c(v)$, or splits v and independently chooses an admissible pruning in every child subtree. The minimum in the second case is the sum of the child minima. This gives the recursion and the reconstruction rule. In an equality case both choices minimize, and the stated rule retains the node. □

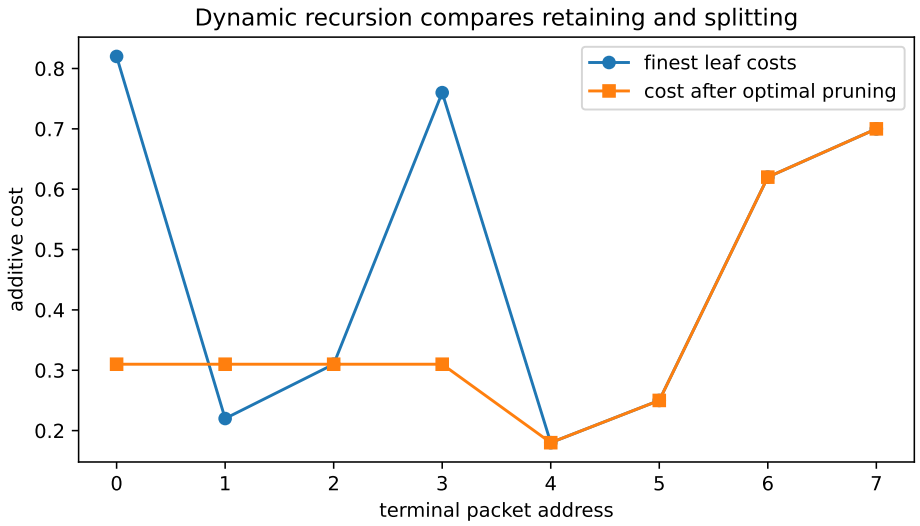


Figure E5. An additive best basis recursion compares the cost of retaining a packet with the total cost of splitting it.

Theorem E6.6 (Stability of the optimal cost)**.** *Let c and $\tilde{c}$ be two node cost functions. For an admissible pruning $\mathcal{L}$, set*

$$\varepsilon(\mathcal{L}) = \sum_{v \in \mathcal{L}} |c(v) - \tilde{c}(v)|$$

and let

$$\varepsilon_* = \max_{\mathcal{L}} \varepsilon(\mathcal{L}).$$

If F_* and $\widetilde{F}_*$ are the two optimal root costs, then

$$|F_* - \widetilde{F}_*| \leq \varepsilon_*.$$

Proof. For every admissible pruning,

$$|C(\mathcal{L}) - \widetilde{C}(\mathcal{L})| \leq \varepsilon_*.$$

Evaluate $\widetilde{C}$ on a minimizer for C to obtain $\widetilde{F}_* \leq F_* + \varepsilon_*$. Reverse the roles to obtain $F_* \leq \widetilde{F}_* + \varepsilon_*$. □

Corollary E6.7 (Stability of the selected basis)**.** *Assume the optimal pruning $\mathcal{L}_*$ for c is unique and at least one competing pruning exists. Define $g = \min_{\mathcal{L} \neq \mathcal{L}_*} (C(\mathcal{L}) - C(\mathcal{L}_*)) > 0$. If*

$$2\varepsilon_* < g,$$

then the optimal pruning for $\tilde{c}$ is the same. If only one admissible pruning exists, it remains selected under every cost change without a gap condition.

Proof. The cost of the original minimizer can increase by at most ε_*, while the cost of every competitor can decrease by at most ε_*. The original gap therefore remains positive. □

E7 Singular packets and exact reconstruction

Trace data identify the singular part

A value jump needs a step packet. A jump in a derivative needs a truncated power of the corresponding order. Subtracting these finite packets matches the one sided traces and leaves the regular remainder covered by the theorem's Sobolev assumptions. The packet construction and the approximation operator play separate roles.

A packet decomposition becomes useful for approximation when it separates a component that should be retained from a component that should be compressed. The simplest singular packets are steps. Higher order packets record jumps in derivatives.

For $m \geq 0$ and $0 < \tau < 1$, define

$$\phi_{m,\tau}(t) = \frac{(t-\tau)_+^m}{m!}.$$

Thus $\phi_{0,\tau} = \mathbf{1}_{[\tau,1]}$. On each side of τ, the packet is a polynomial. Its derivative of order m has a unit jump at τ.

Definition E7.1 (Sobolev step packet class)**.** Fix $r \geq 1$, $1 \leq p \leq \infty$, and an integer $Q \geq 0$. The class $\mathcal{F}_{r,p}(Q)$ consists of functions

$$f = s + \sum_{q=1}^{Q} a_q \phi_{0,\tau_q}$$

with $s \in W^{r,p}(0,1)$ and

$$0 < \tau_1 < \cdots < \tau_Q < 1.$$

No lower bound on the jump amplitudes is required for representation. Recovery results later impose such a bound.

Theorem E7.2 (Higher order singular packet decomposition)**.** *Let*

$$0 = \tau_0 < \tau_1 < \cdots < \tau_Q < \tau_{Q+1} = 1.$$

Suppose the restriction of f to every interval (τ_q, τ_{q+1}) belongs to $W^{r,p}$, and choose the one dimensional Sobolev representatives whose derivatives through order $r-1$ have one sided traces at the endpoints. Define

$$a_{q,m} = \left[f^{(m)}\right]_{\tau_q} = f^{(m)}(\tau_q+) - f^{(m)}(\tau_q-)$$

and

$$j_f(t) = \sum_{q=1}^{Q} \sum_{m=0}^{r-1} a_{q,m} \phi_{m,\tau_q}(t).$$

Then

$$s_f = f - j_f$$

has matching one sided derivatives through order $r-1$ at every breakpoint and belongs to $W^{r,p}(0,1)$. Its weak derivative of order r equals the piecewise classical derivative $f^{(r)}$ almost everywhere.

Proof. For $0 \le \ell \le m$, the classical derivative of $\phi_{m,\tau}$ on the two open sides is

$$\phi_{m,\tau}^{(\ell)}(t) = \frac{(t-\tau)_+^{m-\ell}}{(m-\ell)!}.$$

This derivative has zero jump when $\ell < m$ and a unit jump when $\ell = m$. Derivatives of order larger than m vanish on both open sides. It follows that subtracting the term $a_{q,m}\phi_{m,\tau_q}$ removes exactly the jump in the derivative of order m without changing the other classical trace jumps. Hence s_f has matching traces through order $r-1$.

On each partition interval, j_f is a polynomial of degree at most $r-1$, so its weak derivative of order r is zero there. A piecewise $W^{r,p}$ function whose traces through order $r-1$ match across every breakpoint belongs to $W^{r,p}(0,1)$. Repeated integration by parts on the partition intervals shows that all boundary terms cancel. Thus the weak derivative of order r is the piecewise weak derivative of f. □

Corollary E7.3 (Uniqueness of the trace packet)**.** *Fix the breakpoints τ_q. If*

$$f = s + \sum_{q=1}^{Q} \sum_{m=0}^{r-1} b_{q,m}\phi_{m,\tau_q}$$

with $s \in W^{r,p}(0,1)$, then

$$b_{q,m} = \left[f^{(m)}\right]_{\tau_q}.$$

The finite truncated power packet is therefore the unique packet supported at the declared breakpoints that removes all trace jumps through order $r-1$.

Proof. Every representative in $W^{r,p}(0,1)$ has derivatives through order $r-1$ that admit absolutely continuous representatives on compact subintervals, with matching one sided traces at each interior point. Taking the jump of the derivative of order m therefore removes the contribution of s. The packet ϕ_{m,τ_q} has unit jump in its derivative of order m, while all other declared packets have zero jump at that derivative order and breakpoint. Hence the remaining jump is exactly $b_{q,m}$. □

Remark E7.4. The theorem isolates only finitely many trace jumps. More general free discontinuity models may contain jump sets, Cantor parts, or singular derivatives that are not represented by a finite truncated power sum. The natural ambient theory is related to bounded variation and free discontinuity spaces [AFP00].

Let X be a normed linear space and let $Q : X \to X$ be bounded and linear. The next identity is elementary, but it is the central separation principle.

Theorem E7.5 (Exact retained packet identity)**.** *Let $f = s + j$ in X. Define*

$$\tilde{f} = Qs + j.$$

Then

$$\boxed{f - \tilde{f} = (I - Q)s.}$$

Consequently,

$$\|f - \tilde{f}\| = \|s - Qs\|.$$

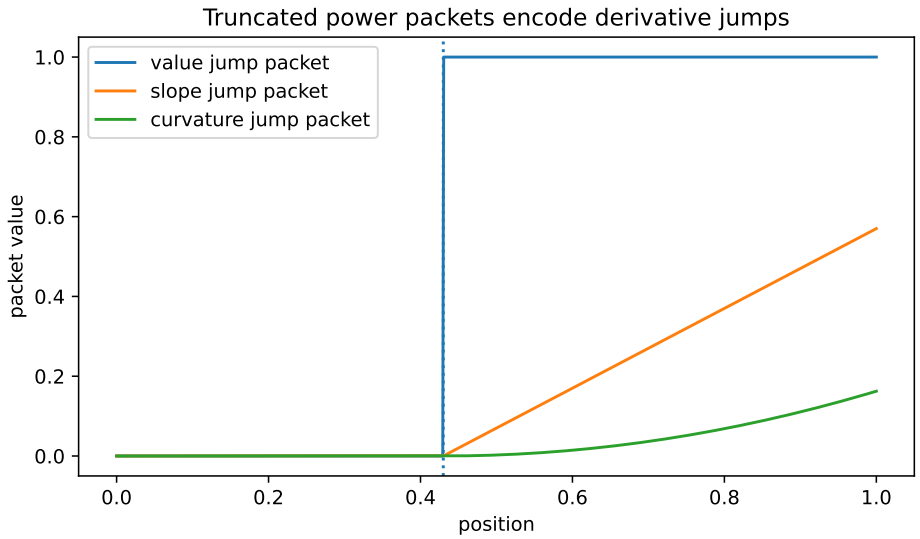


Figure E6. Truncated power packets encode jumps in a function and in its successive derivatives.

Proof. Subtract:

$$f - \tilde{f} = s + j - Qs - j = (I - Q)s.$$

□

Remark E7.6. The theorem assumes that the packet j is known. It does not supply a detector. It also does not say that every representation of f as $s + j$ is useful. The point is that once a meaningful packet has been identified, its approximation error can be removed from the smooth approximation problem exactly.

Corollary E7.7 (Sobolev rate after packet separation). *Suppose Q_m satisfies*

$$\|s - Q_m s\|_{L^p} \le C 2^{-mr} \|s\|_{W^{r,p}}$$

for every $s \in W^{r,p}(0,1)$. If $f = s + j$ and j is retained, then

$$\|f - (Q_m s + j)\|_{L^p} \le C 2^{-mr} \|s\|_{W^{r,p}}.$$

The same conclusion applies to the higher order decomposition in theorem E7.2.

Proof. Use theorem E7.5 and the assumed approximation estimate. □

Theorem E7.8 (Reconstruction with an estimated packet). *Let $Q_m : X \to X$ be linear, let $f = s + j$, let $\hat{j}$ be an estimated packet, and define*

$$\hat{f}_m = Q_m(f - \hat{j}) + \hat{j}.$$

Then

$$\boxed{f - \hat{f}_m = (I - Q_m)s + (I - Q_m)(j - \hat{j}).}$$

If Q_m is bounded, then

$$\|f - \hat{f}_m\| \le \|s - Q_m s\| + (1 + \|Q_m\|)\|j - \hat{j}\|.$$

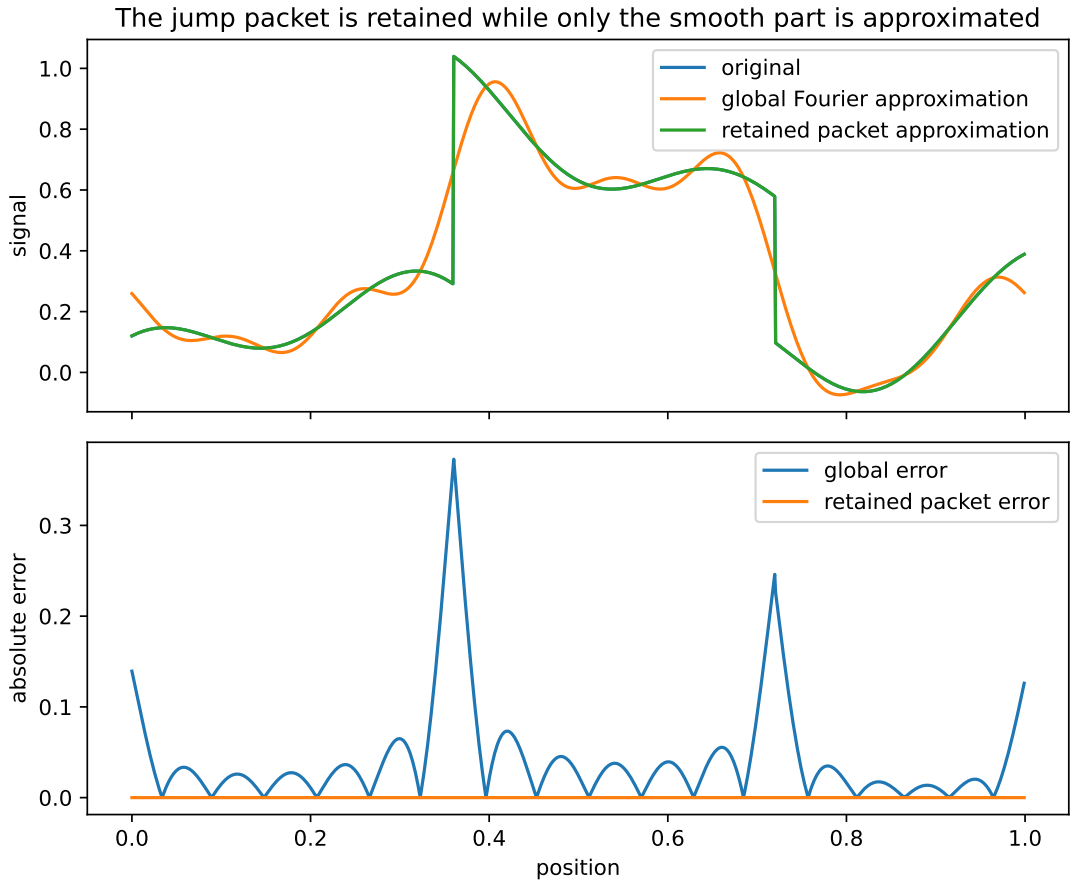


Figure E7. A global Fourier approximation must represent the jumps. A retained packet approximation applies the Fourier truncation only to the smooth component.

Proof. Since $f - \hat{j} = s + (j - \hat{j})$,

$$\hat{f}_m = Q_m s + Q_m(j - \hat{j}) + \hat{j}.$$

Subtract this expression from $s + j$. The norm bound follows from

$$\|(I - Q_m)u\| \le (1 + \|Q_m\|)\|u\|.$$

□

E8 Exact error formulas for estimated packets

The error of an estimated packet is often described by a segmentation score. For approximation, an exact norm formula is more useful because it separates value errors from geometric disagreement.

Theorem E8.1 (Exact scalar region formula). *Let E, F be measurable subsets of a measure space, let $a, b \in \mathbb{C}$, and let $1 \le p < \infty$. Then*

$$\|a\mathbf{1}_E - b\mathbf{1}_F\|_p^p = |a-b|^p \mu(E \cap F) + |a|^p \mu(E \setminus F) + |b|^p \mu(F \setminus E).$$

For equal amplitudes,

$$\|a\mathbf{1}_E - a\mathbf{1}_F\|_p = |a|\mu(E \triangle F)^{1/p}.$$

Proof. The sets $E \cap F$, $E \setminus F$, and $F \setminus E$ are disjoint. The difference takes the values $a - b$, a, and $-b$ on these three sets and is zero elsewhere. Integrating its pth power gives the formula. □

Corollary E8.2 (Location error for one step). *Let $0 \le \tau, \hat{\tau} \le 1$ and $H_\tau = \mathbf{1}_{[\tau,1]}$. For $1 \le p < \infty$,*

$$\|aH_\tau - aH_{\hat{\tau}}\|_p = |a||\tau - \hat{\tau}|^{1/p}.$$

In the supremum norm, the error equals $|a|$ whenever $\tau \neq \hat{\tau}$.

Proof. The symmetric difference of the two intervals has length $|\tau - \hat{\tau}|$. The supremum statement follows because the two steps differ by a on a nonempty interval. □

Theorem E8.3 (Location stability for higher order packets). *Let $m \ge 1$, $1 \le p < \infty$, and $0 \le \tau, \hat{\tau} \le 1$. Then*

$$\|\phi_{m,\tau} - \phi_{m,\hat{\tau}}\|_{L^p(0,1)} \le \frac{|\tau - \hat{\tau}|}{(m-1)!((m-1)p+1)^{1/p}}.$$

For $p = \infty$,

$$\|\phi_{m,\tau} - \phi_{m,\hat{\tau}}\|_\infty \le \frac{|\tau - \hat{\tau}|}{(m-1)!}.$$

Thus location error is Lipschitz for every derivative jump packet of positive order, while a value jump has only the finite L^p modulus in corollary E8.2.

Proof. Assume $\tau < \hat{\tau}$. Differentiation with respect to the location parameter gives

$$\frac{\partial}{\partial u}\phi_{m,u}(t) = -\phi_{m-1,u}(t)$$

for almost every t. Hence

$$\phi_{m,\tau} - \phi_{m,\hat{\tau}} = \int_\tau^{\hat{\tau}} \phi_{m-1,u}\,\mathrm{d}u.$$

Minkowski's inequality gives

$$\|\phi_{m,\tau} - \phi_{m,\hat{\tau}}\|_p \le |\tau - \hat{\tau}| \sup_u \|\phi_{m-1,u}\|_p.$$

The supremum is bounded by the norm of $t^{m-1}/(m-1)!$ on $[0,1]$, which is the stated constant. The supremum norm argument is identical. □

E8.1 Several regions

Let $(E_i)_{i=0}^I$ and $(F_j)_{j=0}^J$ be measurable partitions of the same domain, up to null sets. Let a_i and b_j be the corresponding values. The index zero may be used for a background region.

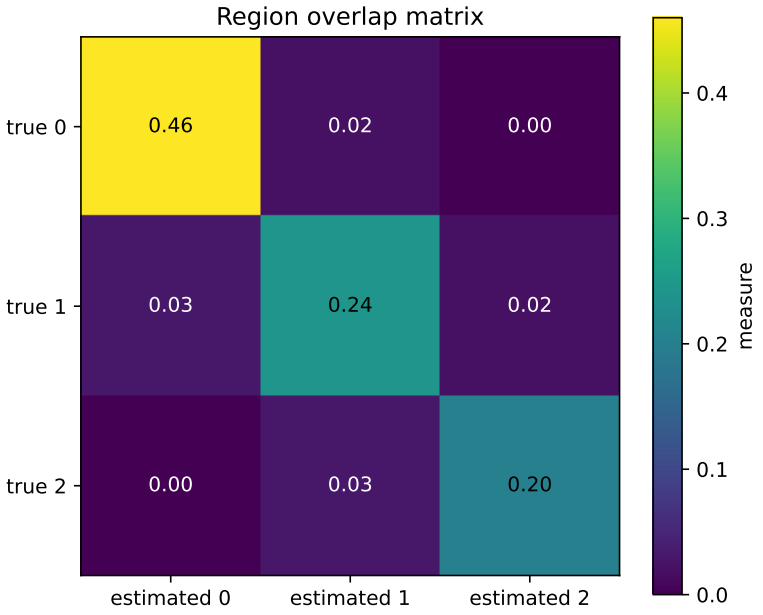


Figure E8. An overlap matrix records both correct regions and every type of misclassification. The exact packet norm weights each entry by the corresponding value difference.

Theorem E8.4 (Overlap matrix formula)**.** *Define*

$$M_{ij} = \mu(E_i \cap F_j).$$

For $1 \le p < \infty$,

$$\left\| \sum_{i=0}^{I} a_i \mathbf{1}_{E_i} - \sum_{j=0}^{J} b_j \mathbf{1}_{F_j} \right\|_p^p = \sum_{i=0}^{I} \sum_{j=0}^{J} |a_i - b_j|^p M_{ij}.$$

The row sums of M *are* $\mu(E_i)$*, and the column sums are* $\mu(F_j)$*.*

Proof. The intersections $E_i \cap F_j$ form a measurable partition. On such an intersection, the two piecewise constant functions have values a_i and b_j. Integrate the constant error over every intersection. The marginal identities follow by summing the partition pieces in a fixed row or column. □

Corollary E8.5 (Background and packet error)**.** *Suppose the true and estimated packets use the same amplitude list* $(a_i)_{i=0}^{I}$*, but possibly different regions. Then*

$$\|j - \hat{j}\|_p^p = \sum_{i,k} |a_i - a_k|^p \mu(E_i \cap F_k).$$

Only off diagonal overlaps contribute.

Proof. Apply theorem E8.4 with $b_k = a_k$. The diagonal terms vanish. □

E8.2 Boundary tube control

For a closed set Γ, write

$$N_\delta(\Gamma) = \{x : \operatorname{dist}(x, \Gamma) < \delta\}.$$

Definition E8.6 (Linear tube bound)**.** A boundary Γ has a linear tube bound if there are constants C_Γ and $\delta_0 > 0$ such that

$$\mu(N_\delta(\Gamma)) \le C_\Gamma \delta$$

for $0 < \delta < \delta_0$.

Bounded Lipschitz domains and many finite perimeter sets have estimates of this form, with constants controlled by geometric size. The next theorem only requires the displayed bound.

Theorem E8.7 (Geometric packet bound)**.** *Let E be a region with boundary Γ, and suppose*

$$E \triangle F \subseteq N_\delta(\Gamma).$$

If Γ has a linear tube bound and $0 < \delta < \delta_0$ lies in its stated range, then for $1 \le p < \infty$,

$$\|a\mathbf{1}_E - a\mathbf{1}_F\|_p \le |a|(C_\Gamma \delta)^{1/p}.$$

If amplitudes a and b differ, then

$$\|a\mathbf{1}_E - b\mathbf{1}_F\|_p \le |a-b|\mu(E \cap F)^{1/p} + (|a| + |b|)(C_\Gamma \delta)^{1/p}.$$

Proof. The equal amplitude case follows from theorem E8.1 and the tube inclusion. For unequal amplitudes, split the error into its value mismatch on $E \cap F$ and the two disagreement pieces. Apply the triangle inequality and the same tube estimate. □

Example E8.8 (A perturbed disk)**.** Let E and F be concentric disks of radii r and $r + \delta$ in $\mathbb{R}^2$, with $\delta > 0$. Then

$$\mu(E \triangle F) = \pi((r+\delta)^2 - r^2) = 2\pi r\delta + \pi\delta^2.$$

For equal amplitude a, the exact L^2 packet error is

$$|a|\sqrt{2\pi r\delta + \pi\delta^2}.$$

This gives the expected square root dependence on boundary displacement.

E9 Stable recovery of separated jumps

The detector needs a visible interval of thresholds

A smooth cell and bounded sample noise give one upper contrast bound. A jump cell gives a lower contrast bound after the same uncertainty is subtracted. Recovery is possible when the lower jump bound exceeds the upper smooth bound. The gap is a condition on the observation model, rather than an automatic consequence of packet coordinates.

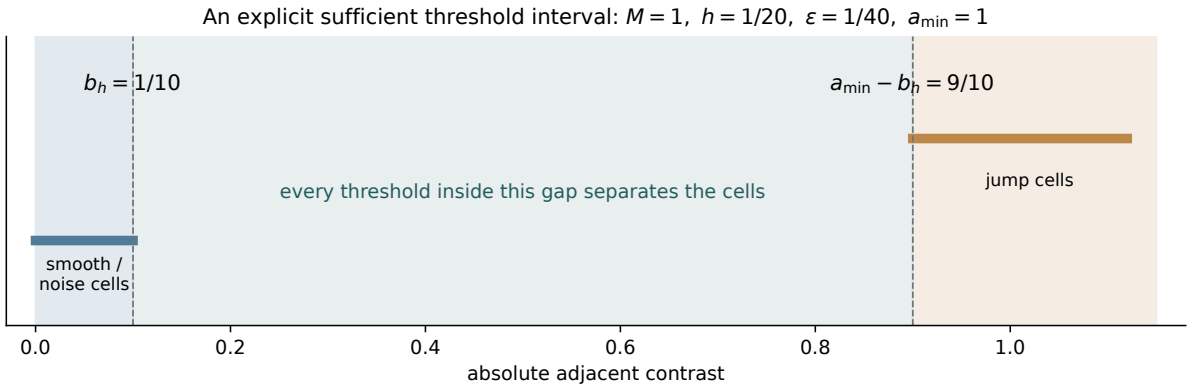


Figure E9. A sufficient threshold interval from exact rational contrast bounds. With the displayed model parameters, smooth and noise contrasts are at most $1/10$ and jump contrasts are at least $9/10$. Every threshold strictly between those values separates the cells under the sampling assumptions stated below. The figure does not assert an optimal threshold for other observation models.

The previous sections describe the error after a packet has been estimated. We now give a direct recovery theorem for one dimensional separated jumps. The detector is intentionally simple because the aim is to expose the exact contrast gap.

Let

$$t_k = kh, \qquad k = 0, \dots, n, \qquad h = \frac{1}{n}.$$

Assume

$$f(t) = s(t) + \sum_{q=1}^{Q} a_q H_{\tau_q}(t), \qquad H_\tau(t) = \mathbf{1}_{[\tau,1]}(t),$$

where s is Lipschitz with constant M, and $Q \geq 1$ is finite with nonzero jump amplitudes. The zero-jump case requires no minimum-amplitude condition. Suppose no jump lies at a sample point and no grid cell contains more than one jump. Observe

$$y_k = f(t_k) + \eta_k.$$

Define the adjacent contrast

$$D_k = y_{k+1} - y_k.$$

Lemma E9.1 (Contrast gap). *Assume $|\eta_k| \leq \varepsilon$ and set*

$$b_h = Mh + 2\varepsilon.$$

If the cell (t_k, t_{k+1}) contains no jump, then

$$|D_k| \leq b_h.$$

If it contains one jump of amplitude a_q, then

$$|D_k - a_q| \leq b_h$$

and therefore

$$|D_k| \geq |a_q| - b_h.$$

Proof. In a cell without a jump,

$$D_k = s(t_{k+1}) - s(t_k) + \eta_{k+1} - \eta_k.$$

The Lipschitz and noise bounds give $|D_k| \le Mh + 2\varepsilon$. In a cell with one jump, the same formula has the additional term a_q, which proves the second estimate. □

Theorem E9.2 (Deterministic jump cell recovery)**.** *Let*

$$a_{\min} = \min_q |a_q|$$

and assume

$$a_{\min} > 2b_h.$$

Choose a threshold θ satisfying

$$b_h < \theta < a_{\min} - b_h.$$

Then

$$\widehat{\mathcal{K}} = \{k : |D_k| > \theta\}$$

is exactly the set of grid cells containing jumps. If $\hat{\tau}_q$ is the midpoint of the detected cell and $\hat{a}_q = D_k$, then after matching by order,

$$|\hat{\tau}_q - \tau_q| \le \frac{h}{2}$$

and

$$|\hat{a}_q - a_q| \le b_h.$$

Proof. By lemma E9.1, every cell without a jump has contrast at most $b_h < \theta$. Every cell with a jump has contrast at least $a_{\min} - b_h > \theta$. Hence the detected set is exact. The midpoint of a cell is within $h/2$ of every point in that cell. The amplitude estimate is the second inequality in lemma E9.1. □

Corollary E9.3 (Jump count and sign recovery)**.** *Under the hypotheses of theorem E9.2, the number of detected cells equals Q, and*

$$\operatorname{sgn}(\hat{a}_q) = \operatorname{sgn}(a_q)$$

for every real valued jump.

Proof. Exact cell recovery gives the jump count. Since

$$|\hat{a}_q - a_q| \le b_h < |a_q|,$$

the amplitude estimate cannot cross zero. □

Corollary E9.4 (Packet reconstruction after detection)**.** *Let*

$$j = \sum_{q=1}^{Q} a_q H_{\tau_q}, \qquad \hat{j} = \sum_{q=1}^{Q} \hat{a}_q H_{\hat{\tau}_q}.$$

Under the hypotheses of theorem E9.2, for $1 \le p < \infty$,

$$\|j - \hat{j}\|_p \le Q b_h + \left(\frac{h}{2} \sum_{q=1}^{Q} |a_q|^p \right)^{1/p}.$$

If Q_m *is bounded and linear and*

$$\hat{f}_m = Q_m(f - \hat{j}) + \hat{j},$$

then

$$\|f - \hat{f}_m\|_p \le \|s - Q_m s\|_p + (1 + \|Q_m\|) \left[Q b_h + \left(\frac{h}{2} \sum_{q} |a_q|^p \right)^{1/p} \right].$$

Proof. Write

$$j - \hat{j} = \sum_q (a_q - \hat{a}_q) H_{\hat{\tau}_q} + \sum_q a_q (H_{\tau_q} - H_{\hat{\tau}_q}).$$

The first sum has norm at most $\sum_q |a_q - \hat{a}_q| \le Q b_h$. The location error interval for the qth jump is contained in its detected grid cell and has length at most $h/2$. Distinct detected cells are disjoint, so the location errors have disjoint supports. Their pth powers therefore add exactly, which gives the displayed location term. The reconstruction estimate follows from theorem E7.8. □

Remark E9.5 (Why finite L^p matters). A shifted step does not converge in the supremum norm until the location is exact. The finite L^p error does converge because the disagreement is confined to an interval whose length tends to zero.

Corollary E9.6 (Deterministic consistency)**.** *Assume* $h \to 0$ *along grids satisfying the preceding sampling assumptions,* $\varepsilon_h \to 0$*, the number of jumps is fixed, and the nonzero jump amplitudes and positive minimum separation remain fixed. Then the detected packet converges to the true packet in every finite* L^p *norm. If* Q_m *has a vanishing smooth approximation error and uniformly bounded norm, the complete reconstruction also converges in* L^p*.*

Proof. The gap condition holds for sufficiently small h. Then $b_h \to 0$, and the bound in corollary E9.4 tends to zero. □

Example E9.7 (A numerical threshold certificate)**.** Take $h = 1/256$, $M = 0.5$, and $\varepsilon = 0.002$. Then

$$b_h = \frac{0.5}{256} + 0.004 < 0.00596.$$

If every jump has magnitude at least 0.08, then $0.08 > 2b_h$. Any threshold between 0.00596 and 0.07404 recovers the exact jump cells. The location error is at most

$$\frac{1}{512}$$

and every amplitude error is less than 0.00596.

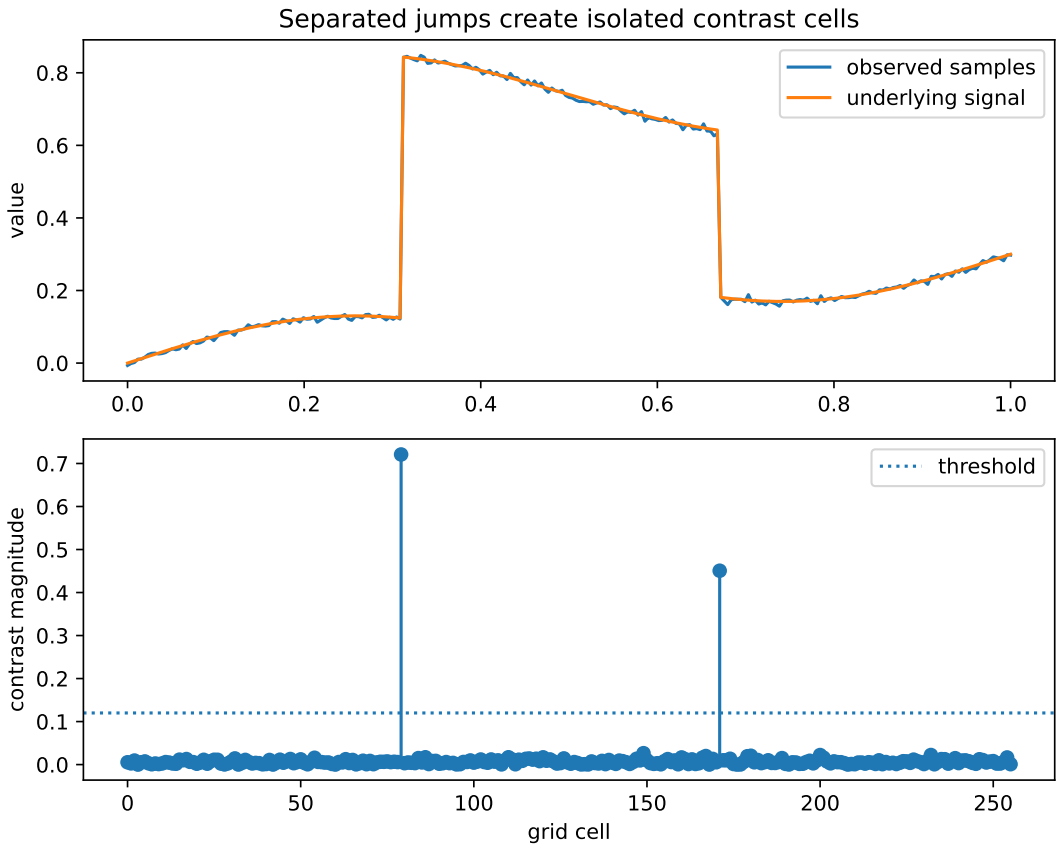


Figure E10. Separated jumps create isolated adjacent sample contrasts above the smooth and noise background.

E9.1 Sub Gaussian noise

Assume the noise variables are independent, centered, and σ sub Gaussian:

$$\mathbb{E}e^{\lambda\eta_k} \le e^{\sigma^2\lambda^2/2}.$$

Theorem E9.8 (Probability recovery bound). *Fix $0 < \delta < 1$ and define*

$$t_{n,\delta} = 2\sigma\sqrt{\log\left(\frac{2n}{\delta}\right)}$$

and

$$b_{h,\delta} = Mh + t_{n,\delta}.$$

With probability at least $1-\delta$, every contrast satisfies the conclusions of lemma E9.1 with b_h replaced by $b_{h,\delta}$.
If

$$a_{\min} > 2b_{h,\delta},$$

then thresholding between $b_{h,\delta}$ and $a_{\min} - b_{h,\delta}$ recovers every jump cell with probability at least $1-\delta$. The same location and amplitude bounds hold with $b_{h,\delta}$.

Proof. If $\sigma = 0$, every centered zero-sub-Gaussian noise variable vanishes almost surely, and the noise-free deterministic conclusion applies. For $\sigma > 0$, the difference $\eta_{k+1} - \eta_k$ is sub Gaussian with variance proxy $2\sigma^2$, so

$$\mathbb{P}(|\eta_{k+1} - \eta_k| > t) \le 2\exp\left(-\frac{t^2}{4\sigma^2}\right).$$

A union bound over the n cells gives

$$\mathbb{P}\left(\max_k |\eta_{k+1} - \eta_k| > t_{n,\delta}\right) \le \delta.$$

On the complementary event, repeat the deterministic proof. □

Corollary E9.9 (Repeated measurements). *Suppose R observations are averaged at every sample location, with all noise variables independent across sites and repetitions and each centered and σ sub Gaussian. Then theorem E9.8 holds with σ replaced by $\sigma/\sqrt{R}$. In particular, a sufficient recovery condition is*

$$a_{\min} > 2Mh + \frac{4\sigma}{\sqrt{R}}\sqrt{\log\left(\frac{2n}{\delta}\right)}.$$

Proof. The average of R independent σ sub Gaussian variables is $\sigma/\sqrt{R}$ sub Gaussian. Substitute this parameter in theorem E9.8. □

Remark E9.10. The displayed uniform noise certificate scales as $\sigma\sqrt{\log n}$. At fixed positive σ, it does not imply consistency of this detector. Decreasing the noise scale or averaging repeated measurements gives sufficient regimes; other averaging schemes require their own analysis.

Corollary E9.11 (Probability consistency). *Let $\sigma_n\sqrt{\log n} \to 0$ and $h = 1/n$. For every fixed $0 < \delta < 1$, along grids satisfying the preceding sampling assumptions, all jump cells are recovered with probability at least $1-\delta$ for sufficiently large n. For the fixed finite jump model above, along grids satisfying the preceding sampling assumptions, the packet error converges to zero in probability in every finite L^p norm.*

Proof. For each fixed $\delta > 0$, $b_{h,\delta} \to 0$. Apply theorem E9.8 and corollary E9.4. For any error tolerance $\epsilon > 0$, the high-probability bound is eventually smaller than ϵ, so the limit superior of the probability that the packet error exceeds ϵ is at most δ. Since δ is arbitrary, convergence is in probability. □

E9.2 Signals with values in a normed space

The recovery proof does not depend on an ordering of the signal values.

Proposition E9.12 (Vector jump recovery)**.** *Let the values lie in a normed space V. Assume*

$$\|s(t) - s(u)\|_V \le M|t - u|, \qquad \|\eta_k\|_V \le \varepsilon,$$

and let the jump vectors satisfy $\|a_q\|_V \ge a_{\min}$. Thresholding $\|D_k\|_V$ gives the same recovery theorem under the condition

$$a_{\min} > 2(Mh + 2\varepsilon).$$

Proof. Only the triangle inequality was used in lemma E9.1 and theorem E9.2. □

E10 Haar localization and annihilating differences

The adjacent difference detector is local in the sample domain. Wavelet coefficients and higher differences give related multiscale packets. In the Haar subsections the signal is defined on $\mathbb{R}$. Here the step convention is $H_\tau(t) = \mathbf{1}_{[\tau,\infty)}(t)$, whose restriction to $(0, 1)$ agrees with the preceding interval step. A chosen extension beyond the observation interval must use this half-line step convention, and the smooth extension must satisfy the stated Lipschitz hypothesis on every displayed wavelet support.

E10.1 Haar coefficient separation

Let

$$I_{j,k} = [k2^{-j}, (k + 1)2^{-j})$$

and let $\psi_{j,k}$ be the normalized Haar wavelet supported on $I_{j,k}$, positive on the left half and negative on the right half.

Theorem E10.1 (Smooth Haar coefficient bound)**.** *If s is Lipschitz with constant M, then*

$$|\langle s, \psi_{j,k}\rangle| \le \frac{M}{4}\, 2^{-3j/2}.$$

Proof. Let $L = 2^{-j}$ and let a be the left endpoint of the support. Pair every point $t \in [a, a + L/2]$ with $t + L/2$. Then

$$\langle s, \psi_{j,k}\rangle = L^{-1/2} \int_a^{a+L/2} \overline{s(t) - s(t + L/2)}\, \mathrm{d}t.$$

The integrand has magnitude at most $ML/2$, and the integration interval has length $L/2$. The result is $ML^{3/2}/4$. □

Theorem E10.2 (Exact Haar coefficient of a step). *Let $\tau \in I_{j,k}$, let $L = 2^{-j}$, and write*

$$u = \frac{\tau - kL}{L} \in [0, 1].$$

Then

$$\left|\langle aH_\tau, \psi_{j,k}\rangle\right| = |a| L^{1/2} \min\{u, 1-u\}.$$

Every Haar coefficient whose support does not cross τ is zero.

Proof. Away from the jump, the step is constant on the support and the Haar wavelet has zero mean. When the jump lies in the support, integrate the positive and negative halves directly. If $u \le 1/2$, the magnitude is $|a|uL^{1/2}$. If $u \ge 1/2$, it is $|a|(1-u)L^{1/2}$. □

Corollary E10.3 (Scale separation). *Suppose $f = s + aH_\tau + \eta$, where s is M Lipschitz and $\|\eta\|_\infty \le \varepsilon$. If the jump lies at relative distance at least ρ from both ends of $I_{j,k}$, then*

$$|\langle f, \psi_{j,k}\rangle| \ge \left(|a|\rho - \varepsilon - \frac{M}{4}L\right) L^{1/2}.$$

A wavelet support without a jump satisfies

$$|\langle f, \psi_{j,k}\rangle| \le \left(\varepsilon + \frac{M}{4}L\right) L^{1/2}.$$

Thus a threshold gap exists whenever

$$|a|\rho > 2\varepsilon + \frac{M}{2}L.$$

Proof. Combine theorems E10.1 and E10.2. The noise coefficient is at most

$$\|\eta\|_\infty \|\psi_{j,k}\|_1 = \varepsilon L^{1/2}.$$

The final inequality makes the lower bound on a jump support larger than the upper bound on a smooth support. □

E10.2 Two shifted grids

A jump on a dyadic boundary can be invisible to a wavelet at that scale. One additional grid removes this exact alignment.

Theorem E10.4 (Half cell shift guarantee). *Fix a cell length $L > 0$. Consider the grid with boundaries kL and the grid with boundaries $(k + 1/2)L$. Every point $\tau \in \mathbb{R}$ lies in a cell of at least one grid at distance at least $L/4$ from both cell boundaries.*

Proof. Reduce τ modulo L and write its representative as $x \in [0, L)$. If

$$L/4 \le x \le 3L/4,$$

then the distance from x to both boundaries of its cell in the original grid is at least $L/4$. If $x < L/4$ or $x > 3L/4$, then x lies in the cell of the shifted grid bounded by $-L/2$ and $L/2$, or in its translate,

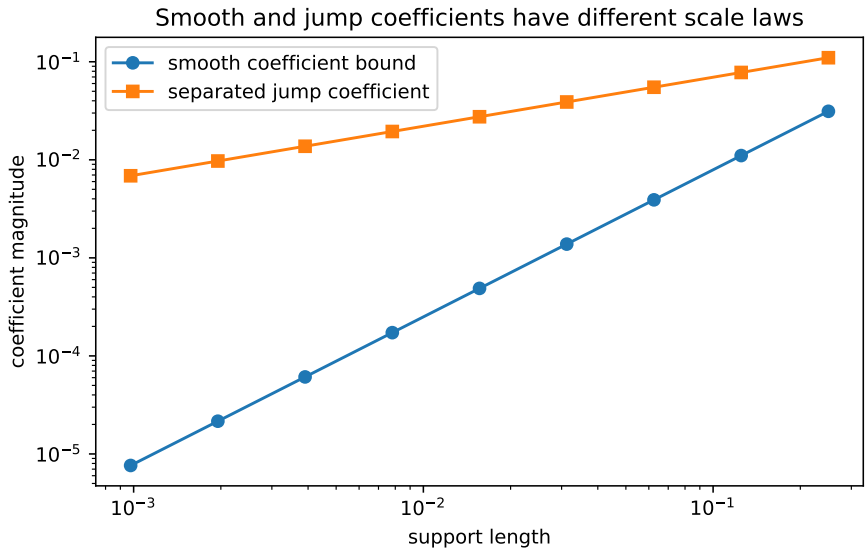


Figure E11. The smooth contribution decays like $L^{3/2}$, while a separated jump contribution decays like $L^{1/2}$.

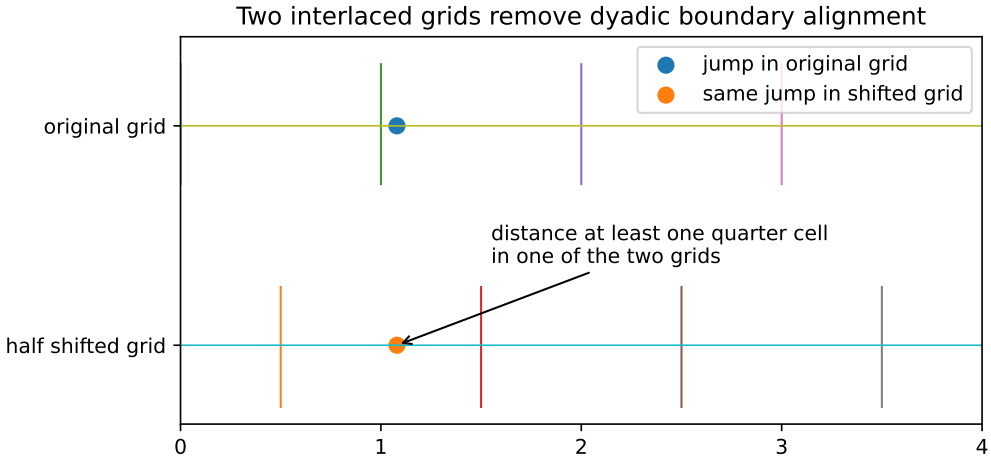


Figure E12. The boundaries of the two grids interlace. Every jump is well inside a cell in at least one grid.

at distance at least $L/4$ from both shifted boundaries. One of the two grids therefore has the required property. □

Corollary E10.5 (Alignment free two grid Haar detection). *Assume the support length L is smaller than the minimum jump separation. Analyze the signal with Haar wavelets on the original grid and on the half shifted grid. Every jump appears in a support with $\rho \geq 1/4$ in one of the two systems. Therefore a threshold gap exists independently of alignment whenever*

$$\frac{|a|}{4} > 2\varepsilon + \frac{M}{2}L.$$

Proof. Apply theorem E10.4 and then corollary E10.3 with $\rho = 1/4$. The separation assumption prevents a selected support from containing two jumps. □

E10.3 Higher differences

Let

$$(\Delta x)(n) = x(n+1) - x(n).$$

Then

$$\Delta^m x(n) = \sum_{r=0}^{m} (-1)^{m-r} \binom{m}{r} x(n+r).$$

Theorem E10.6 (Polynomial annihilation and boundary support)**.** *Let x be a sequence that agrees with a polynomial of degree at most d on each interval of a finite partition of $\mathbb{Z}$. Then*

$$\Delta^{d+1} x(n) = 0$$

whenever the complete stencil

$$\{n, n+1, \dots, n+d+1\}$$

lies inside one polynomial piece. Hence $\Delta^{d+1} x$ is supported in a band of at most $d+1$ addresses before each breakpoint.

Proof. The $(d+1)$st forward difference of a polynomial of degree at most d is zero. The only stencils for which this argument does not apply are those crossing a breakpoint. □

Proposition E10.7 (Noise amplification by differences)**.** *If $\|\eta\|_\infty \le \varepsilon$, then*

$$\|\Delta^m \eta\|_\infty \le 2^m \varepsilon.$$

Therefore no false response above $2^{d+1}\varepsilon$ can occur on a stencil lying inside one polynomial piece.

Proof. The absolute values of the binomial coefficients in Δ^m sum to 2^m. □

Corollary E10.8 (Robust breakpoint bands)**.** *Assume every true breakpoint produces at least one response of magnitude ρ in its $(d+1)$st difference band. If*

$$\rho > 2^{d+2}\varepsilon,$$

then thresholding at any level between $2^{d+1}\varepsilon$ and $\rho - 2^{d+1}\varepsilon$ detects a nonempty cluster near every breakpoint and creates no cluster away from the breakpoint bands.

Proof. Use theorem E10.6 and proposition E10.7. Noise cannot cross the threshold away from a breakpoint. At a response of magnitude ρ, the perturbed magnitude remains at least $\rho - 2^{d+1}\varepsilon$, which is above the threshold. □

E11 Packet separation and the Gibbs phenomenon

A Fourier partial sum is global. When the target has a jump, the partial sum must approximate that jump using continuous trigonometric polynomials. This creates the classical Gibbs oscillation. Standard accounts and recovery methods appear in [Zyg02, GS97].

Standard Fact E11.1 (Classical square-wave Gibbs behavior). Let $q(x) = \frac{1}{2}\operatorname{sign}(\sin x)$, whose jump at zero has size one. For $n \geq 1$, its partial sum through the first n positive odd frequencies is

$$Q_n(x) = \frac{2}{\pi} \sum_{k=0}^{n-1} \frac{\sin((2k+1)x)}{2k+1}.$$

At $x_n = \pi/(2n)$,

$$x_n \longrightarrow 0, \qquad Q_n(x_n) \longrightarrow \frac{\operatorname{Si}(\pi)}{\pi} = \frac{1}{2} + G, \qquad G \approx 0.089489872236,$$

where $\operatorname{Si}(z) = \int_0^z \sin(t)/t\, dt$ and $G = \operatorname{Si}(\pi)/\pi - 1/2 > 0$. Thus a nonzero overshoot persists along points approaching the jump. Scaling by a real amplitude a gives an overshoot or undershoot of magnitude $|a|G$.

For the limit, put $u_k = (k + \frac{1}{2})/n$. The identity

$$Q_n(x_n) = \frac{1}{\pi n} \sum_{k=0}^{n-1} \frac{\sin(\pi u_k)}{u_k} \longrightarrow \frac{1}{\pi} \int_0^1 \frac{\sin(\pi u)}{u}\, du = \frac{\operatorname{Si}(\pi)}{\pi}$$

is a midpoint Riemann sum, since the integrand has continuous value π at zero. This is the normalized classical example in [Nat26, Section 6.16(i), equations 6.16.1–6.16.4].

The square-wave example supplies a classical comparison. The following retained-packet identities do not require a general overshoot theorem. They change the approximation problem because the discontinuity is no longer represented by the Fourier partial sum.

Theorem E11.2 (Uniform convergence with exact jump packets)**.** *Let $f = s + j$ on a compact domain, where j is any bounded singular packet. Suppose $Q_m s \to s$ uniformly. Then*

$$\tilde{f}_m = Q_m s + j$$

converges uniformly to f, even when f is discontinuous:

$$\|f - \tilde{f}_m\|_\infty = \|s - Q_m s\|_\infty \longrightarrow 0.$$

There is no error proportional to the jump size because the jump is shared exactly by f and $\tilde{f}_m$.

Proof. Apply theorem E7.5 in the supremum norm. □

Theorem E11.3 (Estimated packet Gibbs bound)**.** *Let Q_m be linear and uniformly bounded on L^p, with*

$$\sup_m \|Q_m\| \le C_Q.$$

For $f = s + j$ and an estimated packet $\hat{j}_m$, define

$$\hat{f}_m = Q_m(f - \hat{j}_m) + \hat{j}_m.$$

Then

$$\|f - \hat{f}_m\|_p \le \|s - Q_m s\|_p + (1 + C_Q)\|j - \hat{j}_m\|_p.$$

Consequently, smooth approximation and packet recovery may be improved independently. No claim of Gibbs removal is justified unless both terms are controlled in the norm under consideration.

Proof. This is theorem E7.8 with the uniform operator bound. □

Corollary E11.4 (Boundary band error)**.** *Let Γ be the singular boundary and assume*

$$\mu(N_\delta(\Gamma)) \le C_\Gamma \delta$$

for small δ. For finite p,

$$\|f - \tilde{f}_m\|_{L^p(N_\delta(\Gamma))} \le (C_\Gamma \delta)^{1/p} \|s - Q_m s\|_\infty.$$

Proof. The error equals $s - Q_m s$. Bound it by its supremum and multiply by the measure of the boundary tube. □

Example E11.5 (Square wave Fourier tail)**.** Let

$$j(t) = \mathbf{1}_{[-a,a]}(t)$$

on the circle and let s be smooth. If Q_m is a Fourier partial sum, then $Q_m(s + j)$ has the ordinary oscillatory boundary layer. In contrast,

$$Q_m s + j$$

has error exactly $s - Q_m s$. The visual comparison in figure E13 illustrates this change in approximation target. It is not a new Fourier summability theorem.

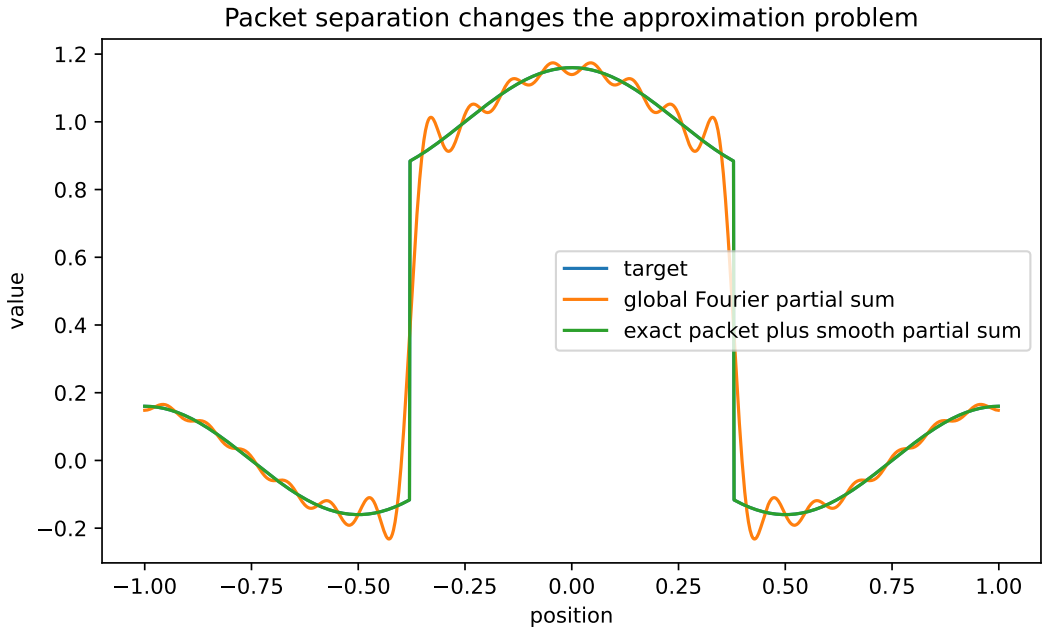


Figure E13. Global Fourier truncation represents the jump and exhibits an oscillatory boundary layer. Packet separation retains the jump and approximates only the smooth component.

E12 Nonlinear interactions in residue coordinates

Linear transfer matrices do not directly describe nonlinear products. Residue coordinates still obey exact conservation laws because integer addresses add modulo the packet modulus.

Theorem E12.1 (Residue law for Cauchy products)**.** *Let*

$$F(z) = \sum_{n \geq 0} f_n z^n, \qquad G(z) = \sum_{n \geq 0} g_n z^n$$

be formal power series. The same statement holds for power series that converge on a common disk. Decompose both series into residue packets modulo N:

$$F = \sum_{r=0}^{N-1} F_r, \qquad G = \sum_{s=0}^{N-1} G_s.$$

If $H = FG$, then its residue packet H_t is

$$\boxed{H_t = \sum_{r+s \equiv t \pmod{N}} F_r G_s.}$$

Proof. Every monomial in $F_r G_s$ has degree congruent to $r + s$ modulo N. Conversely, every coefficient of degree congruent to t is formed from pairs whose residues sum to t. Grouping the Cauchy product by this residue gives the formula. □

Theorem E12.2 (Shifted pointwise monomial law)**.** *Let*

$$y(n) = \prod_{j=1}^{m} x(n - a_j)$$

and write

$$a_j = Nc_j + b_j, \qquad 0 \le b_j < N.$$

For output residue r, define

$$r_j \equiv r - b_j \pmod{N}, \qquad 0 \le r_j < N,$$

and let

$$\kappa_{r,b_j} = \begin{cases} 1, & r < b_j, \\ 0, & r \ge b_j. \end{cases}$$

Then the output channel is

$$\boxed{y_r(q) = \prod_{j=1}^{m} x_{r_j}(q - c_j - \kappa_{r,b_j}).}$$

Proof. For $n = Nq + r$,

$$n - a_j = N(q - c_j) + r - b_j.$$

If $r \ge b_j$, this address has residue $r - b_j$ and coarse index $q - c_j$. If $r < b_j$, add N to the residue and subtract one from the coarse index. Multiplying the resulting channel values gives the formula. □

Corollary E12.3 (Polynomial shift filters)**.** *Every finite polynomial in shifted samples has an exact finite expression in residue coordinates. Each monomial selects a deterministic list of input residues and coarse shifts, and the complete output is their finite sum.*

Proof. Apply theorem E12.2 to each monomial and add the results. □

Example E12.4 (Quadratic nearest neighbor interaction)**.** For

$$y(n) = x(n)x(n - 1)$$

and modulus N,

$$y_r(q) = \begin{cases} x_r(q)x_{r-1}(q), & r \ge 1, \\ x_0(q)x_{N-1}(q - 1), & r = 0. \end{cases}$$

The carry at residue zero is the nonlinear analogue of a transfer crossing a coarse cell boundary.

E13 Finite numerical illustrations

The figures and tables in this section are finite checks and examples. They are not substitutes for the preceding proofs. Their purpose is to show the scale and shape of the terms appearing in the exact estimates.

A fixed depth Haar packet transform and a Fourier basis were applied to the same piecewise smooth test signal. The largest coefficients were retained in each representation.

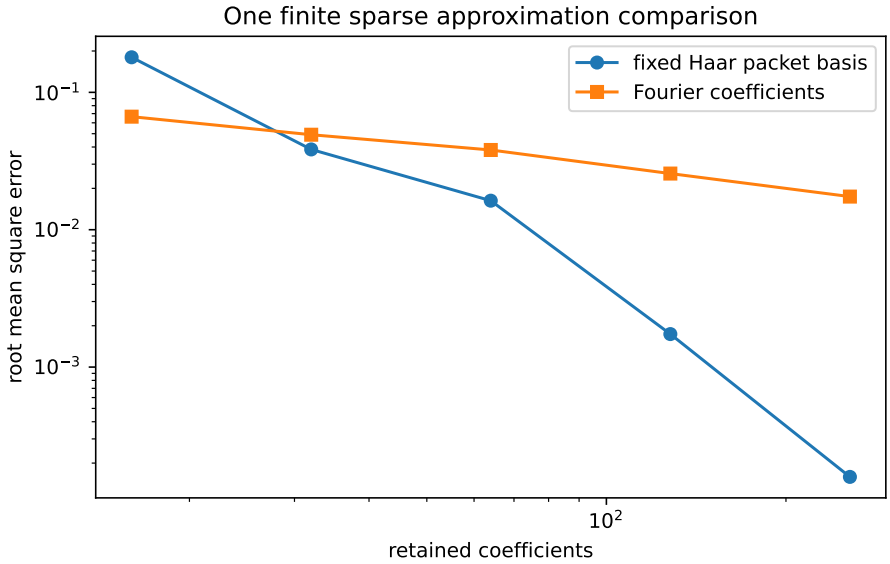


Figure E14. One finite sparse approximation comparison. Fourier coordinates are better at the smallest budget, while the fixed Haar packet basis becomes better after localized edge coordinates are resolved.

Table E1. Finite sparse approximation record for one test signal.

retained	Haar packet RMSE	Fourier RMSE
16	1.7999×10^{-1}	6.6522×10^{-2}
32	3.8414×10^{-2}	4.9153×10^{-2}
64	1.6267×10^{-2}	3.8056×10^{-2}
128	1.7387×10^{-3}	2.5631×10^{-2}
256	1.5870×10^{-4}	1.7424×10^{-2}

Table E2. Finite edge reconstruction record from the original computational study.

case	global	exact packet	estimated packet
one dimensional step	5.4023×10^{-2}	1.3692×10^{-4}	2.4029×10^{-2}
two dimensional disk	3.7643×10^{-2}	6.4752×10^{-5}	3.4043×10^{-3}
multiple regions	3.3740×10^{-2}	5.2118×10^{-7}	not evaluated

The table does not prove that Haar packets dominate Fourier coordinates for every signal. Smooth periodic oscillations may favor Fourier coordinates. Curved edges in two dimensions may favor directional systems. The geometric approximation results in [Don99, CD04] give much deeper statements for specific image classes.

The estimated packet rows used a narrow positive contrast synthetic model. They are not evidence for a general segmentation theorem. The exact packet rows verify theorem E7.5 numerically after the packet is supplied.

E14 Cyclic Cayley coordinates

> **Keep the rotation and its chart separate**
>
> For the phase factorization below, M and N are positive phase orders. The reflection coordinate rotates in the unit disk. The Cayley map expresses that same motion as a fractional linear impedance action. A pole of the chart does not mean that the projective action fails. This realization is independent of the separated jump detector.

This section records a secondary realization from the original signal manuscript. It is logically independent of the recovery theorems. The classical Smith chart uses the Cayley transform between normalized impedance and a reflection coordinate [Smi69].

Let

$$\mathbb{H} = \{z \in \mathbb{C} : \Re z > 0\}$$

and define

$$C(z) = \frac{z-1}{z+1}.$$

It maps $\mathbb{H}$ conformally onto the unit disk $\mathbb{D}$, with inverse

$$C^{-1}(w) = \frac{1+w}{1-w}.$$

For $\theta \in \mathbb{R}$, let

$$R_\theta(w) = \mathrm{e}^{\mathrm{i}\theta} w.$$

Theorem E14.1 (Cyclic Mobius action). *The pullback*

$$\Phi_\theta = C^{-1} R_\theta C$$

is the fractional linear map

$$\boxed{\Phi_\theta(z) = \frac{(1+\mathrm{e}^{\mathrm{i}\theta})z + (1-\mathrm{e}^{\mathrm{i}\theta})}{(1-\mathrm{e}^{\mathrm{i}\theta})z + (1+\mathrm{e}^{\mathrm{i}\theta})}.}$$

It preserves $\mathbb{H}$ and satisfies

$$\Phi_\theta \Phi_\varphi = \Phi_{\theta+\varphi}.$$

For an integer $N \geq 1$ and $\theta = 2\pi/N$, the map has order N.

Proof. Substitute $e^{i\theta}(z-1)/(z+1)$ into C^{-1} and simplify. Preservation of $\mathbb{H}$ follows because C maps it to $\mathbb{D}$, rotation preserves $\mathbb{D}$, and C^{-1} maps back. The group law follows by conjugating the rotation group law. When $\theta = 2\pi/N$, the Nth power is the identity. Conversely, if its kth power is the identity, conjugation by C and evaluation at $w = 1/2$ give $e^{2\pi i k/N} = 1$, so N divides k. Hence the order is exactly N. □

Corollary E14.2 (Impedance and admittance)**.** *For $N = 2$, $\theta = \pi$ and*

$$\Phi_\pi(z) = \frac{1}{z}.$$

Thus the two phase action is normalized impedance and admittance inversion.

Proof. Insert $e^{i\pi} = -1$ in the formula of theorem E14.1. □

Proposition E14.3 (Radial and phase coordinates)**.** *Write*

$$C(z) = \rho e^{i\varphi}, \qquad 0 \leq \rho < 1.$$

Then

$$C(\Phi_\theta(z)) = \rho e^{i(\varphi+\theta)}.$$

The radial mismatch ρ is invariant and the phase coordinate advances by θ.

Proof. This is the defining conjugacy $C\Phi_\theta = R_\theta C$. □

Proposition E14.4 (Coprime phase factorization)**.** *Let M and N be coprime. The cyclic phase labels modulo MN are equivalent to pairs of labels modulo M and modulo N:*

$$\mathbb{Z}/(MN)\mathbb{Z} \cong \mathbb{Z}/M\mathbb{Z} \times \mathbb{Z}/N\mathbb{Z}.$$

Under this identification, the rotation by $2\pi/(MN)$ is determined by its two projected cyclic actions.

Proof. This is the Chinese remainder theorem applied to the additive phase label. A label modulo MN is uniquely determined by its two residues, and addition of labels is preserved. □

E15 Limits and further directions

The one dimensional recovery theorem identifies an explicit admissible threshold interval for an adjacent contrast detector. More general recovery requires a broader observation model. A multiscale average can reduce fixed sample noise, but its bias depends on the smoothness class and the separation of nearby jumps. A useful next theorem should select the averaging scale from the data while retaining a finite probability certificate.

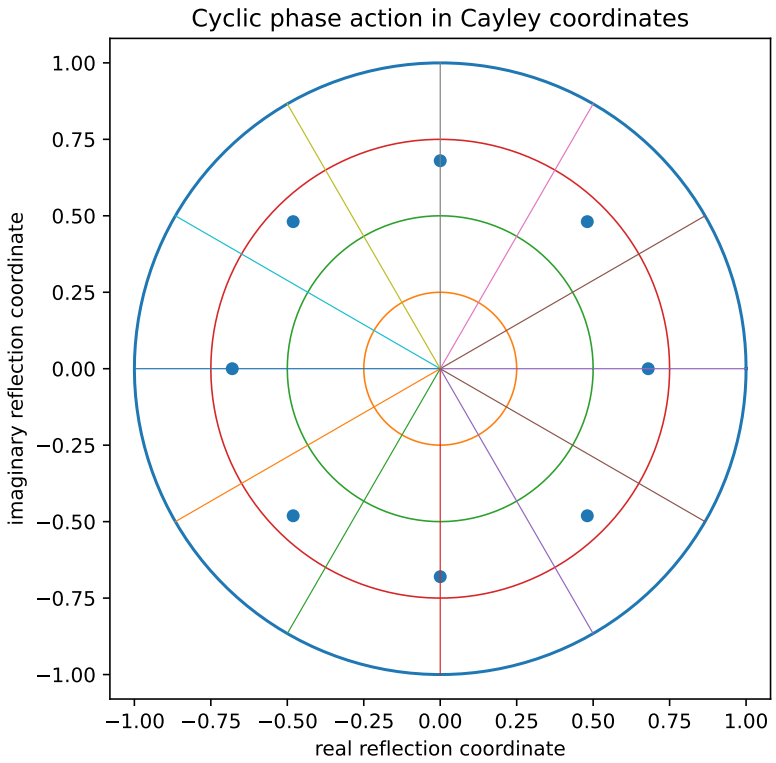


Figure E15. The cyclic action is an ordinary phase rotation in the reflection disk and a fractional linear action in the impedance half plane.

Higher dimensional recovery requires geometry. The overlap and tube formulas in appendix E8 become quantitative once a boundary estimate is known. What remains is a stable method that recovers topology, orientation, curvature, and region values under a declared noise model. Wedgelets and curvelets show why directional geometry is essential for broad image classes [Don99, CD04].

The best basis recursion is exact for additive objectives. Cross packet leakage, shared computation, and global hardware constraints introduce couplings between subtrees. Those problems require a larger compiler or an approximation theorem. The cost stability results in theorem E6.6 and corollary E6.7 identify one condition under which the additive decision survives perturbation.

The higher order singular packet theorem removes finitely many trace jumps. A more complete approximation theory should connect packet norms to geometric measure quantities in BV, piecewise Sobolev spaces, and free discontinuity models. It should also determine when a redundant packet dictionary can identify the derivative order of a singularity rather than merely its location.

Finally, the two shifted Haar grids remove one exact alignment failure, but they are redundant. A complete redundant theory should provide stable synthesis, noise aware coefficient aggregation, and a best basis rule that does not count the same singularity several times.

E16 Conclusion

Finite index sublattices give exact coordinates for lattice signals. In those coordinates, convolution is a matrix of transfer kernels. Perfect reconstruction is a matrix inverse identity. Approximate reconstruction is controlled by a multiplier norm. Frame bounds are pointwise singular value bounds. Lifting

steps are exact triangular coordinate changes. Every admissible packet tree gives a complete coordinate system, and every additive tree objective has an exact dynamic recursion.

The singular packet theory separates representation from recovery. A finite family of truncated powers records jumps in a function and its derivatives, leaving a globally Sobolev remainder under explicit trace assumptions. If the packet is known and retained, the error is exactly the smooth approximation error. If the packet is estimated, exact region overlap and location formulas quantify the remaining defect, while the reconstruction operator contributes a transparent stability factor.

For separated one dimensional jumps, a deterministic contrast gap gives exact cell recovery, midpoint location accuracy, and amplitude control. A sub Gaussian version follows from one union bound, and repeated measurements reduce the effective noise scale. Haar coefficients provide a second separation law because smooth coefficients decay one full power of scale faster than jump coefficients. Two shifted grids remove boundary alignment at a fixed scale. Higher differences annihilate piecewise polynomial interiors and confine their response to breakpoint bands.

The resulting chain is

$$\begin{aligned}&\text{lattice coordinates} \longrightarrow \text{transfer blocks} \longrightarrow \text{stable filter banks} \longrightarrow \text{packet trees}\\ &\longrightarrow \text{singular packet model} \longrightarrow \text{local recovery} \longrightarrow \text{smooth approximation rate.}\end{aligned}$$

Every arrow is exact or quantitatively controlled under the hypotheses stated in the corresponding result.

Part III: Forty worked visual plates

A second route through the mathematics

These forty plates develop the finite models used in the separate visual guide. The identifiers V1–V40 stay fixed across both documents. They lead from exact signal coordinates through filter transfers, adaptive decisions, packet errors, stable banks, and separated jump recovery. Every page gives the relevant manuscript locator. Finite arithmetic and diagrams explain the stated hypotheses and do not extend the formal contract.

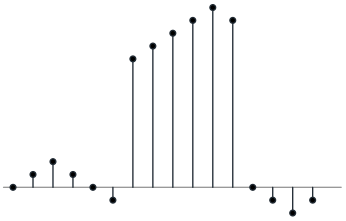
V1 / PAPER V / A WORKED VISUAL COMPANION

Three objects, three different questions

Traditional monograph: Section 1 (p. 2), Section 6 (p. 11), Section 11 (p. 19), Section 13 (p. 24).

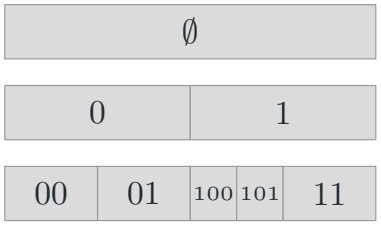
A packet calculus can reorganize a signal exactly, choose among finitely many representations, or describe a nonlinear coordinate geometry. These are not the same task. This guide keeps one concrete object in view for each, so that the reader can compute rather than only follow arrows.

SIGNAL COORDINATES



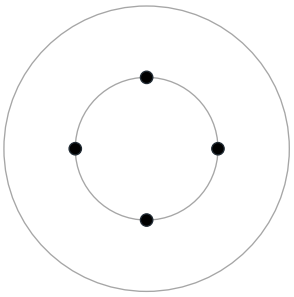
$f = s + j$ in $\mathbb{Q}^{16}$

FINITE TREE CHOICES



26 complete prunings

REFLECTION ORBIT



$\Gamma = \frac{1}{2} i^k$

A signal that can be checked by hand

Our main finite signal is $f = s + j \in \mathbb{Q}^{16}$. The background repeats

$$\tfrac{1}{4}(0, 1, 2, 1, 0, -1, -2, -1),$$

and $j[n] = 3$ at $6 \le n < 12$, with $j[n] = 0$ elsewhere. This is a discrete background model, not an assertion of continuum smoothness. Its energy is exactly 57. We use it for residue coordinates, Haar transforms, coefficient deletion, and known-packet cancellation.

A tree whose alternatives can all be seen

The full binary tree of depth three has only 26 complete prunings. We enumerate all of them, compute a unique mixed-depth optimum, and certify its stability with rational costs. The displayed objective is deliberately explicit, not claimed to be a universal signal-quality score.

A coordinate orbit with no hidden numerical poles

The four reflection points $\Gamma = i^k/2$ map to four exact impedances. A second orbit passes through infinity; homogeneous coordinates make that point an ordinary part of the construction.

> **Read this as:** Exact coordinates preserve information. An optimizer chooses coordinates. An estimator must still identify information not already supplied.

V2 / READING CONVENTIONS / KEEP THE TYPES VISIBLE

An atlas of the objects

Traditional monograph: Locator 5 (p. 34), Locator D (p. 35).

Several symbols in the paper describe different realizations of the same operator language. The following distinctions are used throughout this guide.

Object	Literal meaning	What it is not
S, δ_0	Sample shift and unit impulse	A finite truncation of every ℓ^2 signal
$P_{N,r} f$	A masked signal on the original lattice	The shorter decimated channel
$f_r[q]$	The value $f[Nq + r]$	An average of neighboring samples
D	One channel-index delay	Necessarily one original-sample delay
$E(D), R(D)$	Finite Laurent analysis and synthesis matrices	Values at one test frequency
W_α	The addressed Haar analysis operator	An edge detector by itself
$W_\alpha^* W_\alpha$	A projector on the original signal space	A scalar packet energy
Λ	A complete covering antichain of a finite tree	An arbitrary collection of nodes
$j, \hat{j}$	Known and estimated discontinuity packets	Interchangeable hypotheses
Γ, z	Reflection coefficient and normalized impedance	Coefficients that can be linearly interchanged

Three arithmetic conventions

FIR examples use bilateral sequences with finite support and *zero extension*. Haar examples use vectors of length 16, with lengths divisible by the required powers of two. The three-tap smoother and nonlinear neighbor example use *periodic* indexing. These boundary conventions are stated where they enter. None is silently substituted for another. The polynomial variable t on V – 20 indexes coefficients. The delay symbol D acts on channels. The Smith variable z is impedance. Keeping them separate prevents a visual resemblance from becoming an invalid identity.

> **Read this as:** A correct formula needs the correct object, product, norm, and boundary convention. A familiar-looking matrix does not supply them automatically.

V3 / EXACT ADDRESSES / THE RUNNING SIGNAL

Decimation is a permutation, not a loss

Traditional monograph: Theorem 2.1 (p. 3), Corollary 2.2 (p. 3).

For four phases, write every sample address uniquely as $n = 4q + r$ with $0 \le r < 4$. Analysis stores $f[n]$ at channel address (r, q). Synthesis puts that exact value back at $4q + r$.

FOUR PHASES: EVERY ADDRESS APPEARS ONCE

$r = 0$	$n = 0 :\ 0$	$n = 4 :\ 0$	$n = 8 :\ 3$	$n = 12 :\ 0$	$n = 4q + r$
$r = 1$	$n = 1 :\ \frac{1}{4}$	$n = 5 :\ -\frac{1}{4}$	$n = 9 :\ \frac{13}{4}$	$n = 13 :\ -\frac{1}{4}$	
$r = 2$	$n = 2 :\ \frac{1}{2}$	$n = 6 :\ \frac{5}{2}$	$n = 10 :\ \frac{7}{2}$	$n = 14 :\ -\frac{1}{2}$	$-1 = 4(-1) + 3$
$r = 3$	$n = 3 :\ \frac{1}{4}$	$n = 7 :\ \frac{11}{4}$	$n = 11 :\ \frac{13}{4}$	$n = 15 :\ -\frac{1}{4}$	$-5 = 4(-2) + 3$
	$q = 0$	$q = 1$	$q = 2$	$q = 3$	

Every cell contains an original address and its rational sample value. Shading marks the known jump packet, not an estimated feature or a frequency band.

What has changed? Only where the values are stored

The complete tuple of channels contains sixteen values, just as the original vector does. A single decimated channel is shorter, but keeping all four loses no samples. The residue projector $P_{4,r} f$ is different: it keeps the original lattice and writes zeros outside phase r.

$$\mathcal{S}_4 \mathcal{A}_4 f = f, \qquad \|f\|_2^2 = \sum_{r=0}^{3} \|f_r\|_2^2 = 57.$$

The norm on the channel tuple is the sum-of-squares Hilbert norm, not the maximum of the channel norms. This distinction matters in the infinite-dimensional statement.

Negative addresses are ordinary addresses

Euclidean division, rather than truncation toward zero, gives $-1 = 4(-1)+3$ and $-5 = 4(-2)+3$. The finite tests exercise both positive and negative sample addresses. The algebraic identity applies before any plotting window or finite buffer is chosen.

> **Read this as:** Downsampling one channel discards information. Splitting into all residue channels is an invertible address change.

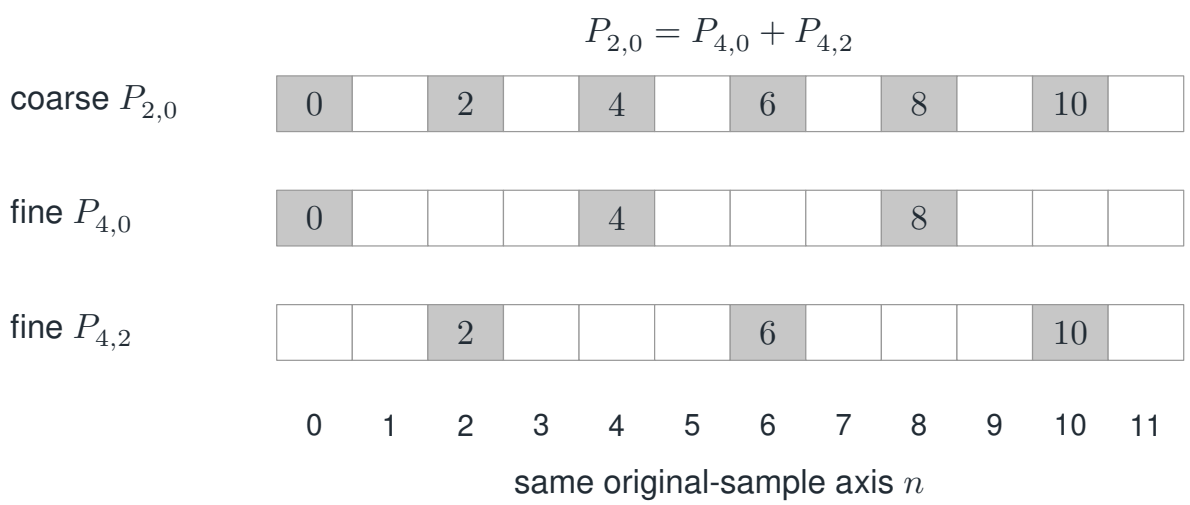
V4 / EXACT REFINEMENT / WHAT CAN BE ADDED

Refine packets on a common lattice

Traditional monograph: Theorem 2.3 (p. 5).

An even sample belongs to exactly one of residues 0 and 2 modulo four. Therefore the coarse even mask is the sum of two disjoint fine masks:

$$P_{2,0} = P_{4,0} + P_{4,2}.$$



The common horizontal axis is the original sample index. Empty cells denote masked-out addresses. There are no interpolated samples between the displayed cells.

Why the coordinate convention matters

The decimated channel $f_0[q] = f[2q]$ has its own index q. At modulus four the descendants are $f[4q]$ and $f[4q+2]$. These shorter arrays must be interleaved to recover the coarse channel. Adding them entrywise instead produces sums of different original samples. For example, at the first descendant address the values $f[0] = 0$ and $f[2] = 1/2$ are two separate values. Their sum $1/2$ cannot tell us both of them. Exact refinement is a disjoint partition, not an averaging rule or a new measurement.

The general formula

When N divides M,

$$P_{N,r} = \sum_{\substack{0 \le a < M \\ a \equiv r \pmod{N}}} P_{M,a}.$$

The divisibility hypothesis ensures that every fine residue class lies entirely inside one coarse class. Without it, this particular descendant relation is not the right refinement rule.

> **Read this as:** Finer coordinates can preserve the object exactly. Compressing their values to averages is an additional operation, with an additional information-loss question.

V5 / FIR TRANSFER / A FOUR-TAP EXAMPLE

A filter becomes a matrix of actual delays

Traditional monograph: Theorem 3.1 (p. 5).

Take the causal filter $h = (1, 2, -1, 1)$, with taps at $0, 1, 2, 3$, acting by $y[n] = \sum_q h[q] f[n-q]$. Resolve the input into even and odd channels. Let D denote one delay in the *channel* index.

$$h = (1, 2, -1, 1), \qquad D : \; u[n] \mapsto u[n-1]$$

	input 0	input 1
output 0	$1 - D$	$D^2 + 2D$
output 1	$D + 2$	$1 - D$

$$y_0 = (1 - D)x_0 + (2D + D^2)x_1$$

Reading one matrix entry

The odd-input contribution to the even output is $(2D+D^2)f_1$. The tap at original delay one reaches the preceding odd channel sample; the tap at delay three reaches the odd channel two positions back. These are different delays despite coming from the same input phase. The two channel equations are

$$y_0[n] = f_0[n] - f_0[n-1] + 2f_1[n-1] + f_1[n-2],$$
$$y_1[n] = 2f_0[n] + f_0[n-1] + f_1[n] - f_1[n-1].$$

Interleaving gives exactly the direct convolution, including its boundary samples under zero extension.

The general address calculation

For N phases, the block from input s to output k has kernel $h_{ks}[m] = h[Nm + k - s]$. This comes from the exact identity $Nn + k - q = N(n - m) + s$. It is a finite reindexing of taps, so no numerical transform of the input is needed. Evaluation of a bilateral transform is a separate step with the summability hypotheses stated in the manuscript.

> **Read this as:** The matrix does not approximate the filter. Its entries record which input phase is used, how far back to read, and what coefficient to multiply.

V6 / DELAY UNITS / AN IMPULSE MAKES THE DIFFERENCE VISIBLE

One sample is not one channel step

Traditional monograph: Theorem 4.1 (p. 7).

A one-sample delay swaps the two phases and wraps one of them into the preceding channel index. Its matrix is $J(D)$, not DI_2.

one original sample two original samples

$$J(D)^2 = \begin{bmatrix} 0 & D \\ 1 & 0 \end{bmatrix} = \begin{bmatrix} D & 0 \\ 0 & D \end{bmatrix}$$

$$\delta_0 \mapsto \delta_1$$

$$\delta_0 \mapsto \delta_2$$

$$y_0[n] = x_1[n-1], \quad y_1[n] = x_0[n]$$

channel delay 1 at $N = 2$ is original-sample delay 2

Trace one impulse

The input δ_0 has a single nonzero value in even channel address zero. Under $J(D)$ it appears in odd channel address zero: this is the original sample δ_1. Under DI_2 it stays even but moves to channel address one: this is δ_2. Thus

$$J(D)^2 = DI_2, \qquad H(D) = I_2 + 2J(D) - J(D)^2 + J(D)^3$$

recovers the previous page's four-tap transfer matrix. The same delay algebra explains both the off-diagonal phase swap and the channel powers.

Signed delays need the same care

For an original-sample delay d at modulus N,

$$y_k[n] = f_{(k-d) \bmod N}\left[n + \left\lfloor \frac{k-d}{N} \right\rfloor\right].$$

This includes advances when $d < 0$. The finite verification checks the formula on signed sample addresses. A bank with product $D^q I_N$ delays the original signal by Nq samples, not q samples.

> **Read this as:** Always state the unit of a delay. A phase permutation and a channel delay together can represent one original sample.

V7 / FILTER BANKS / WHY A FREQUENCY SPOT-CHECK IS INSUFFICIENT

Perfect reconstruction is an operator identity

Traditional monograph: Theorem 4.1 (p. 7).

Consider the finite Laurent bank

$$E(D) = \begin{pmatrix} 1 & D \\ 0 & 1 \end{pmatrix}, \qquad R(D) = \begin{pmatrix} 1 & -D \\ 0 & 1 \end{pmatrix}.$$

Its synthesis cancels the exact delayed cross-channel contribution introduced by analysis.

$E(D)$

1	D
0	1

$R(D)$

1	$-D$
0	1

$$R(D)E(D) = I$$

every impulse is recovered

$$B(D) = \operatorname{diag}(D, 1): \quad B(1) = I, \quad B(D) \neq I$$

testing one frequency cannot detect a channel delay

Two inverses, all inputs

Direct polynomial multiplication gives $RE = ER = I_2$. Since D acts as a shift, these identities imply perfect reconstruction on every bilateral channel sequence. With finite kernels, composition requires only finitely many operations at each address. The converse uses impulses. Insert an impulse in one input channel. Each output channel lists every coefficient of the corresponding transfer polynomial. If all such responses vanish for $RE - I$, every coefficient is zero; hence the polynomial matrix itself is zero.

A deliberately misleading test

The matrix $B(D) = \operatorname{diag}(D, 1)$ satisfies $B(1) = I_2$. At that one transform value it appears perfect. In the time domain, however, it delays only the first channel. An impulse in that channel immediately distinguishes it from the identity. This is why a small set of successful frequency evaluations is not automatically a proof of the full Laurent identity. A separate degree bound and a sufficient interpolation argument would be needed to turn finitely many evaluations into such a certificate.

> **Read this as:** Exact reconstruction concerns every coefficient of the transfer operator, not just an attractive response curve or one evaluation point.

V8 / HAAR ENERGY / EDGE ALIGNMENT

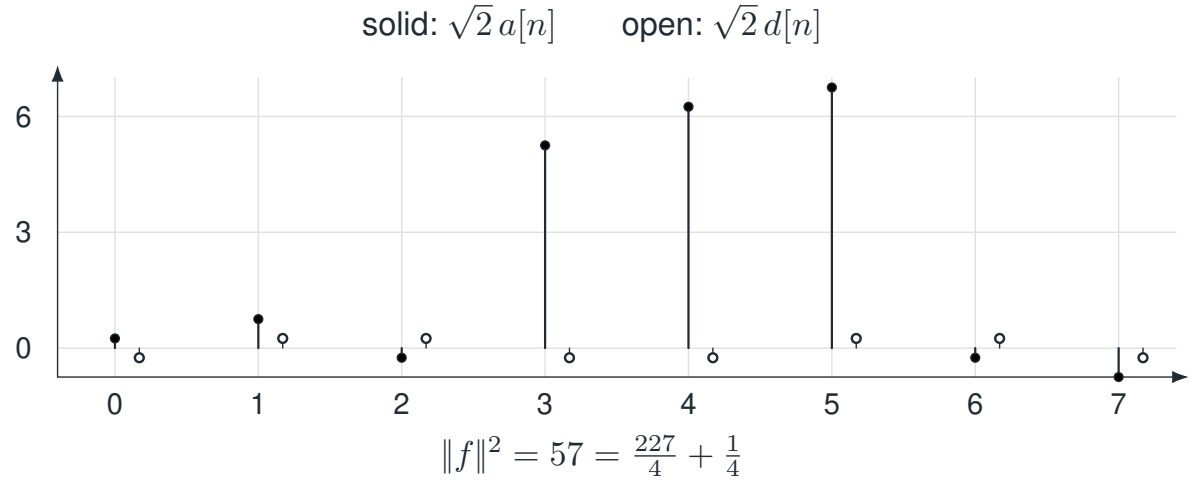
A jump can hide from the first Haar split

Traditional monograph: Corollary 4.2 (p. 8).

For the running signal, Haar analysis gives

$$a[n] = \frac{f[2n] + f[2n+1]}{\sqrt{2}}, \qquad d[n] = \frac{f[2n] - f[2n+1]}{\sqrt{2}}.$$

The plot scales both channels by $\sqrt{2}$ so that all displayed ordinates are rational.



The exact energy calculation

The low channel has energy $227/4$, and the detail channel has energy $1/4$. Their sum is 57, exactly the input energy. The normalization is essential: unnormalized sums and differences would multiply the total energy by two.

Why is the first detail channel so small?

The jump starts at sample 6 and ends just before sample 12. Both lie *between* the pairs $(0,1), (2,3), \ldots, (14,15)$. Inside every pair the jump contributes either $(0,0)$ or $(3,3)$, so its first-level difference is zero. The small detail values come entirely from the discrete background. This does not mean the edge is absent from the transform. The next split of the low channel compares neighboring pairs, and those comparisons do cross the jump. The next pages expose that contribution explicitly.

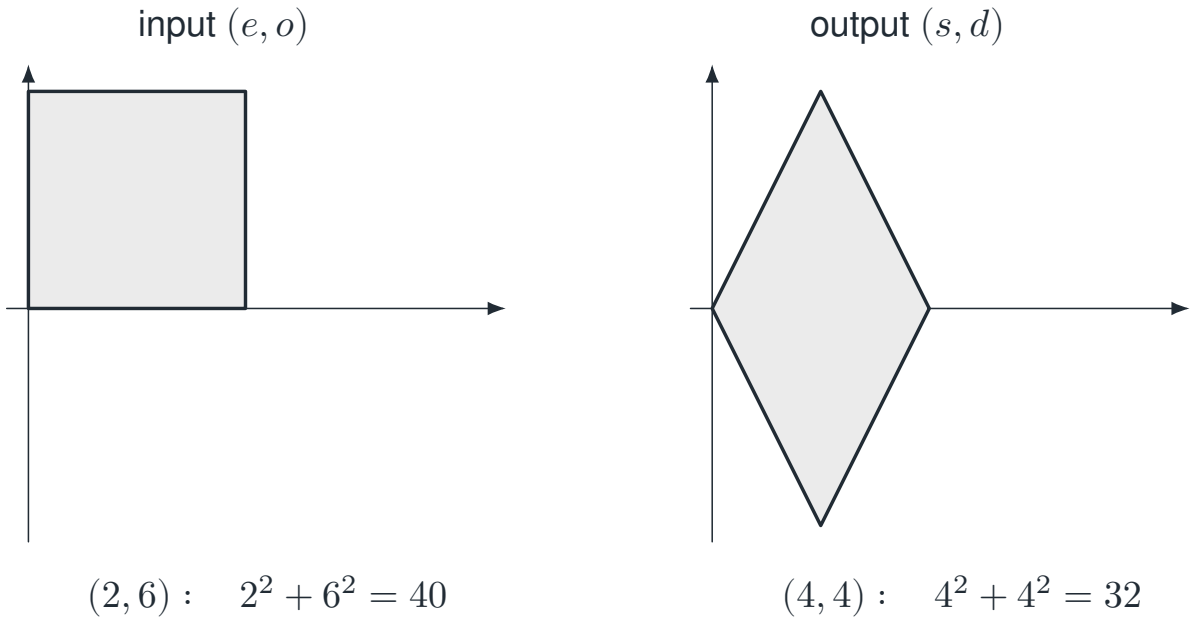
> **Read this as:** Haar energy is exact, but a particular detail level is not a universal edge detector. Edge visibility depends on alignment, scale, and the chosen packets.

V9 / PREDICT–UPDATE / INVERTIBILITY VERSUS ISOMETRY

Lifting preserves information, not energy

Traditional monograph: Theorem 4.3 (p. 10).

For an even/odd pair (e, o), form the prediction residual $d = o - e$, then update $s = e + d/2$. The inverse reads $e = s - d/2$, followed by $o = d + e$.



The square $[0, 4]^2$ and its exact image under the lifting matrix have the same area. The separate pair $(2, 6)$ illustrates that Euclidean energy need not be preserved.

$$\begin{pmatrix} s \\ d \end{pmatrix} = \begin{pmatrix} 1/2 & 1/2 \\ -1 & 1 \end{pmatrix} \begin{pmatrix} e \\ o \end{pmatrix}, \qquad \begin{pmatrix} e \\ o \end{pmatrix} = \begin{pmatrix} 1 & -1/2 \\ 1 & 1/2 \end{pmatrix} \begin{pmatrix} s \\ d \end{pmatrix}.$$

What determinant one does establish

The matrix is invertible, and in these real coordinates it preserves oriented area. The predict and update operations can be undone in reverse order. Applied to each pair, the construction gives exact finite-signal reconstruction.

What determinant one does not establish

The pair $(2, 6)$ becomes $(4, 4)$. Its squared Euclidean norm changes from 40 to 32. The lifting matrix is not unitary. Energy accounting must therefore use its actual coordinate metric or a separately normalized transform; invertibility alone cannot replace the Haar energy identity. All values in this example are rational. Integer-to-integer lifting with a rounding rule is a different algorithm. Its inverse and error conventions require their own specification and are not silently inferred from the displayed rational matrix.

> **Read this as:** Perfect reconstruction, determinant one, and norm preservation are different properties. This transform has the first two, not the third.

V10 / ACTUAL WAVELET PACKETS / FOUR RATIONAL CHANNELS

The second level resolves the hidden change

Traditional monograph: Theorem 5.1 (p. 10).

Apply Haar analysis to *both* children. A binary address records the chronological low/detail choices, with 0 for low and 1 for detail. Each depth-two channel contains four coefficients.

	coefficient positions within each packet				energy
00	$\frac{1}{2}$	$\frac{5}{2}$	$\frac{13}{2}$	$-\frac{1}{2}$	49
01	$-\frac{1}{4}$	$-\frac{11}{4}$	$-\frac{1}{4}$	$\frac{1}{4}$	$\frac{31}{4}$
10	0	0	0	0	0
11	$-\frac{1}{4}$	$\frac{1}{4}$	$-\frac{1}{4}$	$\frac{1}{4}$	$\frac{1}{4}$

$$\sum_{\alpha\in\{0,1\}^2} W_\alpha^* W_\alpha = I_{16}$$

The edge that first-level detail missed

Packet 01 is the detail child of the first low channel. It contains $-11/4$, the large change between neighboring pair averages. Packet 10 vanishes for this particular signal because the first-level differences alternate in cancelling pairs. Neither feature is a universal identity for all inputs. The packet energies are

$$49, \qquad 31/4, \qquad 0, \qquad 1/4,$$

which again sum to 57. Two factors of $1/\sqrt{2}$ explain why the depth-two coefficients are rational halves and quarters.

Coefficients and projectors are different objects

$W_\alpha f$ is the short coefficient vector. The original-space component is $W_\alpha^* W_\alpha f$. Summing these synthesized components, not the short arrays entrywise, reconstructs f:

$$f = \sum_{|\alpha|=2} W_\alpha^* W_\alpha f.$$

The finite verification constructs the actual analysis matrices and checks their product with their adjoints. The paper's ℓ^2 statement additionally establishes boundedness and the existence of the literal Hilbert adjoints.

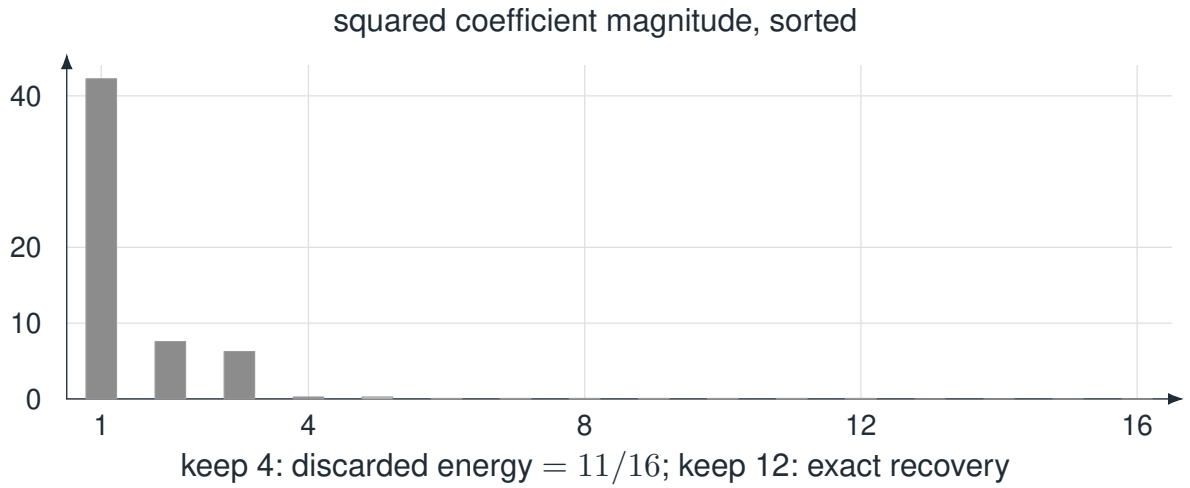
> **Read this as:** A packet address specifies an operator word. To add different packets as signals, synthesize them back into the common signal space first.

V11 / SPARSITY / AN EXACT ERROR LEDGER

Deleting coefficients is the approximation step

Traditional monograph: Section 10 (p. 18).

The complete depth-two transform is exact. Approximation begins only when we discard some of its sixteen coefficients. Order them by squared magnitude, with a deterministic address-and-position rule for ties.



Every discarded square has a meaning

In this fixed orthonormal basis, the squared reconstruction error equals the sum of the squared discarded coefficients. For our running signal:

kept coefficients k	1	2	4	8	12	16
squared error	$59/4$	$115/16$	$11/16$	$1/4$	0	0

The four zero coefficients belong to packet 10, so twelve coefficients suffice for exact reconstruction here. This is a property of the selected signal and basis, not a guarantee that all edge signals need only twelve coefficients.

Do not compare incompatible budgets

A cutoff m in a one-dimensional signed Fourier spectrum means $2m + 1$ bins, including zero. A budget of k largest coefficients is a different rule. Real Fourier synthesis may also require conjugate-pair closure. Neither count alone equals a bit-storage budget once amplitudes, phases, indices, or a selected tree must be encoded. The manuscript's Fourier-versus-Haar experiment is a finite comparison, not a proof that one basis dominates every signal class. Here we isolate the part that can be checked exactly: reconstruction error within one fixed finite basis.

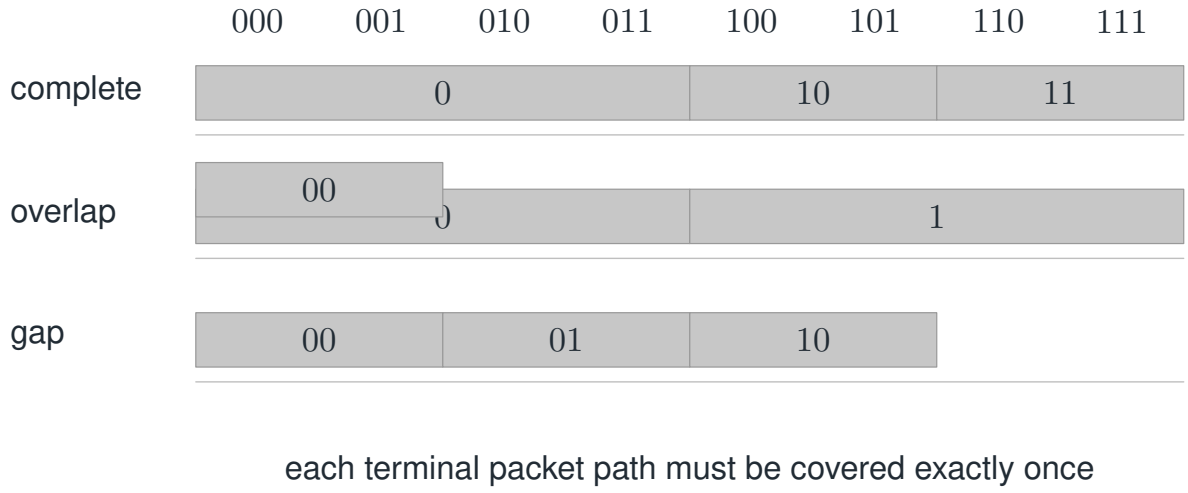
> **Read this as:** Changing coordinates creates no error. Throwing away coefficients does, and orthogonality makes that error exactly accountable.

V12 / COMPLETE PRUNINGS / NO GAPS AND NO DOUBLE COUNTING

A mixed-depth basis must cover every branch

Traditional monograph: Definition 11.1 (p. 19), Theorem 11.2 (p. 20).

A complete pruning chooses nodes of a finite refinement tree so that every root-to-terminal path meets exactly one selected node. The horizontal positions below are *terminal packet addresses*, not time intervals in the original signal.



Three candidate selections

The complete selection $\{0, 10, 11\}$ covers every terminal branch once. The selection $\{0, 00, 1\}$ covers the 00 branch twice: it is not an antichain. The selection $\{00, 01, 10\}$ misses the 11 branch entirely. For actual Haar packets, set $P_v = W_v^* W_v$. Parent-to-child conservation gives

$$P_v = P_{v0} + P_{v1}.$$

Replacing unselected parents by their children until the complete pruning is reached proves $\sum_{v \in \Lambda} P_v = I$. This is why the coefficients at different depths still form an exact coordinate system.

An exhaustive finite check

At depth three the pruning count obeys $a_0 = 1$ and $a_{d+1} = 1 + a_d^2$, giving $1, 2, 5, 26$. The supplied suite checks all 26 covering conditions and all 26 actual 16×16 projector-sum identities. These finite checks illustrate, but do not replace, the universal tree theorem.

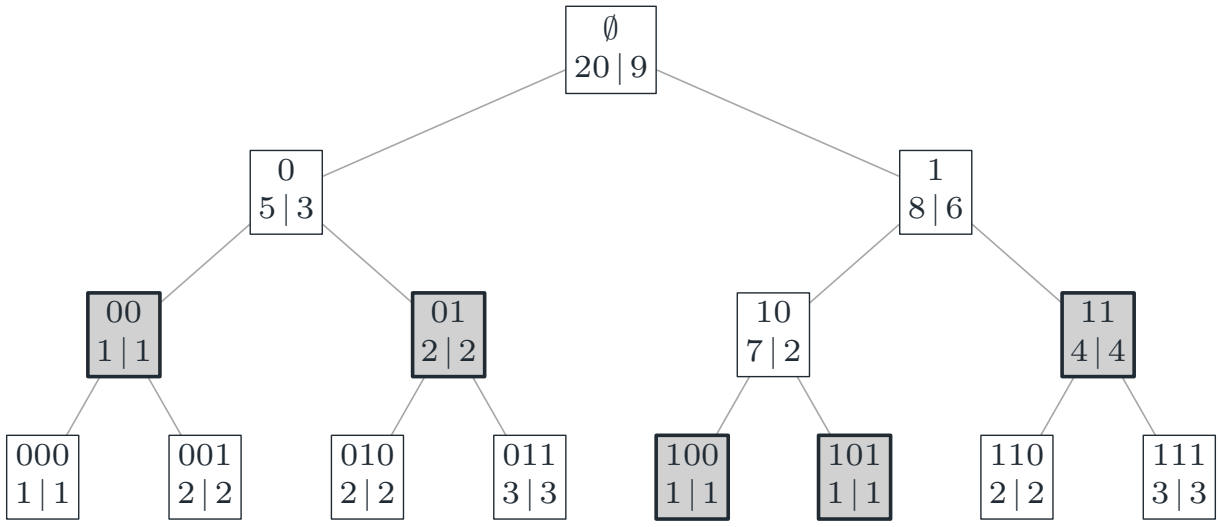
> **Read this as:** Mixed depth is allowed. Missing a terminal path or selecting an ancestor and its descendant is not.

V13 / ADDITIVE COSTS / EXACT DYNAMIC PROGRAMMING

Solve every alternative without searching every alternative

Traditional monograph: Theorem 11.3 (p. 20), Theorem 11.4 (p. 21).

Give every node the rational stop cost shown below. A node may either stop and pay its own cost, or refine and pay the already optimized costs of its children. The shaded nodes form the selected complete pruning.



node labels: stop cost c_v | optimal subtree cost $V(v)$

$$V(v) = \min\{c_v,\ V(v0) + V(v1)\}, \qquad V(v) = c_v \text{ at a terminal node.}$$

Read the calculation from the bottom upward

At 10, the children cost $1 + 1 = 2$, better than stopping for 7. At 11, stopping costs 4, better than $2 + 3 = 5$. The right subtree therefore costs 6, better than its stop cost 8. The left subtree costs $1 + 2 = 3$, better than 5. At the root, $3 + 6 = 9$ beats 20. The unique optimum is

$$\Lambda_* = \{00, 01, 100, 101, 11\}, \qquad J(\Lambda_*) = 9.$$

All 26 complete prunings are separately enumerated and give the same minimum. At equality, the rule stops, making the selector deterministic. A singleton tree needs no comparison. The costs here are supplied numbers. The theorem optimizes that stated additive objective; it does not prove those numbers encode the best denoising criterion. Coupled costs that cannot be written as a sum of selected-node costs need a different optimizer.

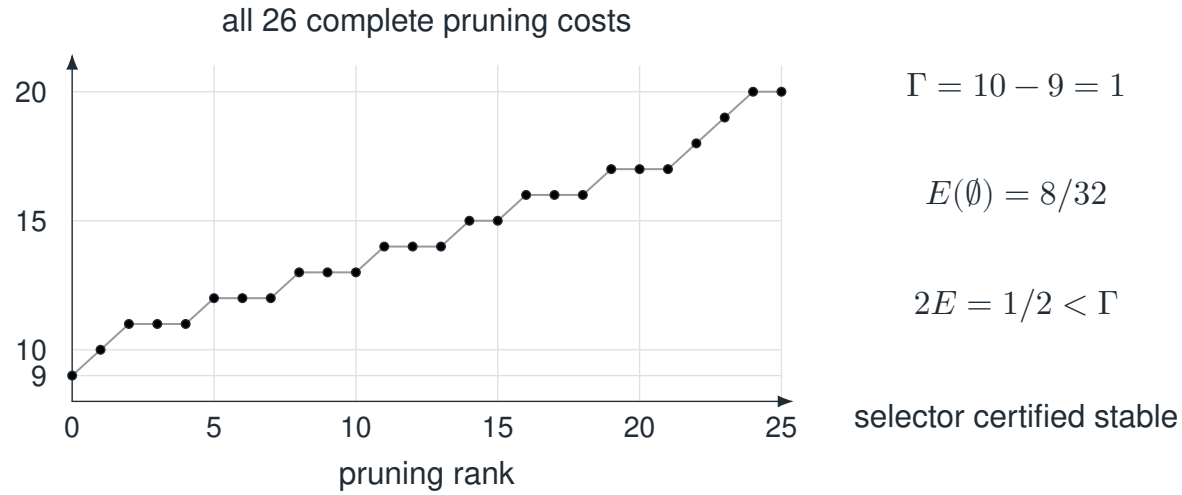
> **Read this as:** Global optimality follows from the exact stop-or-refine decomposition of a complete pruning, not from a greedy assumption.

V14 / A GLOBAL MARGIN / NOT A LOCAL HEURISTIC

How far can the costs move before the tree changes?

Traditional monograph: Theorem 11.3 (p. 20), Corollary 11.5 (p. 21).

The best pruning on the previous page costs 9; the cheapest competitor costs 10. Its exact global gap is therefore $\Gamma = 1$. The plate lists every complete-pruning cost in sorted order, giving each pruning its own horizontal rank.



Propagate an error budget as carefully as a cost

Suppose every node cost changes by at most $\varepsilon_v = 1/32$. A pruning may select as many as eight leaves, so its total cost can change by at most $8/32 = 1/4$. The recursive envelope proves this without guessing which pruning will be selected:

$$E(v) = \max\{\varepsilon_v,\ E(v0) + E(v1)\}, \qquad E(\emptyset) = \tfrac{1}{4}.$$

For any competitor Λ, the changed cost difference is bounded below by

$$J'(\Lambda) - J'(\Lambda_*) \geq \Gamma - 2E(\emptyset) = \tfrac{1}{2} > 0.$$

Thus the optimum is unchanged for *every* permitted simultaneous perturbation, not just a sampled noise realization. The envelope is over all feasible prunings, not just the five nodes in the current optimum.

Strict inequality has content

If two competing costs are 9 and 10, moving them to 9.5 and 9.5 removes uniqueness. Equality in $2E = \Gamma$ is therefore not a unique-selector certificate. For ordinary probability, the random node costs and the joint good event must be measurable. Separate nodewise probability bounds do not automatically give the probability of that joint event.

> **Read this as:** The exact selector is stable because its global gap exceeds the total worst-case movement of both competing costs.

V15 / AN EXACT IDENTITY / A CONDITIONAL INPUT

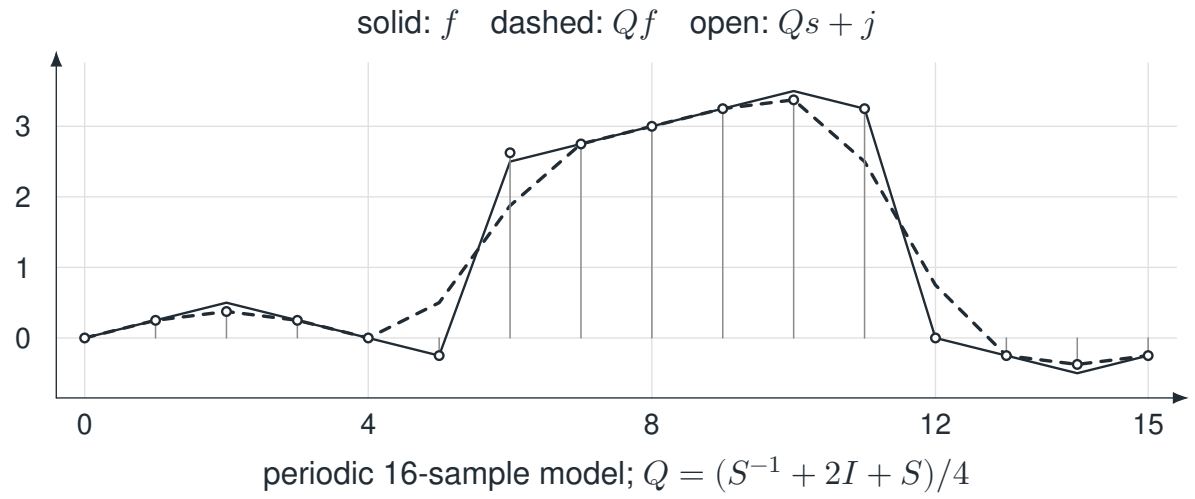
Retain the jump and approximate the other packet

Traditional monograph: Theorem 6.1 (p. 12), Corollary 6.2 (p. 12).

Return to the running signal $f = s + j$. For a concrete finite calculation, use the periodic three-tap smoother

$$(Qx)[n] = \tfrac{1}{4}x[n-1] + \tfrac{1}{2}x[n] + \tfrac{1}{4}x[n+1], \qquad n \in \mathbb{Z}/16\mathbb{Z}.$$

The plots compare smoothing the full signal with retaining its supplied jump packet. Every plotted sample is a rational number computed from the displayed formula.



The cancellation is the theorem

Define $\tilde{f} = Qs + j$. Then, sample by sample,

$$\boxed{f - \tilde{f} = s - Qs.}$$

By contrast, linearity gives

$$f - Qf = (s - Qs) + (j - Qj).$$

The second error includes a new term caused by smoothing the discontinuity. In this finite example that term is concentrated near the two jump boundaries. The identity itself requires no linearity of the approximation applied to s; linearity is used only in the comparison with Qf.

The input is not discovered by subtraction

The data here include the correct j. Replacing it with a wrong $\hat{j}$ retains the error $j - \hat{j}$, even when s is approximated perfectly. Multiple amplitudes and overlapping shapes are allowed if their full sum is supplied, but the identity does not estimate that sum from observations. Our finite periodic smoother is an illustration, not a new continuum approximation theorem. Its chosen boundary convention is part of the experiment.

> **Read this as:** Known-edge reconstruction removes the jump from the approximation problem. It does not remove the need to identify the jump.

V16 / A CONTINUOUS PULSE / EXACT ENDPOINT VALUES

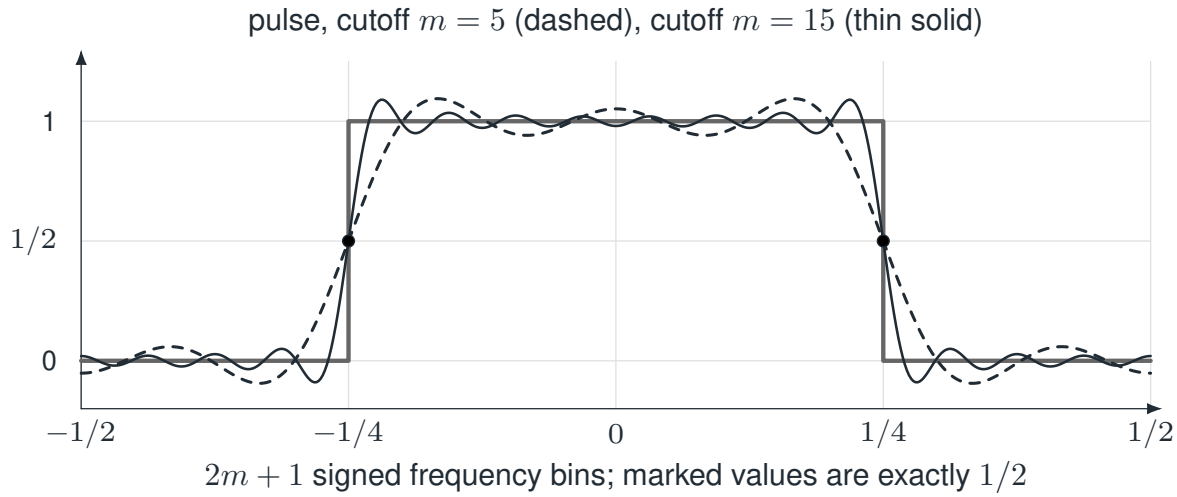
Why a Fourier cutoff cannot reproduce this jump pointwise

Traditional monograph: Section 6 (p. 11), Section 8 (p. 13).

Use a separate period-one example on $[-1/2, 1/2)$:

$$j(t) = \mathbf{1}_{\{|t|<1/4\}}, \qquad S_m j(t) = \tfrac{1}{2} + \frac{2}{\pi}\sum_{n=1}^{m} \frac{\sin(\pi n/2)}{n}\cos(2\pi n t).$$

This is the exact finite Fourier formula. The drawn curves sample it numerically; the endpoint calculation below is symbolic.



One value is fixed at every cutoff

At $t = \pm 1/4$, every summand vanishes because $\sin(\pi n/2)\cos(\pi n/2) = 0$ for integer n. Hence

$$S_m j(\pm 1/4) = \tfrac{1}{2} \qquad \text{for every } m \geq 0.$$

A larger cutoff resolves a narrower transition, but it does not make the finite trigonometric polynomial discontinuous. The two displayed cutoffs retain 11 and 31 signed frequency bins, respectively, not five and fifteen coefficients.

An exact known-packet comparison

Take $s(t) = \frac{1}{4}\cos(2\pi t) + \frac{1}{10}\cos(6\pi t)$. For $m \geq 3$ this smooth packet is already in the retained Fourier span. Thus $S_m s + j = s + j$ exactly in this special model, whereas $S_m(s + j)$ still replaces the pulse by $S_m j$. The values assigned at the two endpoints matter for pointwise error, but do not affect an L^p norm for finite p. The illustrated ringing is not a root enclosure or an asymptotic error certificate.

> **Read this as:** Increasing spectral resolution and retaining a known discontinuity are different operations, with different pointwise consequences.

V17 / MASK GEOMETRY / TRANSLATION BY ONE SIXTEENTH

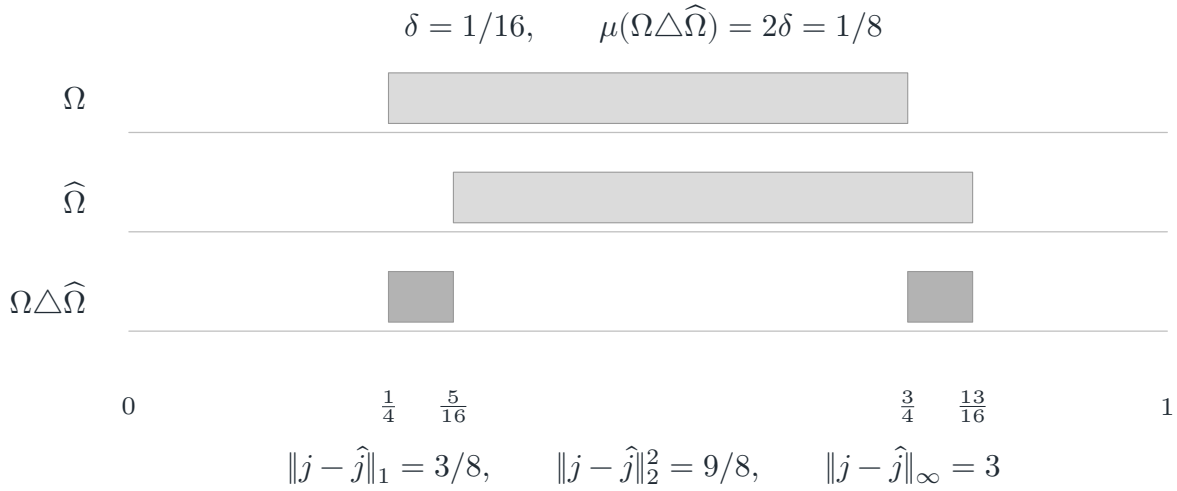
Small location errors, different norms

Traditional monograph: Theorem 7.1 (p. 13).

In Lebesgue measure on the line, let

$$\Omega = [\tfrac{1}{4}, \tfrac{3}{4}], \qquad \widehat{\Omega} = [\tfrac{5}{16}, \tfrac{13}{16}], \qquad a = \hat{a} = 3.$$

The two intervals have the same length. Their disagreement consists of one missed strip and one extra strip, each of width $1/16$.



$$\|j - \hat{j}\|_1 = 3/8, \qquad \|j - \hat{j}\|_2^2 = 9/8, \qquad \|j - \hat{j}\|_\infty = 3$$

$$|\Omega \triangle \widehat{\Omega}| = \tfrac{1}{8}, \qquad j - \hat{j} = 3(\mathbf{1}_\Omega - \mathbf{1}_{\widehat{\Omega}}).$$

error measure	L^1 norm	squared L^2 norm	L^∞ norm
exact value	$3/8$	$9/8$	3

Area shrinks while the missed jump keeps its height

For a translation by δ with $0 < |\delta| < 1/2$, the symmetric difference has measure $2|\delta|$. At finite p,

$$\|j - \hat{j}\|_p = 3(2|\delta|)^{1/p}.$$

It tends to zero as the displacement tends to zero. The essential supremum stays 3 for every nonzero displacement, because the error reaches height 3 on a set of positive measure. At exactly zero displacement all norms vanish. A nonempty disagreement set of measure zero would be different: it can affect the pointwise supremum while leaving the essential norm unchanged. This is why the paper distinguishes the two statements.

> **Read this as:** A shrinking boundary strip can give small integrated error and still contain a full-height jump error.

V18 / COUNTING MEASURE / AN EXACT FINITE BUDGET

Separate amplitude error from mask error

Traditional monograph: Theorem 7.1 (p. 13).

On the 16 sample addresses, let $\Omega = \{6, \dots, 11\}$ and $\widehat{\Omega} = \{7, \dots, 12\}$. Use true amplitude $a = 3$ and estimate $\hat{a} = 5/2$. There are six true samples, five overlapping samples, and two disagreement samples.

$$a = 3, \quad \hat{a} = 5/2, \quad |\Omega| = 6, \quad |\Omega \triangle \widehat{\Omega}| = 2$$

	4	5	6	7	8	9	10	11	12	13	14
j	0	0	3	3	3	3	3	3	0	0	0
$\hat{j}$	0	0	0	$\frac{5}{2}$	$\frac{5}{2}$	$\frac{5}{2}$	$\frac{5}{2}$	$\frac{5}{2}$	$\frac{5}{2}$	0	0
$j - \hat{j}$	0	0	3	$\frac{1}{2}$	$\frac{1}{2}$	$\frac{1}{2}$	$\frac{1}{2}$	$\frac{1}{2}$	$-\frac{5}{2}$	0	0

$$\|j - \hat{j}\|_1 = 3 + 5(1/2) + 5/2 = 8$$

The residual splits exactly as

$$3\mathbf{1}_\Omega - \tfrac{5}{2}\mathbf{1}_{\widehat{\Omega}} = \tfrac{1}{2}\mathbf{1}_\Omega + \tfrac{5}{2}(\mathbf{1}_\Omega - \mathbf{1}_{\widehat{\Omega}}).$$

The missed sample has error 3, the five shared samples have error $1/2$, and the extra sample has error $-5/2$. With *counting measure*,

$$\|j - \hat{j}\|_1 = 8, \qquad \|j - \hat{j}\|_2^2 = \tfrac{33}{2}, \qquad \|j - \hat{j}\|_\infty = 3.$$

Read the theorem as a budget, not an equality claim

Here the L^1 bound is attained:

$$|3 - \tfrac{5}{2}|\,|\Omega| + \tfrac{5}{2}|\Omega \triangle \widehat{\Omega}| = \tfrac{1}{2} \cdot 6 + \tfrac{5}{2} \cdot 2 = 8.$$

The L^2 triangle bound is $\frac{1}{2}\sqrt{6} + \frac{5}{2}\sqrt{2}$, and need not be sharp. A background estimate adds another term $\|s - \hat{s}\|_p$; cancellation between terms can make the total smaller than the bound. Normalized RMSE divides the L^2 norm by $\sqrt{16}$. A boundary-band RMSE uses the band size instead. Changing that denominator changes the reported quantity.

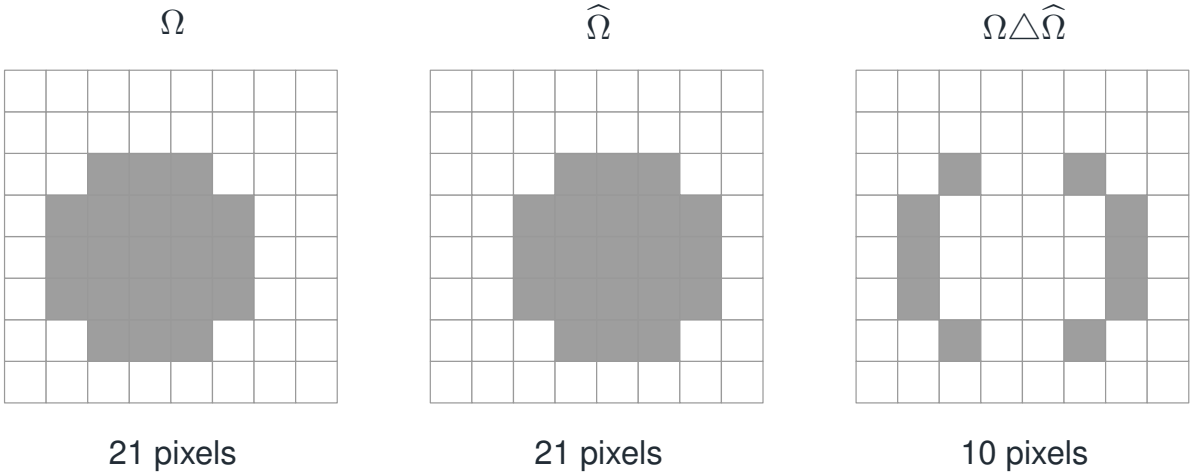
> **Read this as:** Mask error, amplitude error, and background error are separate mathematical inputs. A single reconstruction score conceals that separation.

V19 / A FINITE IMAGE / AN AMBIGUOUS OBSERVATION

Geometry localizes error while data may leave it ambiguous

Traditional monograph: Section 7 (p. 12), Section 9 (p. 15).

On the integer 8×8 grid, choose the disk-shaped mask $\Omega = \{(i, j) : (i-3)^2 + (j-3)^2 \le 5\}$ and translate it one pixel to the right. Each mask contains 21 pixels; their symmetric difference contains exactly 10.



A geometric error calculation is not a segmentation algorithm

For a common amplitude a, the squared counting-measure error is $10a^2$, entirely on the disagreement pixels. The full-image mean squared error is $10a^2/64$. Both are exact, but answer different normalization questions. Now consider the four-sample observation

$$y = (0, \tfrac{3}{2}, 3, 3).$$

It is consistent with either true signal

$$u = (0, 0, 3, 3), \qquad v = (0, 3, 3, 3)$$

under deterministic sup-norm noise at most $3/2$. Indeed $y = (u + v)/2$, and both error norms equal $3/2$. A rule receiving only y and that noise bound cannot be guaranteed to select both distinct true masks correctly.

What additional structure would have to do

A lower noise level, separation, contrast, geometry, or a specified prior can change the identification problem. The example rules out a guarantee at the *stated* noise radius and signal pair, not all recovery results. The manuscript's positive-contrast estimator is deliberately narrower than a universal segmentation method.

> **Read this as:** Exact synthesis can preserve an identified boundary. It cannot decide between two boundaries that the observation model makes indistinguishable.

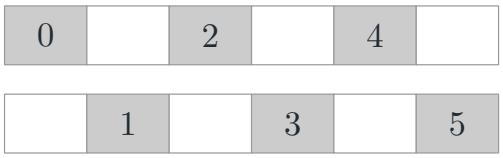
V20 / POINTWISE SIGNALS VERSUS CAUCHY COEFFICIENTS

Two products, two packet laws

Traditional monograph: Theorem 12.1 (p. 24).

The word “product” must be typed. Multiplying two signal values at the same time address is not the same operation as multiplying generating series. The distinction changes which packets can interact.

POINTWISE SIGNAL PRODUCT



$$(P_{2,0}x)\,(P_{2,1}y) = 0$$

CAUCHY COEFFICIENT PRODUCT

0	1	2
1	2	0
2	0	1

output label $(i + j) \bmod 3$

$$A = 1 + 2t + 3t^2,\ B = 2 + t^2 : \qquad P_{3,0}(AB) = 2 + 2t^3$$

Pointwise multiplication preserves the same address

For time-residue masks, $(P_{N,i}x)[n](P_{N,j}y)[n] = 0$ when $i \neq j$. Therefore

$$P_{N,k}(x \cdot y) = (P_{N,k}x) \cdot (P_{N,k}y).$$

Here the dot means multiplication at the same sample, not convolution.

Cauchy multiplication adds degrees

For formal series $A(t), B(t)$, the coefficient of t^n is a sum over $a + b = n$. Consequently the output residue is $i + j \pmod N$:

$$P_{N,k}(AB) = \sum_{i+j\equiv k\ (N)} (P_{N,i}A)(P_{N,j}B).$$

For $N = 3$, take $A = 1 + 2t + 3t^2$ and $B = 2 + t^2$. Direct multiplication gives

$$AB = 2 + 4t + 7t^2 + 2t^3 + 3t^4, \qquad P_{3,0}(AB) = 2 + 2t^3.$$

The $2t^3$ term comes from residues $1 + 2$, not $0 + 0$. At power zero, the empty product contributes 1 only in residue zero. These are formal coefficient identities and require no convergence assumption.

> **Read this as:** Before applying a packet multiplication rule, specify whether multiplication acts on sample values or on series coefficients.

V21 / FULL INPUT TUPLES / EXACT CYCLIC INDEXING

Nonlinear neighbors cross channel boundaries

Traditional monograph: Section 12 (p. 24).

For the periodic running signal define

$$F(x)[n] = x[n] + \tfrac{1}{2}x[n]x[n-1].$$

This is nonlinear and not a convolution operator. Nevertheless its two-channel representation is exact, provided the neighbor comes from the correct channel and index.

$$F(x)[n] = x[n] + \tfrac{1}{2}x[n]x[n-1]$$

$$F_0[n] = e[n] + \tfrac{1}{2}e[n]o[n-1] \qquad F_1[n] = o[n] + \tfrac{1}{2}o[n]e[n]$$

$$e[1] = 1/2, \quad o[0] = 1/4 \qquad o[1] = 1/4, \quad e[1] = 1/2$$

$$F(x)[2] = 9/16 \qquad F(x)[3] = 5/16$$

phase wrap changes the neighbor address; it does not remove the mixed term

Put $e[q] = x[2q]$ and $o[q] = x[2q+1]$, with channel indices taken modulo eight. Then

$$F(x)[2q] = e[q] + \tfrac{1}{2}e[q]o[q-1],$$
$$F(x)[2q+1] = o[q] + \tfrac{1}{2}o[q]e[q].$$

The even output needs the *previous* odd sample; the odd output needs the current even sample. This is the same carry in the address system that appeared in the one-sample delay matrix.

Check two actual outputs

The running values are $x[1] = 1/4$, $x[2] = 1/2$, and $x[3] = 1/4$, so

$$F(x)[2] = \tfrac{1}{2} + \tfrac{1}{2}\tfrac{1}{2}\tfrac{1}{4} = \tfrac{9}{16}, \qquad F(x)[3] = \tfrac{1}{4} + \tfrac{1}{2}\tfrac{1}{4}\tfrac{1}{2} = \tfrac{5}{16}.$$

Applying the same formula independently within each decimated array would use the wrong neighbors. Keeping the full channel tuple avoids that loss of information. The supplied suite compares every output sample in the two implementations using exact rational arithmetic. No convergence, contraction, or approximation property follows merely from writing these exact coordinates. Those require hypotheses on the nonlinear map and the problem being solved.

> **Read this as:** Exact packet coordinates remain available for nonlinear maps. They do not turn cross-channel interactions into independent channel problems.

V22 / THE CAYLEY CHART / EXACT QUARTER TURNS

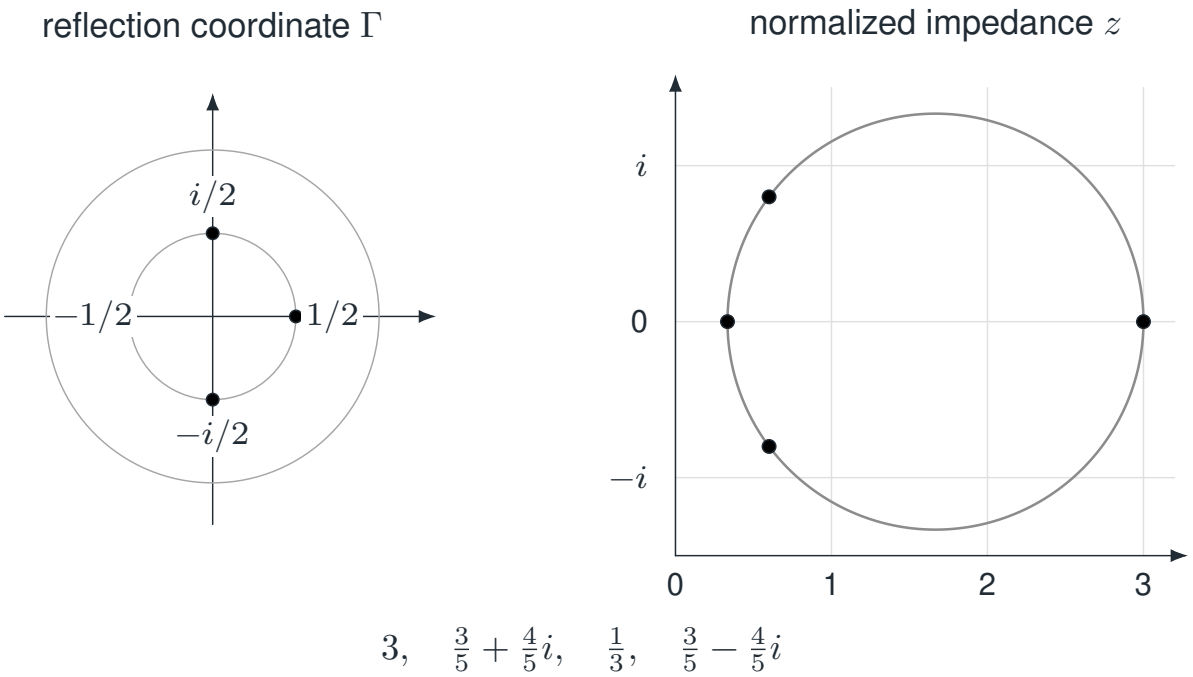
One reflection circle, four very different impedances

Traditional monograph: Theorem 13.2 (p. 26).

Use normalized impedance z and reflection coefficient Γ:

$$\Gamma = \frac{z-1}{z+1}, \qquad z = \frac{1+\Gamma}{1-\Gamma}.$$

The circle $|\Gamma| = 1/2$ is a constant-mismatch orbit. Its four quarter-turn points map to the exact impedances shown below.



$$3, \quad \frac{3}{5}+\frac{4}{5}i, \quad \frac{1}{3}, \quad \frac{3}{5}-\frac{4}{5}i$$

Γ	$1/2$	$i/2$	$-1/2$	$-i/2$
z	3	$3/5+4i/5$	$1/3$	$3/5-4i/5$

The coordinates preserve structure, not Euclidean distances

A quarter turn is a rotation in the reflection disk. After pulling back, it is a Möbius map, not a Euclidean rotation of the impedance plane. Equal reflection magnitudes need not give equal impedance magnitudes. The opposite points $1/2$ and $-1/2$ become 3 and $1/3$. The continuous impedance locus is the circle $(\operatorname{Re} z - 5/3)^2 + (\operatorname{Im} z)^2 = 16/9$, also drawn in the plate. Finite passive impedances with $\operatorname{Re} z \geq 0$ map to the closed disk except $\Gamma = 1$. That missing point is obtained only by adjoining impedance infinity. The interior maps to the open right half-plane. The classical Smith grid supplies the geometry; the cyclic labels specify exact rotations on it. Neither a new physical law nor a new optimal sampling theorem is implied by this coordinate description.

> **Read this as:** A simple action in one chart can be nonlinear in another. Conjugacy preserves the action law, not the apparent shape of a displacement.

V23 / HOMOGENEOUS COORDINATES / NO DIVISION BY ZERO

A pole is a chart boundary, not a broken group action

Traditional monograph: Theorem 13.2 (p. 26), Corollary 13.3 (p. 26).

Represent impedance by a nonzero pair $[u : v]$, where $[cu : cv] = [u : v]$ for $c \neq 0$. A finite impedance is $[z : 1]$; infinity is $[1 : 0]$. For a nonzero reflection multiplier w, use

$$A(w) = \frac{1}{2}\begin{pmatrix} 1+w & 1-w \\ 1-w & 1+w \end{pmatrix}.$$

$$A(i) = \tfrac{1}{2}\begin{pmatrix} 1+i & 1-i \\ 1-i & 1+i \end{pmatrix}$$



$z = 0$	$z = -i$	$z = \infty$	$z = i$
$\Gamma = -1$	$\Gamma = -i$	$\Gamma = 1$	$\Gamma = i$

$A(i)^4 = I$: the fourth step returns to $[0 : 1]$

The action is defined before a ratio is taken

The determinant is w, so the matrix cannot send a nonzero pair to zero. Direct multiplication gives

$$A(w)A(w') = A(ww'), \qquad A(1) = I.$$

For $w = i$, the orbit through zero is

$$[0 : 1] \longmapsto [-i : 1] \longmapsto [1 : 0] \longmapsto [i : 1] \longmapsto [0 : 1].$$

The third point is a legitimate projective point, even though a finite impedance formula has a zero denominator there. The second iterate is $A(-1)$, which swaps the two coordinates. Thus a half turn exchanges 0 and ∞ and sends each finite nonzero z to $1/z$. The matched point $\Gamma = 0$, equivalently $z = 1$, is fixed by every phase multiplier. It is not part of the boundary orbit above. The exact checks test homogeneous pairs and their rescaling equivalence, rather than introducing an artificial complex value for $1/0$.

> **Read this as:** Compute with homogeneous pairs first. A denominator becomes a chart-selection issue rather than an exception to the cyclic action.

V24 / DYADIC–ODD FACTORIZATION / TWELVE ADDRESSES

Residue labels are not impedance averages

Traditional monograph: Proposition 14.1 (p. 29).

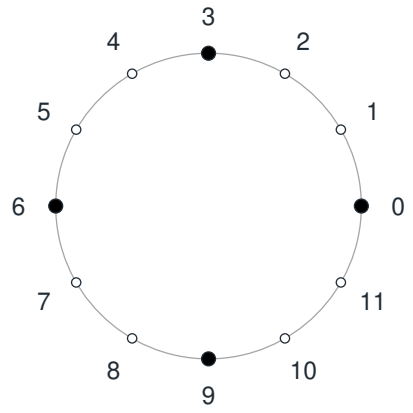
At phase order $12 = 4 \cdot 3$, the map

$$k \longmapsto (k \bmod 4,\ k \bmod 3)$$

is a bijection from twelve residue addresses to the 4×3 grid. Every cell below contains its unique original address.

	0	1	2
0	0	4	8
1	9	1	5
2	6	10	2
3	3	7	11

row $j \bmod 4$, column $j \bmod 3$



filled: the four coarse rays; open: the eight new rays

The factorization is an intersection of conditions

For integer sample addresses, including negative ones,

$$P_{12,k} = P_{4,k \bmod 4}\, P_{3,k \bmod 3}.$$

The product on the right is composition of two residue masks: both congruences must hold. Coprimality makes their intersection a single class modulo twelve. It is not a formula for multiplying or adding impedances.

Nested samples and nested projectors are different statements

The four coarse reflection rays occur at indices $0, 3, 6, 9$ of the twelve-ray grid. Thus the geometric sample set is nested. Separately, a coarse coefficient projector is the sum of its fine descendants in a common coefficient space. There is no corresponding rule saying that a coarse impedance is the average of its descendants. The inverse Cayley map is nonlinear. Even opposite reflection points have impedances 3 and $1/3$ in the preceding example; their average $5/3$ is not the impedance 1 of their averaged reflection coefficient zero.

> **Read this as:** CRT factors addresses. Refinement conserves coefficient packets. Neither operation authorizes linear averaging through a nonlinear chart.

V25 / LOCAL DERIVATIVES / FINITE INCREMENTS

Sensitivity grows before the pole is reached

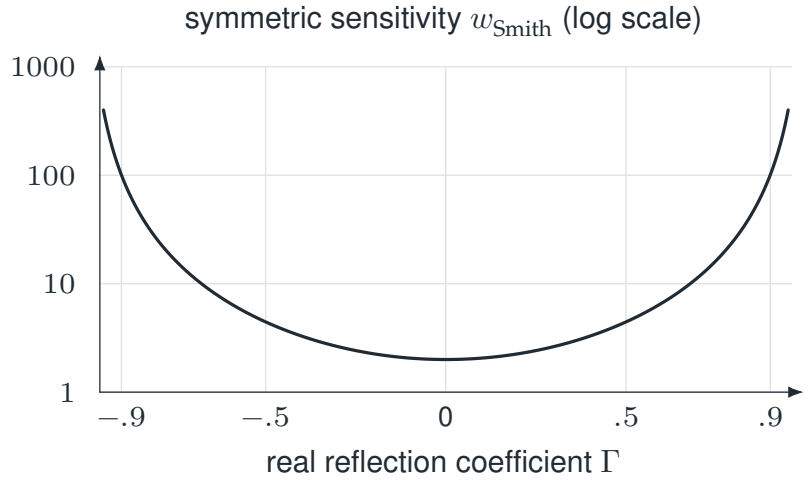
Traditional monograph: Section 14 (p. 29).

Away from $\Gamma = 1$, the inverse Cayley map satisfies

$$\frac{dz}{d\Gamma} = \frac{2}{(1-\Gamma)^2}.$$

Along the real axis, three exact derivatives already show the scale change:

$$\Gamma = \tfrac{1}{2} : 8, \qquad \Gamma = \tfrac{9}{10} : 200, \qquad \Gamma = \tfrac{99}{100} : 20000.$$



Γ	$\lvert dz/d\Gamma \rvert$
$1/2$	8
$9/10$	200
$99/100$	20000

$$\Delta z = 20/9 \neq 2$$

A differential is not the full finite-error formula

For a finite increment ε, with both denominators nonzero,

$$z(\Gamma+\varepsilon) - z(\Gamma) = \frac{2\varepsilon}{(1-\Gamma-\varepsilon)(1-\Gamma)}.$$

At $\Gamma = 9/10$ and $\varepsilon = 1/100$, the actual increment is $20/9$, while derivative times increment is 2. Both are calculated exactly. Their difference comes from using a differential in place of a finite increment. The derivative gives a first order approximation.

What a proposed weight can and cannot certify

Impedance is sensitive near $\Gamma = 1$, and admittance near $\Gamma = -1$. The symmetric weight

$$w(\Gamma) = |1-\Gamma|^{-2} + |1+\Gamma|^{-2}$$

reflects both chart sensitivities. Its growth motivates denser sampling near the endpoints, but does not establish an optimal grid, interpolation rule, or measurement allocation. A finite-error estimate must also control how close the perturbed point comes to either pole.

> **Read this as:** Use the exact finite difference for an error budget. A large derivative diagnoses conditioning. Choosing an optimal algorithm requires further input.

What the reader can now verify

Traditional monograph: Locator D (p. 35), Section E15 (p. 78).

Three worked structures, three distinct kinds of conclusion

Structure	What is established in the original worked layer
Finite signal	Exact signed addressing, filter transfer, Haar reconstruction and energy, sparse coefficient error, and full-tuple nonlinear evaluation.
Finite packet tree	All 26 complete prunings, actual projector sums, the unique cost-9 optimum, and a strict perturbation-margin certificate.
Reflection orbit	Exact rational-complex coordinates, a pole-safe projective action, CRT labels, and finite sensitivity calculations.

What each evidence layer means

Manuscript theorems. The preserved v1.1.0 release maps twenty theorem-like statements to 225 supporting Lean targets in 23 proof modules. Its saved compiler and axiom records remain inherited evidence. No fresh Lean run is claimed for this edition. The additional Part II developments remain outside this twenty-result map.

Current exact examples. The symbolic visual suite was rerun for this monograph. All 181 rational, algebraic, symbolic, and exhaustive finite checks passed. Seven deliberately false assertions were rejected. Numerical samples draw the continuous Fourier and sensitivity curves; they are not promoted to interval enclosures or universal error bounds.

Current executions. The fresh source-release checker passed 20 exact tests containing 305,933 assertions and passed 16 verifier tests, including positive and negative controls. The expanded-source numerical audit passed 11,052 finite checks, mixing exact and numerical calculations. The new extension examples separately passed 38 grouped exact checks and four false controls. These counts measure different operations and are not combined as theorem counts.

Reproducibility. The package preserves the original sources and their reports. Run `python3 build.py` here for an isolated PDF build. The extension finite checker is `checks/verify_extension_examples.py`; its contract and raw execution manifest are included. The original visual checker requires the listed optional dependencies. PDF assembly does not run Lean or either mathematical checker.

The remaining boundaries are not decorative disclaimers

Known-edge synthesis requires the correct packet. A finite cost optimum depends on the supplied objective. An infinite packet tree, a universal segmentation procedure, minimax recovery rates, and optimal Smith sampling require additional theorems. The core's broad edge-recovery problems are not resolved by these finite examples. V27 introduces the additional separated-jump recovery results and their explicit hypotheses. The 16-sample running signal is not the 1024-sample manuscript experiment; the 26-pruning example is not its 458,330-pruning benchmark. Their smaller sizes allow every relevant number to be inspected exactly.

> **Read this as:** Coordinates, approximation, identification, optimization, and physical interpretation are separate layers. The examples make their interfaces visible without erasing their hypotheses.

V27 / PART II / REPRESENTATION BECOMES CONDITIONAL RECOVERY

What the extended developments add

Traditional monograph: Locator D (p. 35), Section E1 (p. 39), Section E15 (p. 78).

The first twenty-six pages follow the corrected twenty-result formal core. The traditional paper's second part restores the broader mathematical developments of the earlier expanded manuscript. The next thirteen worked pages make their additional hypotheses and conclusions visible.

Four transitions, with the missing input made explicit

Transition	Additional input	Resulting control
Residues to lattices	A finite-index sublattice and one representative per coset	Exact addresses in several dimensions
Invertibility to stability	Positive lower frame bound and bounded perturbation	Quantified coefficient and reconstruction error
Known jumps to recovery	Separated jumps, sampling, a Lipschitz background, and a strict contrast gap	Exact jump cells and bounded location/amplitude error
Recovered packets to approximation	A bounded linear approximation operator and its norm	A complete two-term error estimate

The two parts have different formal evidence

The inherited Lean map covers the twenty designated results of Part I through its 225 supporting targets. The additional traditional proofs in Part II are not silently included in that map. The new pages below are mathematical explanations and exact worked specializations of those developments, with a separate finite-example checker. The original manuscript's broad edge-recovery questions remain broader than separated one-dimensional jumps. Conditions such as one jump per sample cell, an available wavelet support, and a positive detection margin do real work. In particular, the ambiguous observation on V19 still rules out an unrestricted recovery guarantee at its stated noise radius.

How to read the extension

V28 to V30 extend coordinates and stability. V31 to V34 identify what a singular packet contains and measure its error. V35 to V39 give three detection mechanisms. V40 closes the route by combining packet accuracy with a specified approximation operator.

> **Read this as:** A positive recovery theorem can coexist with an impossibility example. Their sampling models, noise bounds, and signal classes decide which conclusion applies.

V28 / LATTICE COORDINATES / A RECTANGULAR EXAMPLE

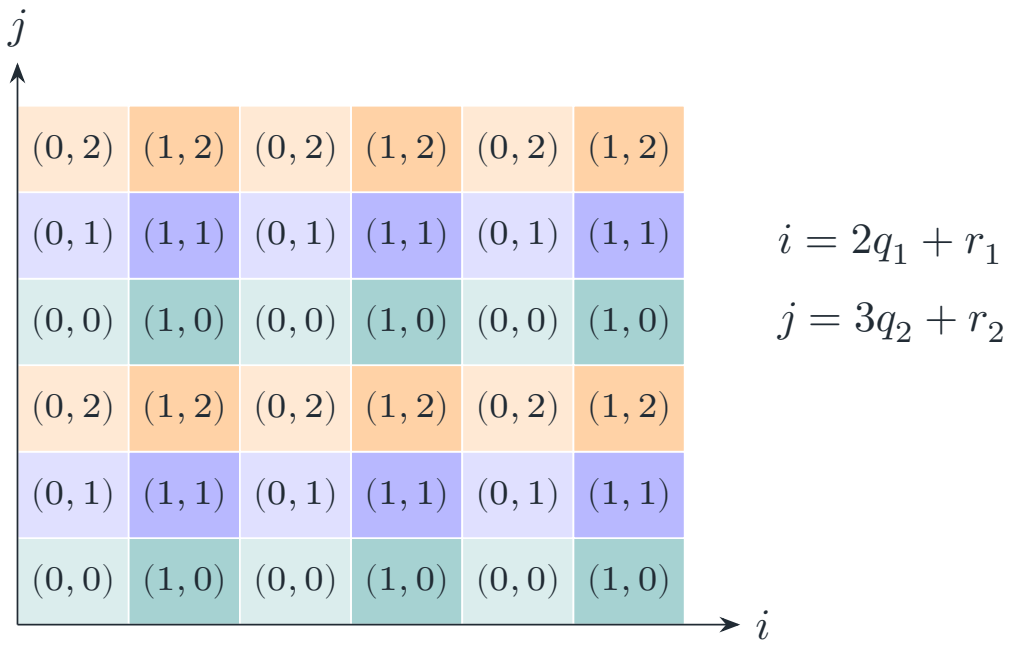
Six image phases are six exact address classes

Traditional monograph: Theorem E3.2 (p. 43), Theorem E3.5 (p. 44), Remark E2.2 (p. 43).

Take $L = 2\mathbb{Z} \times 3\mathbb{Z}$ inside $\mathbb{Z}^2$, with representatives

$$R = \{0, 1\} \times \{0, 1, 2\}.$$

Every address has a unique expression $(i, j) = (r_1, r_2) + (2q_1, 3q_2)$. The six channels are $x_r(2q_1, 3q_2) = x(r_1 + 2q_1, r_2 + 3q_2)$.



Each cell shows its residue label. Colors identify six disjoint classes; they do not average neighboring image pixels.

A negative address is still unique

The point $(-1, 7)$ has representative $(1, 1)$ and lattice displacement $(-2, 6)$, hence channel index $(-1, 2)$. Floor division gives the correct answer in both coordinates. For finite p, the channel norm uses the sum of the pth powers. At $p = \infty$, it uses their maximum. Both equal the norm on the original lattice because the cosets partition all addresses. In ℓ^∞, this coordinate identity does not imply that translates of an impulse are dense: their closure is only c_0.

Refinement partitions a class again

For $L' = 4\mathbb{Z} \times 6\mathbb{Z} \subset L$, the coarse representative $(1, 2)$ has fine representatives

$$(1, 2),\ (3, 2),\ (1, 5),\ (3, 5).$$

Their original-lattice masks sum to the coarse mask. As on V4, decimated arrays are interleaved, not added entrywise.

> **Read this as:** Dimension changes the address tuple. Unique coset decomposition still supplies exact synthesis and the correct norm identity.

V29 / FRAME STABILITY / AN EXACT TWO-CHANNEL BANK

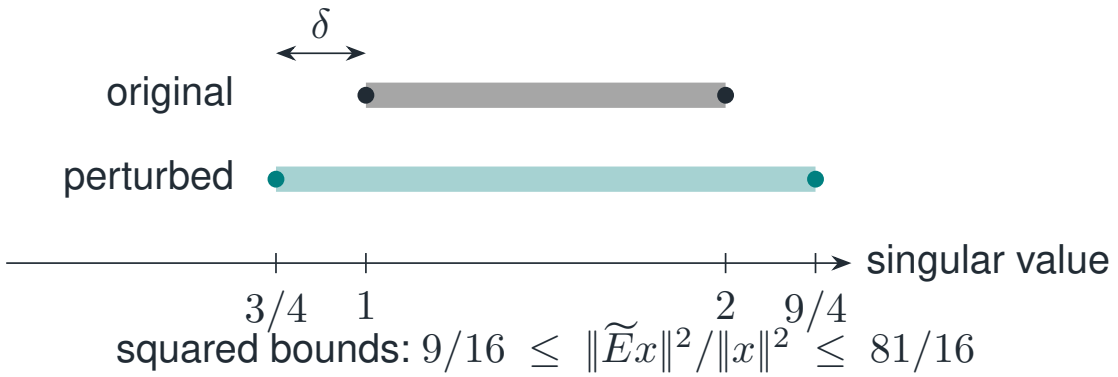
A positive singular-value gap survives perturbation

Traditional monograph: Theorem E5.2 (p. 49), Theorem E5.7 (p. 50), Corollary E5.6 (p. 50).

Consider the constant analysis bank

$$E = \begin{pmatrix} 1 & 0 \\ 0 & 2 \end{pmatrix}, \qquad E^*E = \operatorname{diag}(1, 4).$$

It has frame bounds $A = 1$, $B = 4$. For every perturbation with operator norm at most $\delta = 1/4$, the squared-norm bounds remain at least $(1 - 1/4)^2 = 9/16$ and at most $(2 + 1/4)^2 = 81/16$.



Both bounds can be attained

Choose $\Delta E = \operatorname{diag}(-1/4, 1/4)$. Then $\widetilde{E} = \operatorname{diag}(3/4, 9/4)$ has precisely those two frame bounds. Its inverse has operator norm $4/3$. A coefficient error $\nu = (3/4, 0)$ therefore produces signal error $(1, 0)$, attaining the noise bound. The strict condition $\delta < \sqrt{A}$ prevents the lower bound from vanishing. At $\delta = 1$, the perturbation $\operatorname{diag}(-1, 0)$ destroys the first channel entirely.

An inverse and an approximate inverse answer different questions

If the original synthesis $R = \operatorname{diag}(1, 1/2)$ is retained after this perturbation, then

$$R\widetilde{E} - I = \operatorname{diag}(-1/4, 1/8).$$

Its defect norm is $1/4$. Every input has relative reconstruction error at most that value, with equality on the first coordinate. For frequency-dependent banks the theorem uses an essential supremum on the unit circle, not a few sampled frequencies.

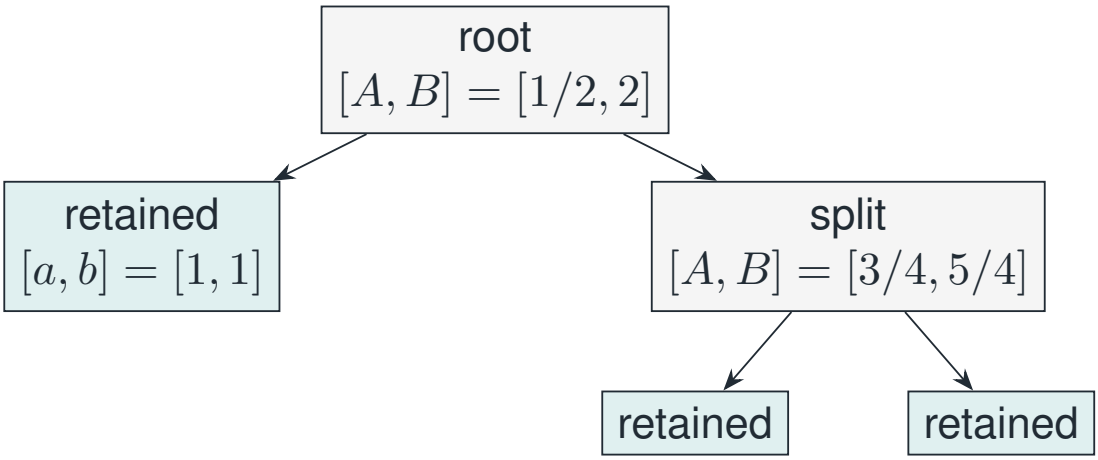
> **Read this as:** A lower singular-value gap quantifies stable recovery. A reconstruction defect quantifies the error of the actual synthesis bank being used.

V30 / LOCAL FRAME CONSTANTS / A MIXED-DEPTH CERTIFICATE

Nonunitary tree bounds propagate along branches

Traditional monograph: Proposition E6.4 (p. 53).

Suppose the root split has nonnegative squared-norm bounds $A = 1/2$ and $B = 2$. Retain the left child. Split the right child with bounds $3/4$ and $5/4$, then retain both grandchildren.



Start with one at every retained node

The left subtree has bounds $a_0 = b_0 = 1$. The right subtree has $a_1 = 3/4$ and $b_1 = 5/4$. The recursive certificate gives

$$a_{\mathrm{root}} = \tfrac{1}{2}\min\{1, \tfrac{3}{4}\} = \tfrac{3}{8}, \qquad b_{\mathrm{root}} = 2\max\{1, \tfrac{5}{4}\} = \tfrac{5}{2}.$$

Consequently the total leaf coefficient energy lies between $3/8$ and $5/2$ times the root energy. These are guaranteed bounds; no assertion that every admissible collection of local maps attains both constants is needed.

Why a minimum and maximum appear

After the root split, its energy may distribute unevenly between the two children. The lower estimate must survive the least favorable child lower bound. The upper estimate must survive the largest child upper bound. Replacing these by an unweighted average would presume an energy distribution that the hypotheses do not supply. When all local maps are unitary, every factor is one and the recursion recovers exact energy conservation. For general local maps, a positive lower bound alone establishes injectivity and stable inversion on the range; it does not by itself assert surjectivity onto every possible leaf tuple.

> **Read this as:** Exact tree coverage and good conditioning are separate inputs. The first chooses a coordinate route; the second bounds what that route does to norms.

V31 / TRACE DATA / A STEP AND A RAMP

Derivative jumps have their own packets

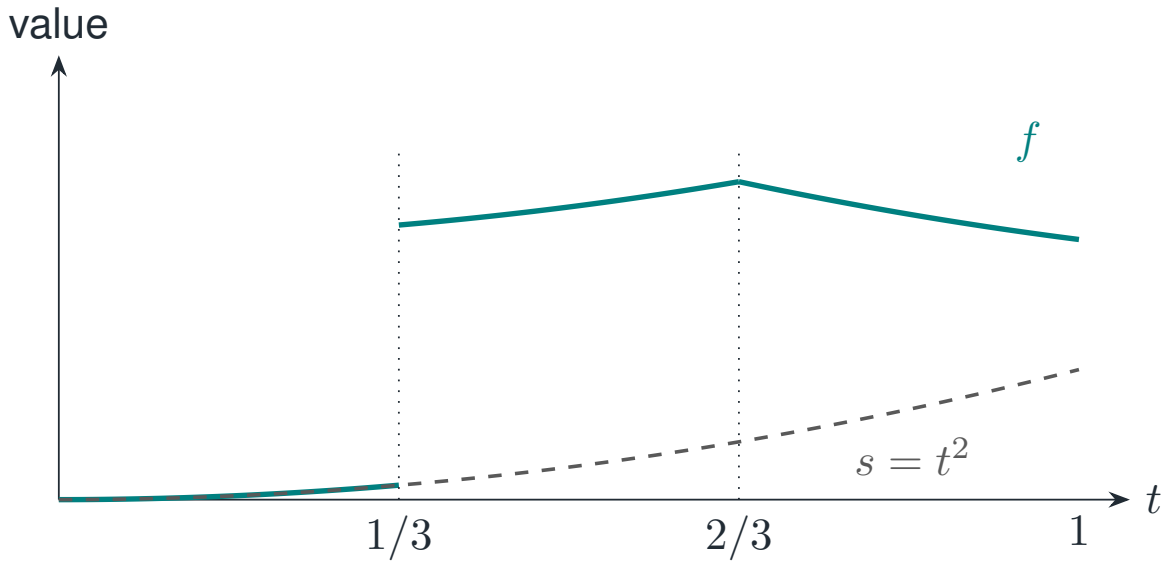
Traditional monograph: Theorem E7.2 (p. 56), Corollary E7.3 (p. 57).

On $[0,1]$, let $H_\tau = \mathbf{1}_{[\tau,1]}$ and take

$$f(t) = t^2 + 2H_{1/3}(t) - 3(t-2/3)_+.$$

The function has a value jump 2 at $1/3$ and a first-derivative jump -3 at $2/3$. Its packet and remainder are

$$j_f(t) = 2\phi_{0,1/3}(t) - 3\phi_{1,2/3}(t), \qquad s_f(t) = t^2.$$



The displayed curves are exact polynomial pieces. The solid jump is not connected across its discontinuity. The dashed curve is the global smooth remainder.

The normalization makes the trace coefficient literal

The general packet is $\phi_{m,\tau}(t) = (t-\tau)_+^m/m!$. Its derivative of order m has a unit trace jump, while its other classical trace jumps vanish. Thus its multiplier is exactly the jump being removed, with no hidden factorial. Here the remainder has matching value and first-derivative traces and belongs to $W^{2,p}(0,1)$ for every $1 \le p \le \infty$. Its second weak derivative is 2. The singular packet accounts for the distributional boundary terms that would otherwise arise at the breakpoints.

What the general theorem requires

Each piece must lie in the stated Sobolev class and possess the specified one-sided traces. Subtracting the finite trace packet then joins those pieces into a global Sobolev remainder. This is a theorem about finitely many declared breakpoints, not a representation of every possible singular measure or arbitrary image boundary.

> **Read this as:** A value jump uses a step. A slope jump uses a ramp. The derivative order determines the packet and its normalization.

V32 / ESTIMATED PACKETS / AN EXACT AMPLIFICATION EXAMPLE

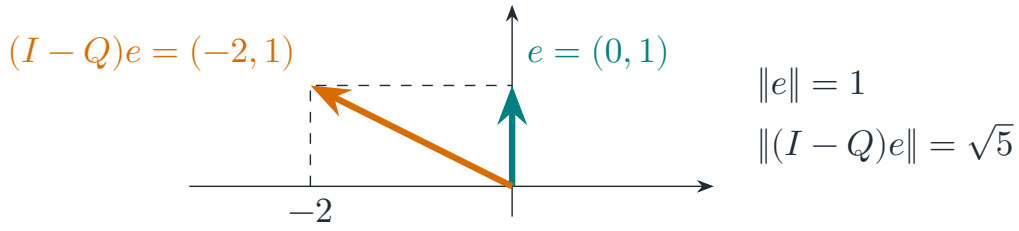
The approximation operator also acts on packet error

Traditional monograph: Theorem E7.8 (p. 58).

Let Q be a bounded *linear* operator and set $e = j - \hat{j}$. Substituting $f = s + j$ into $\hat{f} = Q(f - \hat{j}) + \hat{j}$ gives

$$f - \hat{f} = (I - Q)s + (I - Q)e.$$

The second term includes the action of Q on the packet error. Linearity is required for this split.



An oblique projection can increase the error

In $\mathbb{R}^2$, choose

$$Q = \begin{pmatrix} 1 & 2 \\ 0 & 0 \end{pmatrix}, \qquad s = (1,0), \qquad e = (0,1).$$

Then $Q^2 = Q$ and $Qs = s$, but $(I - Q)e = (-2, 1)$. The smooth error is zero while the unit packet error becomes a reconstruction error of norm $\sqrt{5}$. For a fully specified realization, take $j = e$ and $\hat{j} = 0$. Then $f = (1, 1)$, $\hat{f} = Qf = (3, 0)$, and their difference is exactly $(-2, 1)$.

Use the actual operator bound

The always-valid estimate in this setting is

$$\|f - \hat{f}\| \le \|s - Qs\| + (1 + \|Q\|)\|e\|.$$

Here $\|Q\| = \sqrt{5}$, so the bound is conservative. For an orthogonal projection, $\|I - Q\| \le 1$ gives a sharper estimate. The operator's geometry determines which bound can be used.

> **Read this as:** Recovering the packet and approximating the background are separate tasks, but the chosen approximation operator couples their final errors.

V33 / REGION VALUES / EVERY MISCLASSIFICATION HAS A WEIGHT

An overlap matrix is an exact error ledger

Traditional monograph: Theorem E8.1 (p. 59), Theorem E8.4 (p. 61).

Let two piecewise-constant signals have region values $a = (0, 2, 5)$ and $b = (0, 2, 5)$ on a counting-measure domain of twelve samples. Suppose their overlap counts are

$$M = \begin{pmatrix} 3 & 1 & 0 \\ 0 & 2 & 1 \\ 1 & 0 & 4 \end{pmatrix}.$$

The row totals $(4, 3, 5)$ are the true region sizes. The column totals are also $(4, 3, 5)$, although three samples are assigned to the wrong values.

	$b_0 = 0$	$b_1 = 2$	$b_2 = 5$
$a_0 = 0$	3	1	0
$a_1 = 2$	0	2	1
$a_2 = 5$	1	0	4

off-diagonal squared error

$$1 \cdot 2^2 + 1 \cdot 3^2 + 1 \cdot 5^2$$

$$= 38$$

Equal error counts need not mean equal reconstruction error

The three off-diagonal entries contribute one sample each. Their value differences have magnitudes 2, 3, and 5, so

$$\|j - \hat{j}\|_1 = 2 + 3 + 5 = 10, \qquad \|j - \hat{j}\|_2^2 = 4 + 9 + 25 = 38.$$

The counting-measure supremum error is 5. The full-domain mean squared error is $38/12 = 19/6$. A mismatch fraction of $3/12$ reports a different statistic and omits all three amplitude weights.

The formula requires partitions

For measurable partitions (E_i) and (F_j), with $M_{ij} = \mu(E_i \cap F_j)$,

$$\|j - \hat{j}\|_p^p = \sum_{i,j} |a_i - b_j|^p M_{ij}, \qquad 1 \le p < \infty.$$

Each location belongs to exactly one intersection. Overlapping indicator packets that are summed at the same location must first be converted to their actual combined value regions before this partition formula is applied.

> **Read this as:** Geometry supplies the overlap counts. Signal values supply the weights. Their combination gives the norm relevant to reconstruction.

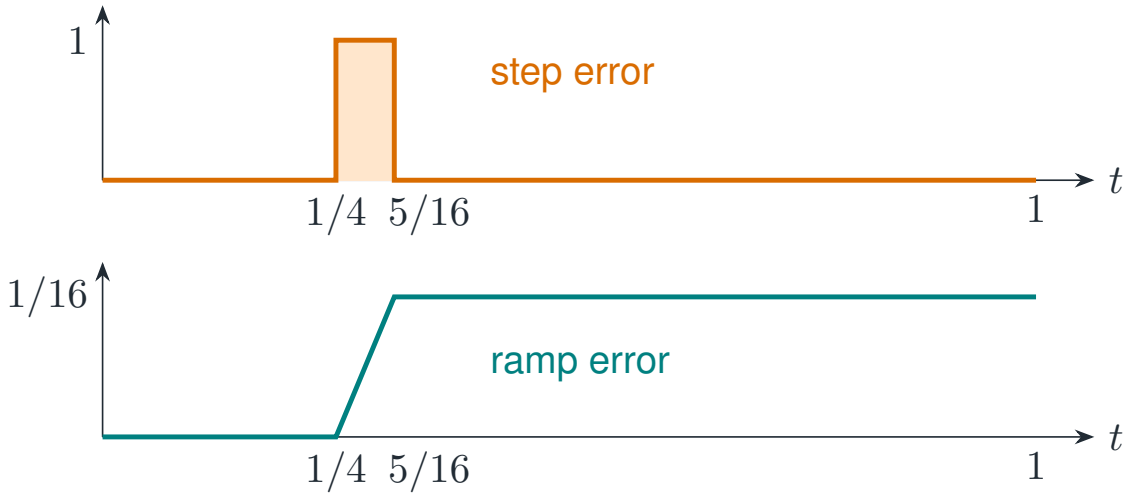
V34 / LOCATION STABILITY / A ONE-SIXTEENTH DISPLACEMENT

A shifted step and a shifted ramp have different moduli

Traditional monograph: Corollary E8.2 (p. 60), Theorem E8.3 (p. 60), Theorem E8.7 (p. 62).

Set $\tau = 1/4$, $\hat{\tau} = 5/16$, and $\delta = 1/16$. A unit step differs only on the interval between its two locations:

$$\|H_\tau - H_{\hat{\tau}}\|_2 = \sqrt{\delta} = \tfrac{1}{4}, \qquad \|H_\tau - H_{\hat{\tau}}\|_\infty = 1.$$



For a ramp, the error height shrinks too

Write $r_\tau(t) = (t - \tau)_+$. The difference grows linearly from zero to δ on $[\tau, \hat{\tau}]$ and stays at δ on $[\hat{\tau}, 1]$. Direct integration gives

$$\|r_\tau - r_{\hat{\tau}}\|_2^2 = \frac{\delta^3}{3} + (1 - \hat{\tau})\delta^2 = \frac{17}{6144} < \frac{1}{256} = \delta^2.$$

Thus the L^2 ramp error is at most δ, and its supremum error is exactly δ. Positive-order truncated powers are Lipschitz in location, with the order-dependent constants supplied by the theorem.

The geometric analogue needs a tube hypothesis

If $E \triangle F \subseteq N_\delta(\partial E)$ and the tube measure is bounded by $C\delta$ for the stated range $0 < \delta < \delta_0$, then an equal-amplitude packet has finite-p error at most $|a|(C\delta)^{1/p}$. A mere visual impression that two boundaries are close does not establish the inclusion or the tube estimate.

> **Read this as:** A displaced value jump keeps its full height on a smaller set. A displaced derivative-jump packet also decreases in height.

V35 / DETERMINISTIC RECOVERY / A NUMERICAL CERTIFICATE

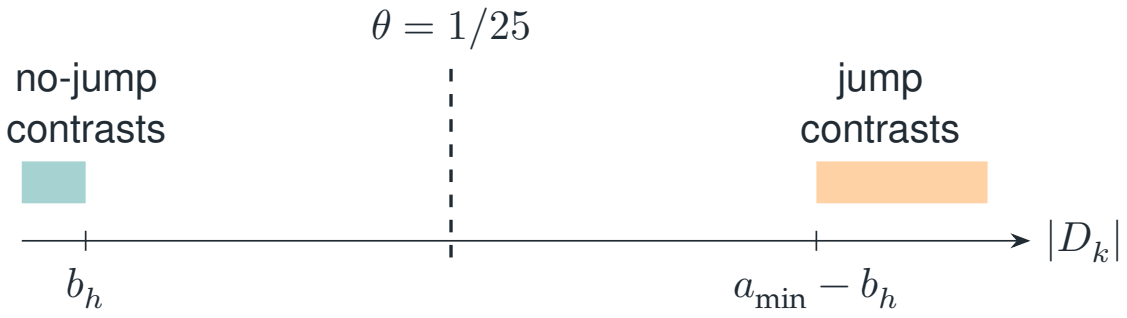
A strict contrast gap locates every separated jump cell

Traditional monograph: Lemma E9.1 (p. 63), Theorem E9.2 (p. 64), Example E9.7 (p. 65).

Assume a real signal is a Lipschitz background plus jumps. No jump occurs at a sample point, and each grid cell contains at most one jump. With spacing h, background constant M, and sample noise bounded by ε, write

$$b_h = Mh + 2\varepsilon.$$

A no-jump contrast has magnitude at most b_h. A jump contrast differs from its true amplitude by at most b_h.



Use the manuscript's exact numerical inputs

For $h = 1/256$, $M = 1/2$, $\varepsilon = 1/500$, and $a_{\min} = 2/25$,

$$b_h = \frac{381}{64000} < \frac{3}{500}, \qquad 2b_h < \frac{2}{25}.$$

The threshold $\theta = 1/25$ lies strictly between b_h and $a_{\min} - b_h$. Thresholding $|y_{k+1} - y_k|$ therefore identifies exactly the jump-containing cells. Their midpoints locate each jump within $1/512$, and each estimated amplitude differs by at most $381/64000$.

The recovered object is a cell, then an estimate

The theorem does not claim the exact real-valued breakpoint from a finite grid. It supplies the correct cell and a controlled representative of that cell. For real jumps, the amplitude error is too small to reverse the sign. Two opposite jumps in one cell could cancel in the contrast, which is why the separation assumption cannot be dropped. For Q jumps the finite-p packet bound contains both Qb_h and the location term $(\frac{h}{2}\sum_q |a_q|^p)^{1/p}$. A growing number of jumps or shrinking separation requires its own analysis.

> **Read this as:** Exact detection means exact cell identification under a strict margin. Location and amplitude remain quantitative estimates with explicit errors.

V36 / SUBGAUSSIAN RECOVERY / A CONSERVATIVE SAMPLE BUDGET

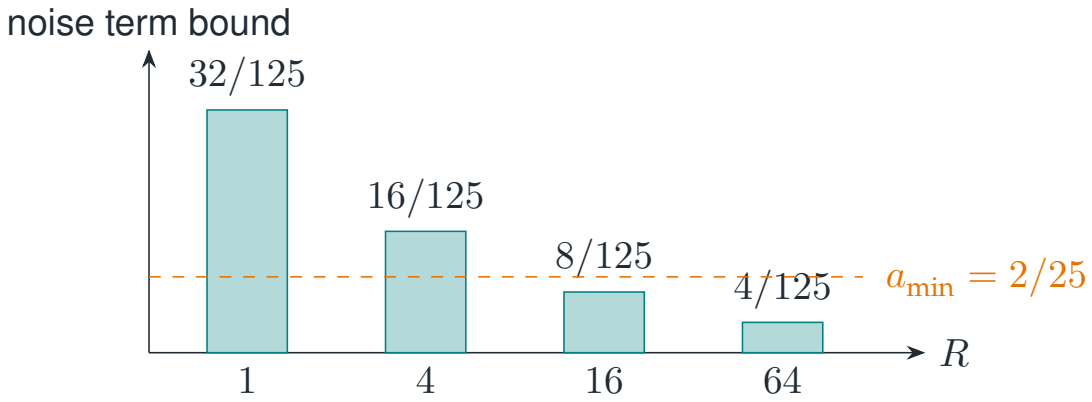
Repeated observations shrink the noise side of the gap

Traditional monograph: Theorem E9.8 (p. 67), Corollary E9.9 (p. 67), Corollary E9.11 (p. 67).

Suppose all noise observations are independent and centered, with moment-generating bound $\mathbb{E}e^{\lambda\eta} \le e^{\sigma^2\lambda^2/2}$. Averaging R observations at each of $n+1$ sample sites replaces σ by $\sigma/\sqrt{R}$. A sufficient recovery condition is

$$a_{\min} > 2Mh + \frac{4\sigma}{\sqrt{R}}\sqrt{\log(2n/\delta)}.$$

The probability of simultaneous recovery is then at least $1-\delta$, subject to the same separated-jump sampling model.



One explicit conservative choice

Take $n = 256$, $M = 1/2$, $\sigma = 1/50$, $\delta = 1/20$, and $a_{\min} = 2/25$. Since $\log(10240) < 10 < (16/5)^2$, choosing $R = 16$ makes the right-hand side strictly less than

$$\frac{1}{256} + \frac{1}{50}\frac{16}{5} = \frac{2173}{32000} < \frac{2}{25}.$$

Thus sixteen independent observations per sample site suffice for this bound. It is a sufficient budget, not a claim of optimal sample complexity. The exact checker certifies $e^{10} > 10240$ using a rational Taylor partial sum, so the displayed logarithm bound is not based on rounded numerical logarithms.

Dependence between adjacent contrasts is allowed

Neighboring differences share one sample. The proof does not require those differences to be independent: it bounds each tail and applies a union bound across all cells. Independence of the underlying sample noises supplies the stated subGaussian difference proxy. For a fixed separated signal model, a noise scale satisfying $\sigma_n\sqrt{\log n} \to 0$ gives the stated recovery consistency in probability. A fixed positive noise scale with one observation per site does not satisfy that condition.

> **Read this as:** More grid points and more repeated observations affect different terms. Finer spacing reduces background variation; averaging reduces noise.

V37 / SCALE SEPARATION / A QUANTIFIED THRESHOLD

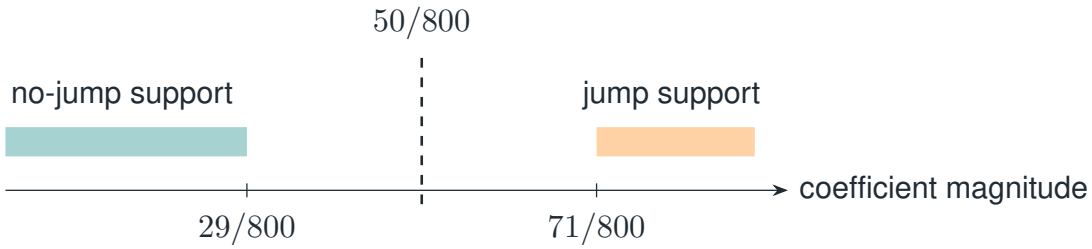
Haar sees a jump only through its position in the support

Traditional monograph: Theorem E10.1 (p. 68), Theorem E10.2 (p. 69), Corollary E10.3 (p. 69).

Use a normalized Haar wavelet on an available interval of length L on the real line, positive on its left half and negative on its right half. Here H_τ is the half-line step $\mathbf{1}_{[\tau,\infty)}$, so there is no artificial second endpoint jump. If u is the relative jump position in the support, then

$$|\langle aH_\tau, \psi\rangle| = |a|\sqrt{L}\min\{u, 1-u\}.$$

The coefficient vanishes when the jump lies exactly at a support boundary.



A worked gap with all three contributions

Take $L = 1/4$, $M = 1$, noise bound $\varepsilon = 1/100$, jump size $|a| = 1$, and relative boundary distance at least $\rho = 1/4$. The smooth and noise contributions together are bounded by

$$\frac{M}{4}L^{3/2} + \varepsilon\sqrt{L} = \frac{1}{32} + \frac{1}{200} = \frac{29}{800}.$$

The jump contributes at least $|a|\rho\sqrt{L} = 1/8$. The observed coefficient therefore has magnitude at least $71/800$. The threshold $1/16 = 50/800$ separates every such jump support from every support containing no jump.

The available support is part of the hypothesis

A fixed extension is needed if the observation domain ends inside a desired wavelet support. Also, the selected support must contain only the specified jump. An unmodeled second jump can reinforce or cancel the coefficient.

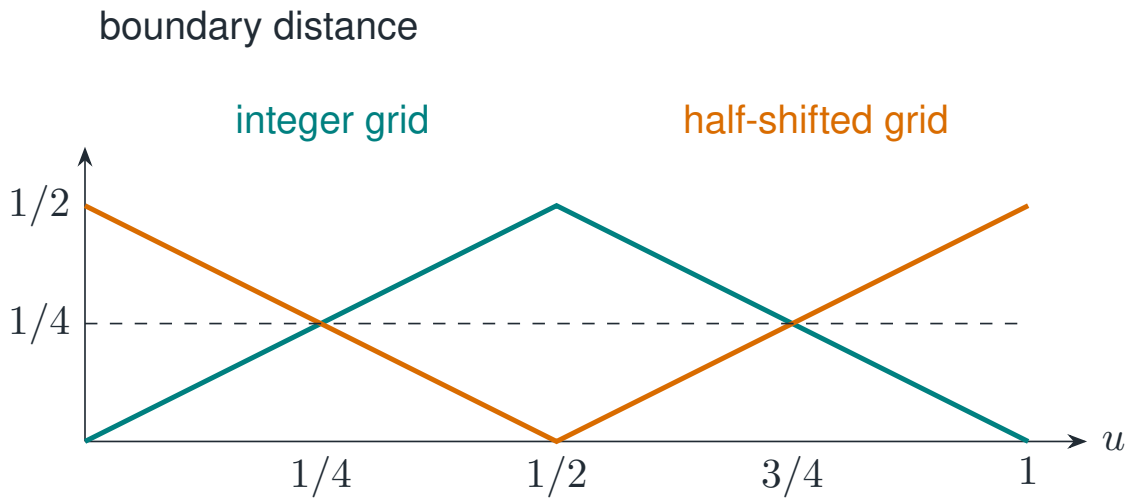
> **Read this as:** Scale determines the smooth contribution, but alignment determines the jump contribution. A detection guarantee needs both.

V38 / HAAR SUPPORT GEOMETRY / A QUARTER-CELL GUARANTEE

Two half-shifted grids remove exact alignment failure

Traditional monograph: Theorem E10.4 (p. 69), Corollary E10.5 (p. 70).

Normalize the support length to $L = 1$. The first grid has boundaries at integers; the second has boundaries at half-integers. For a point at position u modulo one, consider its distance to the nearest boundary of each grid.



At least one distance is one quarter or larger

If $1/4 \le u \le 3/4$, the original cell works. Outside that range, a shifted cell works. At $u = 1/8$, the original margin is $1/8$ but the shifted cell $[-1/2, 1/2)$ gives margin $3/8$. At $u = 1/4$, both margins equal $1/4$, showing that the uniform constant cannot be increased for these two grids. Restoring L, every jump has a support with boundary distance at least $L/4$ in one grid. If L is smaller than the minimum jump separation, that support contains no other jump.

Insert the geometric guarantee into the analytic estimate

The alignment-independent gap condition is

$$\frac{|a|}{4} > 2\varepsilon + \frac{M}{2}L.$$

For the numbers on V37, the right side is $1/50 + 1/8 = 29/200$, strictly below $1/4$. Hence one of the two grids supplies a detectable support for every jump, regardless of its position relative to the original grid. This certifies a useful support per jump. It does not by itself specify a unique rule for merging duplicate detections from two grids into exact breakpoint estimates.

> **Read this as:** A second grid repairs a geometric blind spot. The contrast inequality and separation hypotheses still supply the recovery guarantee.

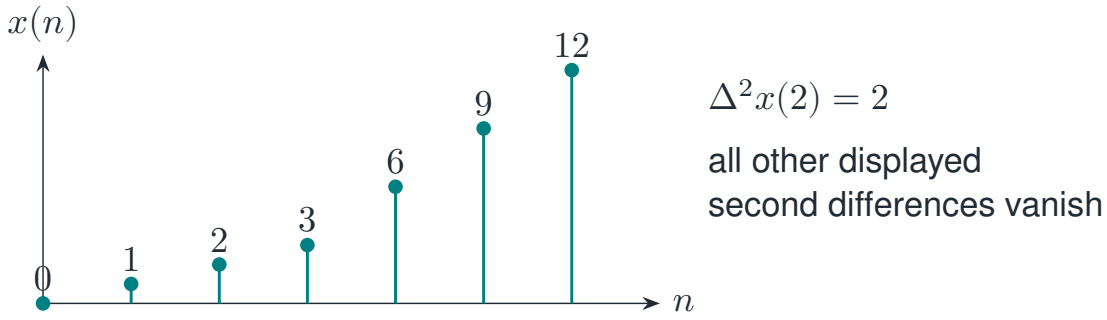
V39 / BOUNDARY STENCILS / SIGNAL RESPONSE AND NOISE GAIN

Higher differences annihilate polynomial interiors

Traditional monograph: Theorem E10.6 (p. 71), Proposition E10.7 (p. 71), Corollary E10.8 (p. 71).

Let $x(n) = n + 2(n-3)_+$ on the integer line. Its slope changes from one to three at the breakpoint 3. The second forward difference is

$$\Delta^2 x(n) = x(n+2) - 2x(n+1) + x(n).$$



An exact small stencil calculation

The values at $n = 0, \dots, 6$ are $(0, 1, 2, 3, 6, 9, 12)$. The second differences at $n = 0, \dots, 4$ are $(0, 0, 2, 0, 0)$. The only nonzero stencil straddles the slope change. For a piecewise polynomial of degree at most d, Δ^{d+1} vanishes whenever its complete stencil lies inside one polynomial piece. Candidate responses are confined to at most $d + 1$ starting addresses before each breakpoint. They are boundary bands, not necessarily exact breakpoint locations.

Differencing also acts on noise

The absolute binomial coefficients of Δ^m sum to 2^m. With $\|\eta\|_\infty \le 1/16$, second-difference noise is bounded by $4/16 = 1/4$. The true response 2 remains at least $7/4$, while all responses away from the breakpoint band remain at most $1/4$. Threshold one separates them. The general robust-band statement assumes that each breakpoint has at least one sufficiently large true response. A breakpoint can fail that assumption through its amplitude or local configuration. Annihilation away from boundaries does not prove a lower bound at every boundary.

> **Read this as:** A vanishing interior response is structural. Reliable detection also requires the boundary response to exceed the amplified noise.

V40 / THE TWO ERRORS / A COMPLETE READING CONTRACT

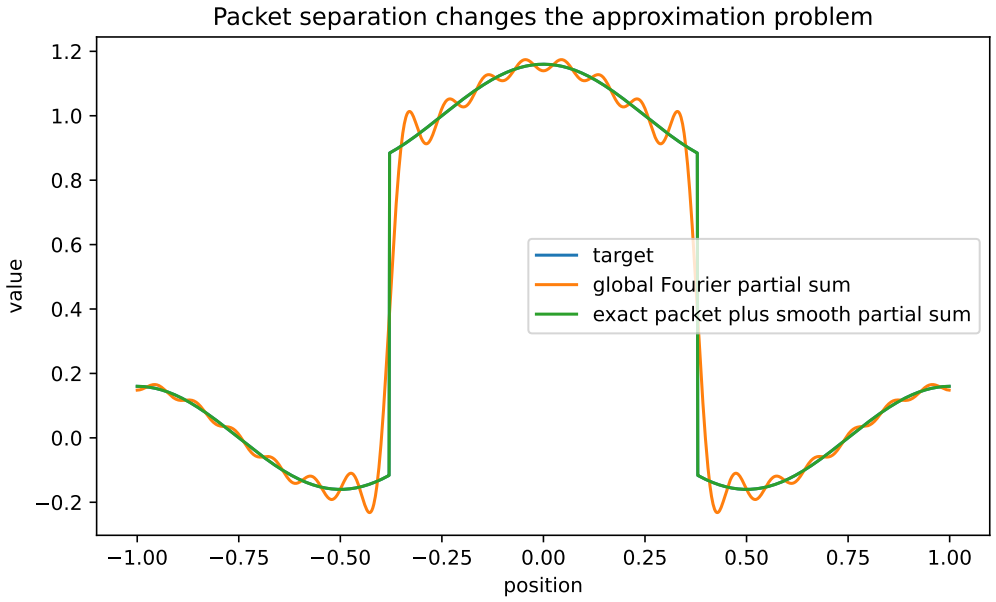
Conditional Gibbs control closes the reconstruction estimate

Traditional monograph: Theorem E11.2 (p. 72), Theorem E11.3 (p. 73).

The exact retained-packet approximation shares the same discontinuity as its target. If $f = s + j$ and $Q_m s \to s$ uniformly, then

$$\|f - (Q_m s + j)\|_\infty = \|s - Q_m s\|_\infty \longrightarrow 0.$$

The approximants themselves may be discontinuous. There is no conflict with the failure of continuous Fourier polynomials to converge uniformly to a jump.



Preserved vector figure from the expanded source. It illustrates the choice of approximation target; it is not an independent universal recovery certificate.

Estimated packets need the operator norm too

If the bounded linear operators satisfy $\sup_m \|Q_m\|_{L^p \to L^p} \le C_Q$, then

$$\|f - \hat{f}_m\|_p \le \|s - Q_m s\|_p + (1 + C_Q)\|j - \hat{j}_m\|_p.$$

For an orthogonal L^2 projection one may use $\|I - Q_m\| \le 1$, sharpening the packet multiplier to one. Such a bound must be justified in the norm actually being used. In particular, uniform boundedness of Fourier partial sums in the supremum norm is not supplied by this theorem.

What the complete guide establishes

V1 to V26 preserve the original worked layer. V27 to V40 explain the additional traditional developments, outside the inherited twenty-result Lean map. The new exact examples have their own finite arithmetic record. They do not extend the formal coverage merely by appearing beside formally mapped results. The final package keeps current computations and inherited compiler reports attached to their stated scope. The symbolic visual suite was rerun, with 181 checks passed and seven invalid controls rejected. Lean compiler evidence remains inherited. No fresh Lean run is claimed.

> **Read this as:** A complete error claim specifies the signal class, the recovered packet, the approximation operator, and the norm. Each term can then be improved and checked on its own terms.

References

[AFP00] Luigi Ambrosio, Nicola Fusco, and Diego Pallara. *Functions of Bounded Variation and Free Discontinuity Problems*. Oxford University Press, Oxford, 2000.

[CD04] Emmanuel J. Candès and David L. Donoho. New tight frames of curvelets and optimal representations of objects with piecewise smooth singularities. *Communications on Pure and Applied Mathematics*, 57(2):219–266, 2004.

[CDF92] Albert Cohen, Ingrid Daubechies, and Jean Christophe Feauveau. Biorthogonal bases of compactly supported wavelets. *Communications on Pure and Applied Mathematics*, 45(5):485–560, 1992.

[CR83] Ronald E. Crochiere and Lawrence R. Rabiner. *Multirate Digital Signal Processing*. Prentice Hall, Englewood Cliffs, New Jersey, 1983.

[CW92] Ronald R. Coifman and Mladen Victor Wickerhauser. Entropy based algorithms for best basis selection. *IEEE Transactions on Information Theory*, 38(2):713–718, 1992.

[Dau92] Ingrid Daubechies. *Ten Lectures on Wavelets*, volume 61 of *CBMS NSF Regional Conference Series in Applied Mathematics*. Society for Industrial and Applied Mathematics, Philadelphia, 1992.

[DeV98] Ronald A. DeVore. Nonlinear approximation. *Acta Numerica*, 7:51–150, 1998.

[Don99] David L. Donoho. Wedgelets: Nearly minimax estimation of edges. *The Annals of Statistics*, 27(3):859–897, 1999.

[DS98] Ingrid Daubechies and Wim Sweldens. Factoring wavelet transforms into lifting steps. *Journal of Fourier Analysis and Applications*, 4(3):247–269, 1998.

[GS97] David Gottlieb and Chi-Wang Shu. On the gibbs phenomenon and its resolution. *SIAM Review*, 39(4):644–668, 1997.

[Mal09] Stéphane Mallat. *A Wavelet Tour of Signal Processing*. Academic Press, Burlington, Massachusetts, third edition, 2009.

[MH92] Stéphane Mallat and Wen Liang Hwang. Singularity detection and processing with wavelets. *IEEE Transactions on Information Theory*, 38(2):617–643, 1992.

[Nat26] National Institute of Standards and Technology. NIST Digital Library of Mathematical Functions, section 6.16(i): The gibbs phenomenon. `https://dlmf.nist.gov/6.16.i`, 2026. Version 1.2.8, released 15 September 2026. Equations 6.16.1–6.16.4. Accessed 20 October 2026.

[Smi69] Phillip H. Smith. *Electronic Applications of the Smith Chart*. McGraw Hill, New York, 1969.

[SN96] Gilbert Strang and Truong Nguyen. *Wavelets and Filter Banks*. Wellesley Cambridge Press, Wellesley, Massachusetts, 1996.

[Swe96] Wim Sweldens. The lifting scheme: A custom design construction of biorthogonal wavelets. *Applied and Computational Harmonic Analysis*, 3(2):186–200, 1996.

[Vai93] P. P. Vaidyanathan. *Multirate Systems and Filter Banks*. Prentice Hall, Englewood Cliffs, New Jersey, 1993.

[VK95] Martin Vetterli and Jelena Kovačević. *Wavelets and Subband Coding*. Prentice Hall, Englewood Cliffs, New Jersey, 1995.

[Zyg02] Antoni Zygmund. *Trigonometric Series*. Cambridge University Press, Cambridge, third edition, 2002.